THE USE OF RADAR DATA TO DERIVE AREAL REDUCTION FACTORS FOR SOUTH AFRICA

by

TODD JASON THOMAS

Thesis presented in fulfilment of the requirements for the degree of Master of Civil Engineering (Hydrology) in the Faculty of Engineering at Stellenbosch University.

Supervisor: Professor J.A. Du Plessis

DECEMBER 2019

DECLARATION

By submitting this thesis, I declare that the entirety of the work contained therein is my own, original work, that I am the sole author thereof (save to the extent explicitly otherwise stated), that reproduction and publication thereof by Stellenbosch University will not infringe any third party rights and that I have not previously in its entirety or in part submitted it for obtaining any qualification.

Sign: _____

ABSTRACT

An areal reduction factor (ARF) can be defined as a factor that is applied to point rainfall depths to convert these depths to an average rainfall over a specific catchment area. The concept of ARFs provide a powerful mechanism for the analyses of the spatial variability of various hydrological processes. However, a plethora of methods used to derive ARFs are dependent rainfall stations. With the decline in population of reliable rainfall stations, radar data has been reviewed as an alternative for applications in hydrology and consequently ARFs. Radar data appears to be more efficient than using rain gauge networks as radar data is able to capture the internal and spatial distribution of a rainfall event.

This research made use of using the storm centred approach based on its incorporation of high spatial and temporal resolution, with radar imagery. Meteorological Data Volume (MDV) files were converted to network common data form (netcdf) files, for compatibility in ArcGIS. ArcGIS was used to delineate single cellular storms, find the maximum point rainfall and calculate the isohyetal rainfall, to produce ARFs. Precipitation Arrays were abstracted from the netcdf files, for the validation of ArcGIS storm outputs: storm area and isohyetal areal rainfall.

The ArcGIS storm outputs, storm area and isohyetal areal rainfall, had significantly high correlation with Precipitation Array outputs, confirming the results thereof suitable for use in deriving ARFs. Furthermore, the ARFs that were obtained using Precipitation Arrays and ArcGIS had high correlation and significance.

The influence of storm area on the radar derived ARFs was determined. It was found that storm area had a significant effect on the ARFs; stronger influence on storm durations of 3 hours, and weaker influence on storm durations of 24 hours. Satisfactory correlation was found between the maximum point rainfall and the resulting ARF. Moreover, a strong inverse proportional relationship was found to exist between the maximum point rainfall intensity and the resulting ARF, for storms of different durations. For various rainfall processes, convective rainfall regions produced higher ARFs, than the ARFs produced in frontal rainfall regions.

A comparison between the radar derived ARFs and the ARFs currently implemented in South Africa was carried out. The radar derived ARFs were lower than ARFs in South Africa for storm areas less than 200 km^2, for smaller catchments. For larger catchments, it was found that radar derived ARFs were lower than ARFs in South Africa for storm durations of more than 1 hour. The radar derived ARFs for the 1 hour storm events were found to be overestimated. In general, the radar derived ARFs were more conservative. Finally, using radar data for the derivation of ARF has exposed the high potential of its use in hydrology.

ACKNOWLEDGEMENTS

The honorary participants that assisted on my journey toward completing this document, and consequently, my success, goes beyond the acknowledgement within this document. Countless days and nights filled with hard work, stress and energy drinks, were endured. Thus, I would like to endlessly thank the following people and organisations:

- My family (Mom, Dad and Sisters). Thank you for listening, motivating and never giving up on me. Many times, I felt like I could not do this, but was reassured through your love and support.
- My friends and partner. Thank you for having an ultimate level of understanding and relatability. We are on our way to making our communities proud and breaking the cycle. Thanks for the fast food errands, assisting me all forms of admin and helping me break away from the stress.
- My supervisor. Thank you for your patience and guidance. Thank you for making opportunities available for me within the Civil Engineering industry. Your knowledge, constructive critique and meaning input is highly appreciated.
- Karel De Waal. Thank you for your patience and assistance with regards to the conversion of files. You input is highly praised.
- SANRAL, especially Rhona Erasmus. Thank you so much for the financial support. Thank you for giving me the opportunity obtain a master's degree.
- Water Resource Commission and SANCOLD. Thank you for giving the opportunity to explore and share my research with extremely talented individuals.
- South African Weather Services. Thank you for your cooperation with regards to providing the radar data. A special mention goes to Morné Gijben, thank you having the patience and lending some time for the queries I had.
- My office colleagues. Thanks for the socials, cake and stress relief. These were very much needed.
- God. For none of this would even be remotely possible without you.

TABLE OF CONTENTS

LIST OF TABLES

LIST OF FIGURES

LIST OF ABBREVIATIONS

AEP	Annual Exceedance Probability
AMS	Annual Maximum Series
AP	Anomalous Propagation
ARF	Areal Reduction Factor
ARI	Average Recurrence Interval
AWS	Automatic Weather Station
CAPPI	Constant Altitude Plan Position Indicator
CSIR	Council for Scientific and Industrial Research
CA_1	Cell Area
dB	Decibel
DDF	Depth-duration-frequency
DWAF	Department of Water Affairs and Forestry
DWS	Department of Water and Sanitation
EV1	Extreme Value Type I
GEV	General Extreme Value
GIS	Geographical Information System
MAP	Mean Annual Precipitation
MDV	Meteorological Data Volume
netcdf	Network Common Data Form
NEXRAD	Next Generation Radar
NCAR	National Center for Atmospheric Research
NOAA	National Oceanic and Atmospheric Administration
NWS	National Weather Services
PDS	Partial Duration Series
PMP	Probable Maximum Precipitation
RAL	Research Application Laboratory
RSA	Republic of South Africa

RDAS	Radar Data Acquisition System
SANRAL	South African National Roads Agency Limited
SAWB	South African Weather Bureau
SAWS	South African Weather Services
T_C	Time of concentration
TITAN	Thunderstorm Identification, Tracking, Analysis and Nowcasting
TP	Technical Paper
USA	United States of America
FSR	United Kingdom Flood Studies Report
WRC	Water Research Commission

1 INTRODUCTION

1.1 Background

Areal Reduction Factors (ARFs) are used for the development and formulation of design areal rainfalls, which are essential for the design and planning of hydraulic structures. ARFs are essential in the design of hydrologic extremes and form part of key functions of storm characteristics such as storm size and shape. ARFs have mostly been developed in the US, UK and New Zealand. The use of ARFs are convenient as the networks of rain gauges with long rainfall records are typically sparse and do not account for appropriate characterisation of associated spatial rainfall patterns (Svensson and Jones, 2010).

An ARF is typically defined as a factor that is applied to point rainfall depths to convert these rainfall depths to an average rainfall over a specific catchment area (Gill, 2005). The two main types of ARFs are derived either by considering a specific fixed graphical location (referred to as the geographically fixed method) or a storm event (referred to as the storm centred method). The geographically fixed method consists of analysing rainfall data at a specific geographical location and contains more statistical significance than the storm centred method. On the other hand, the storm centred method typically focuses more on analysing aspects of a specific storm event, irrelevant of locale.

Radar data appears to be more efficient than using rain gauge networks as radar data is able to capture the internal and spatial distribution of a rainfall event. Moreover, rain gauge networks produce poor spatial characteristics of rainfall events, as it is highly dependent on the density of the rain gauge network. A major challenge that comes with radar data is obtaining reliable and accurate precipitation values. An abundance of limitations exists in the conversion process and differs from radar to radar. These limitations can include radar reflectivity calibration, high estimates due to frozen and wet frozen precipitation and partial beam filling that generally results in signal degradation, which leads to rainfall rates being reduced.

The use of radar data in South Africa has only been used to a limited extent. Currently, there is a significant level of uncertainty with the use of radar data in hydrological research field, not only due the problems associated with the production of many inaccuracies, but also on the grounds of cost, technical infrastructure and topography.

1.2 Problem Statement

Currently, the Areal Reduction Factors (ARFs) used in engineering applications in South Africa to arrive at design rainfalls were mainly produced in 1965 (ARFs for smaller areas) and 1969 (AFRs for larger areas). Although these ARFs were used to calculate many areal design rainfalls, they are now considered outdated as a significant amount of geomorphology, historic rainfall patterns and behaviour changes has since occurred. A significant volume of additional historic information is also now available. With this, an evolution of technology has occurred, and weather data capturing is currently more convenient and accessible than before. With traditional rainfall station data under pressure due to a lack of maintenance, radar data could potentially act as a suitable means to obtain areal precipitation data to calculate ARFs. Furthermore, of the two main methods to obtain ARFs, a storm centred approach would be better suited as rain gauges used in other ARF derivation methods tend to exclude the spatial characteristic of a specific storm event.

1.3 Research Objectives

The main objective of this research is to investigate the potential to develop ARFs using radar data provided from a service provider, in South Africa. These objectives are achieved by completing the following sub-objectives:

a) Obtain estimates of precipitation values derived from raw radar data;
b) Identify potential obstacles that could hinder the use of radar data;
c) Use radar rainfall data to establish storm centred depth area relationships for convective and frontal rainfall regions in South Africa;
d) Calculate Areal Reduction Factors using radar data from a reliable radar(s) in South Africa;
e) Compare the ARFs calculated from radar data to the ARFs currently implemented in South Africa;
f) Explore various aspects that could affect ARFs, namely storm area and duration, with radar data;
g) Expose the potential of the use of radar data, specifically for the hydrologic environment.

1.4 Assumptions

The research implemented the following assumptions within methodology and results:

- The radar imagery received from the service provider is reliable enough for any analysis
- The default Marshall-Palmer relationship holds true for all storm events
- All radar imagery captured inland is assumed to be a convective rainfall region
- All radar imagery captured along and close the coast is assumed to be a frontal rainfall region
- The influence of return period does not affect the derivation of areal reduction factors

1.5 Limitations of Research

The scope of this research is limited by the following:

- The availability of radars;
- The historic record of radar data available for analysis;
- The location of the radars; convective region and frontal regions;
- Type of storm events captured by radars for analysis;
- The available different storm duration(s) (1h, 3h and 24h) data as captured by radar service provider
- The area of the storms as captured by the radar(s)

1.6 Report Layout

The report layout provides an overview of the critical aspects considered in each chapter.

Chapter 1 provides a background and problem statement, and explains the objectives, assumptions and limitations of the research.

A literature review was conducted in Chapter 2 on ARFs on a global and national scale. Thereafter, literature was reviewed on radar data and its use within hydrology and specifically for ARFs.

Chapter 3 extensively explains the methodology followed to arrive at an ARF from the radar data. This specifically looks at the conversion process of radar data into a GIS compatible format, and thereafter, the analysis in the GIS software.

Chapter 4 discussed the results obtained from carrying out the methodology in Chapter 3. The validation of storm outputs, factors influencing ARFs and the comparison of ARFs were explained.

Chapter 5 concludes the main findings of this research.

Chapter 6 provides recommendations for further research, based on this research.

2 LITERATURE REVIEW

2.1 Introduction

This section reviews the derivation of Areal Reduction Factors (ARFs) by specifically discussing factors influencing ARFs, methods of deriving ARFs and the current ARFs for South Africa. Thereafter, radars, and radar data, was reviewed by looking at the current radar network in South Africa and radar reflectivity problems. The use of radar data present in hydrology was explained. Finally, the use of radar data for the derivation of ARFs was discussed.

2.2 Areal Reduction Factors

Areal Reduction Factors has many definitions that allude to calculating the same intrinsic value. This results from the calculation of the ARF either incorporating the return period, catchment area or storm duration of a particular rainfall event; or any combination of these three characteristics. Thus, a basic definition of an ARF can be defined as a factor that is applied to a point rainfall to arrive at an average rainfall for a specific catchment area. The analyses of spatial variability of various hydrological processes is fully encompassed by the concept of ARFs (Gill, 2005)

The design of hydraulic structures requires the measurement of precipitation that is likely to fall over a specific catchment area for a certain duration of time. Conventional flood risk assessments are highly dependent on ARFs. The incorrect estimation or derivation of ARFs could produce a plethora of errors on the estimates of design rainfall and discharge, specifically for flood frequency analyses. A point rainfall only describes the rainfall for a very minuscule area. For larger areas, the maximum observed point rainfall has a great probability of being greater than the average areal rainfall (Svensson and Jones, 2010). ARFs have the tendency to be highly influenced by predominant weather types, return periods and seasons. Thus, ARFs play an essential role for catchments with an inadequate historical rainfall record or weak spatial rain gauge density. Moreover, ARFs provides the facilitation of the development of engineering guidelines, as well as incorporated the spatial smoothing of sample variations.

The methods of deriving ARFs can be split into two categories: empirical and statistical methods. From a traditional stance, the derivation of ARFs typically follow an empirical approach, which tend to disregard the influence of return period. More recently, analytical methods of deriving ARFs were researched and applied accordingly in various countries (Svensson and Jones, 2010). Empirical methods tend to disregard the influence of return period for the derivation of ARFs. That is, until Svensson and Jones (2010) conducted a review study and found that research articles that clearly show that some influence of the return period exists within the derivation of ARFs. In addition, Bell 1976 derived ARFs from rainfall frequency curves and found that ARFs are influenced by return period.

For South Africa, Du Plessis and Loots (2019) re-evaluated the current implemented ARFs, using 19 test sites well spread over South Africa. In turn, this added approximately 20 years of data to the previous set used during the development of ARFs for South Africa, by various researchers. It was concluded, based on the test sites, that return period has an impact on ARFs for South Africa.

Incorrect estimation and derivation of ARFs could have the effect of producing colossal errors for the estimation of areal rainfall intensity, included the analysis of design storms. This directly offers an impact on subsequent flood risk estimates (Wright, Smith and Baeck, 2014). ARFs should at least represent the rudimentary properties of an observed storm structure, along with its variability, based on the premise that flooding is the end product of highly complex meteorological systems and not idealised design storms. Thus, this suggests that the basic characteristics and properties of an observed storm structure, with its variability, should at least be addressed by the ARFs.

2.2.1 Factors Influencing Areal Reduction Factors

Various factors affect the ratio between the maximum point rainfall and the areal rainfall over a specific catchment area. These issues include factors that relate to the characteristics of rainfall as well as the geographical characteristics of the catchment. This includes the data and various methods that are used to derive an ARF.

2.2.1.1 Catchment Characteristics

Most research conducted on the estimation of ARFs concluded that catchment geomorphology (e.g., area, shape and topography) has an insignificant influence on ARFs (Svensson and Jones, 2010). In catchments with areas less than 800 km², the catchment or storm area and point rainfall intensity governs the derivation of ARFs. This is a direct influence from the predominant relationship between the infiltration rate of the soil and point rainfall intensity. In catchments with areas less than 30 000 km², but greater than 800 km², the storm or catchment area and storm duration governs the derivation of the ARFs (Alexander, 2001; SANRAL, 2013). Lambourne and Stephenson (1986) demonstrated that the ARF will decrease from unity with an increasing catchment area.

Elongated catchment shapes tend to result in variable ARFs, with a dependency on typical rainfall isohyets that are aligned along or perpendicular to the catchment. Veneziano and Langousis (2005) investigated deriving ARFs from a theoretical multifractal perspective and rainfall fields. It was concluded that the influence of the shape of a catchment was minimal. In addition, the researchers noted that profoundly elongated catchments are scarce in hydrology.

Windward and leeward effects of mountainous and hilly regions potentially have an influence on ARFs. For the calculation of areal precipitation, which is essential for the derivation of ARFs, using Thiessen polygons with inverse distance weighting methods are not true representatives of the topography being examined. This comes as a potential challenge at higher elevations where the network of rain gauges tend to be less dense (Prudhomme, 1999). With this 'new' knowledge at the time, Allen and DeGaetano (2005) developed a topographical bias adjustment factor to combat the inaccuracy that comes with simple precipitation interpolation procedures in mountainous regions. This bias acted as a means of modifying the areal precipitation values that were given by the interpolation procedures. Their research concluded that the biases appeared to be insignificant for the derivation of ARFs.

A study conducted by Huff (1995) analysed ARFs derived for urban areas and its surrounding rural areas and found a potential difference from the resulting ARFs. The study area, Chicago, produced several storms that were found to have a slower decay for the derivation of ARFs, for a radius of 500 km^2 from the urban storm centre, when compared to several other rural storms. For larger areas, it was found that the decay in ARFs for urban storms exceeded that for rural storms. The sample size of the storms used for the study was relatively small, and the variability in spatial rainfall characteristics for storms is generally larger. Thus, Huff (1995) deduced that this oddity could potentially be a result of the natural variability, instead of the urban rainfall effect.

2.2.1.2 Rainfall Characteristics

Skaugen (1997) conducted research in Norway, on the scaling properties of areal rainfall occurring daily. The rainfall events were classified into small- and large-scale storm events, based on their statistical pattern recognition. The rainfall events were also classified into frontal and convective rainfall events. It was concluded that minimal reduction in magnitude resulted from the spatial averages for large scale frontal storm events, with increasing storm area as opposed to the small scale convective rainfall events. According to Huff and Shipp (2002), different synoptic weather types produced various pattern of spatial rainfall. Huff and Shipp (2002) used a detailed classification method and found that lower pressure centres occur in smaller storm events, which consisted of a lower rate of decrease in spatial correlation, as opposed to the fronts that are typically associated with mid-latitude cyclones. Further, the greatest spatial correlation occurred in air mass storms.

2.2.1.3 Climate and Rainfall Types

The climate can be considered highly variable within South Africa. As a result, nine distinctive climatological regions were defined by making use of hydrological and climatological information for South Africa (Alexander, 2010). This is displayed in Figure 2.1: Climatological Regions for South Africa (Alexander, 2010; Adapted From Du Plessis (2019))

In the South-Western Cape, the climate is predominantly characterised by warm windy summers and winter rainfall. On the other hand, highly variable, extreme temperatures and non-seasonal rainfall tends to occur in the Karoo (KAR) region. Typically, hot summers with convective thunderstorms and cold winters are on the Highveld. Mesic-subtropical conditions dominate on the KwaZulu-Natal coast (Davies and Day, 1998; Alexander, 2010). With this, the MAP has a tendency to decrease, while potential evaporation generally increases westwards and northwards across South Africa. The spatial and temporal distribution quality of rainfall is highly fluctuant on a seasonal and annual level due to the rainfall being produced by different weather mechanisms in different regions, at varying times of the year (Davies and Day, 1998). In winter, the north-westerly winds produce high rainfall in the western part of the South Africa, while the southern interior and Karoo usually remains dry. Summer rainfall is generally higher in the north and east. However, rainfall is typically low in the western part of South Africa due to dry high-pressure air masses that persists for prolonged periods of time (Davies and Day, 1998).

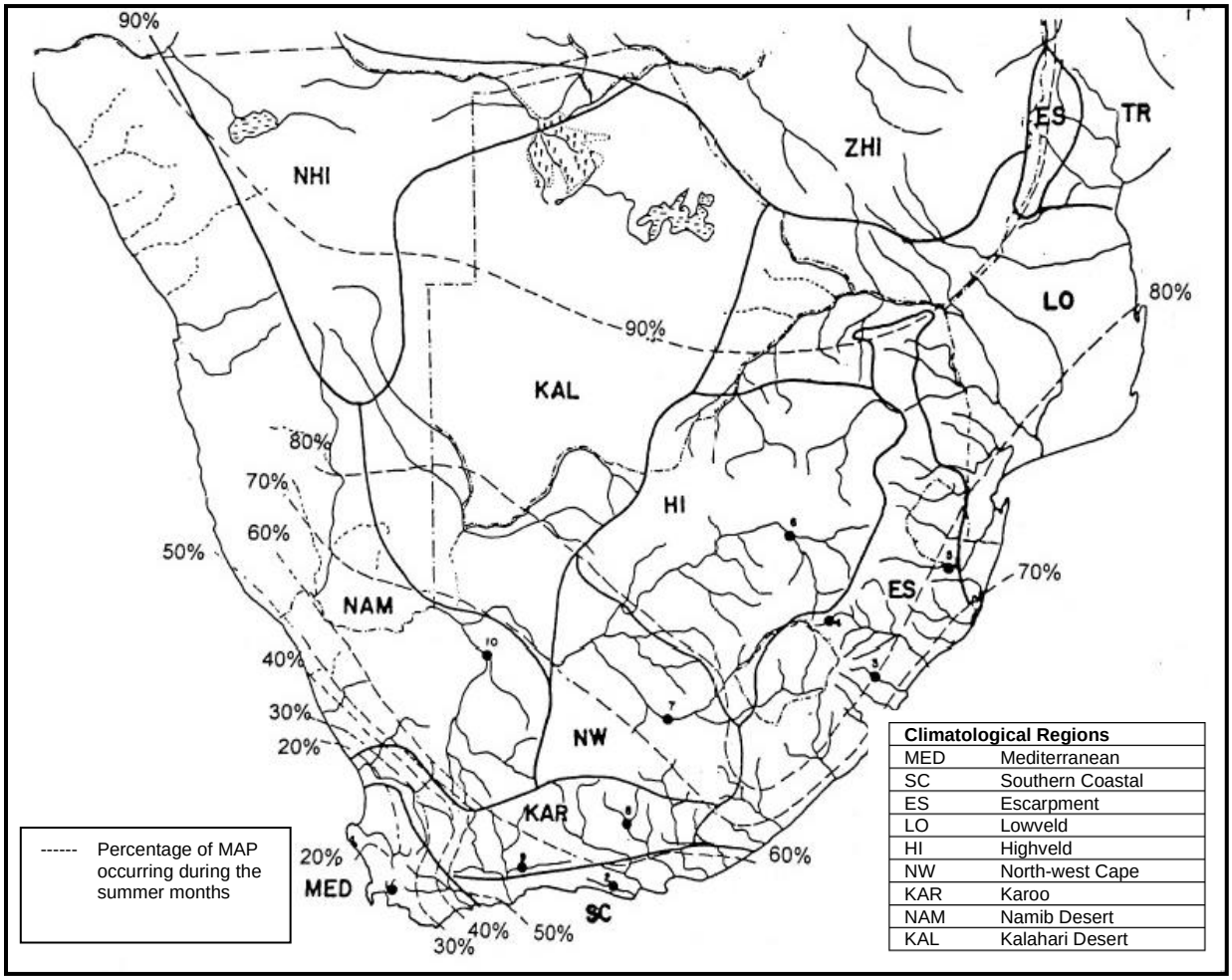

Figure 2.1: Climatological Regions for South Africa (Alexander, 2010; Adapted From Du Plessis (2019))

Bárdossy and Pegram (2018) emphasised that a 10-year return period rainfall event in the UK would likely be greater that the same return period event occurring in Germany, due to their differences in catchment area. Climate possibly affects rainfall distribution, rainfall intensity, duration and variability, and these variables happen to all be interdependent on one another. In South Africa, four major rainfall processes occur that has the potential to affect the interdependency of these variables, which are affected by the climate. In turn, these variables affected by the climate would have numerous influences on the estimation of ARFs. The four major rainfall processes that occurs in South Africa is summarised as follows (Haarhoff and Cassa, 2009; Van der Spuy and Rademeyer, 2018):

a) Convective rainfall: This process occurs during the warmer season when air layers saturated with water vapour are heated and subsequently are inclined to rise and cool down, resulting in cloud formation and rainfall. The rainfall intensity is generally high and is associated thunder activity. Convective rainfall is characteristic of the Highveld regions in South Africa.
b) Cyclonic rainfall: This rainfall process occurs over an open sea and forms when cyclones grow. The growth allows moist air to be drawn into the cyclone vortex and additionally allowing mist to be lifted into the centre. Thus, this results in gale force winds and considerably high rainfall intensities.
c) Frontal rainfall: This inland rainfall process occurs when cold or warm fronts move across South Africa and interact with one another. The cold air tends to move underneath the warm air. As a result, the warm air is deflected upwards by the trailing edge of the cold air. In both cases, the warm air is lifted into the colder region, which produces rainfall.
d) Orographic rainfall: This process usually occurs near the coast when wind blows over an open sea towards land carrying air that is saturated with water vapour until it reaches a mountain range. At the mountain range, the saturated air is forced upwards to result in condensation and rainfall. The rainfall intensity is generally moderate and dependent on wind blowing inland.

The rainfall types listed in (a) to (d) were considered to highlight and describe the influence of various rainfall processes on the estimation and derivation of ARFs. The magnitude of ARFs are highly dependent on multiple storm mechanisms that are associated with the different rainfall types. In a region with frequent convective rainfall occurring than frontal rainfall, the observed point rainfall Annual Maximum Series (AMS) for that specific region would likely consist of rainfall values associated with convective activity (rainfall with rapidly changing intensity).

On the other hand, the frontal rainfall values would be more representative of the actual rainfall process in that particular region. This may result in much lower probabilistically correct ARFs (thunderstorms with high intensities), as opposed to the probabilistically higher ARFs represented by the frontal activity (Siriwardena and Wienmann, 1996).

Considering ARFs with rainfall types (a) and (c), Skaugen's (1997) research in Norway, as mentioned in Section 2.2.1.2, found that the difference in ARF curves between frontal and convective rainfall events had become more distinct for longer return periods. There is a considerably higher decay in ARFs for convective rainfall events than for frontal events; both frontal and convective rainfall events' ARFs decrease with an increase in return period. Allen and DeGaetano (2005) conducted research on determining return intervals, using radar derived precipitation estimates, for extreme areal precipitation amounts, in USA. This research concluded that ARFs are smaller in warmer seasons than in the colder seasons presumed to be responsive to the increased convection over the summer season. Huff and Shipp (2002) found a comparative seasonal difference in ARFs: the decrease with distance in precipitation with regard to the spatial correlation pattern was smaller in the colder seasons than the warmer seasons. The decay in ARFs with the increase in return period could potentially bring to light the significance of convection in the production of large point rainfalls.

Skaugen (1997) pointed out that convective rainfall events, with the associated point rainfall extremes, tend to occur inland, as opposed to the maxima of the large-scale rainfall events that typically occur along the coast.

Allen and DeGaetano (2005a) deduced that the warmer seasons within Eastern United States regions (April – September) produced ARF values that decay at a rate faster than when compared to the colder seasons (October – March). This was said to be attributed to the precipitation mechanisms, which are season dependent, and the corresponding spatial variability of rainfall.

2.2.1.4 Return Period

Bell (1976) conducted a study that specifically focused on areal reduction factors in rainfall frequency estimations. Bell (1976) re-examined the ARFs produced by the Flood Studies Report (FSR), by focusing on the influence of return period. Two methods were used to test the significance of the influence of return period: an adaption of the t-test, for the comparison of means of samples from populations with different variances, and a non-parametric sign test.

The non-parametric sign test emphasised the variation between the group values for any pair of return periods to be significant at 95 percent level, for the 24-hour ARFs. Similarly, its application to the short duration ARFs showed increasing significance at 99 percent levels. With the t-test significant differences were also found between the 2 year and 20-year return periods for the 24-hour ARFs, at 95 percent level. This suggests that the data provided rational evidence that an increase in return period implies a decrease in ARFs. Bell (1976) points out that the values of ARFs in the FSR similarly matches the return periods of 5 to 10 years, with a tendency to be underestimated for greater return periods.

Stewart (1989) carried out a study on ARFs that were used for design storm areal rainfalls by using rain gauge and radar data. Stewart (1989) followed Bell's (1976) methodology which consisted of relying on obtaining ARFs directly from frequency curves. The study introduced a standardisation of rainfall data by the division of the mean annual maximum rainfall. In this way, rainfall growth curves were used to derive the ARFs, instead of rainfall frequency curves. This enhanced the influence of locational variations that mean annual maximum values were represented by, while influence of the return period were represented by the growth data. The findings were concurrent to Bell's (1976) findings, in that the ARF had the tendency to decrease for longer return periods. Allen and DeGaetano (2005a) calculated ARFs with a high rain gauge density, following the geographically fixed method and found that ARF values for a 2-year return period decayed exponentially. It was also found that higher return periods were associated with lower ARF values.

In terms of the methods used to derive ARFs, Omolayo (1993) suggests that storm centred ARFs tend to be incorrect by using point rainfalls to estimate areal rainfall for a particular frequency, as point rainfalls are mainly suited for probable maximum precipitation (PMP) studies.

Du Plessis and Loots (2019) re-evaluated ARFs and their impacts on floods within South Africa. The study focuses primarily evaluate the validity of ARFs, through the use of statistical methods, currently implemented in South Africa through the FSR and Alexander (1990). Within the re-evaluation, it was found that the ARFs had a tendency to decrease with an increase in return period. Adding on, the ARFs generally decreased with an increase in area. Although the general trend was a decrease in ARFs, it was mentioned that the results were somewhat inconsistent, resulting from the influences of the catchment size or shape, geographical location and climatic conditions. Comparatively, the results showed that Alexander’s method for estimating ARFs in South Africa could potentially be overestimated, by as much as 32%, for return periods ranging from 5 to 200 years. The study suggested that return period should be considered when deriving ARFs.

2.2.1.5 Spatial Variability of Rainfall

Kim *et al.* (2019) studied the role of rainfall spatial variability in deriving ARFs. The research highlighted the effect of internal spatial variability of storms on ARFs. For a six year period, composite radar data was used in a storm identification algorithm to classify some 55 000 elliptically-shaped extreme storms. Thereafter, an investigation on various storm characteristics with the corresponding ARF values were carried out. The main assumption was accepting that the ARF generally increases with duration, with an inverse relationship to storm area. The coefficient of variation of radar pixel rainfall estimates was used to comment on the spatial variability within a storm, as the coefficient, along with storm area and duration, proved to be a useful predictor of the ARF value. The average difference in ARF values between storms of circular shape and storms with an elliptical shape, for the same catchment area, was found to approximately 20%. These findings suggest that the current design framework for areal rainfall estimates could be enhanced by the integration of storm shape and the spatial variability of rainfall.

2.2.2 Methods of Deriving Areal Reduction Factors

Theoretical approaches for deriving ARFs were developed analysing the relationship characteristics of extreme storm events and the extent to which their characteristics associate with one another. The earliest attempt at deriving an ARF followed an empirical approach that focused on single storm events, dating back to 1957 (US Weather Bureau, 1957). These approaches had the tendency to disregard the influence of return period and were pioneering for countries like Italy, where they are frequently used for defining design storms for urban drainage systems (Supino, 1964). By including reduction parameters and variance functions, the theoretical approach was extended (Rodriguez-Iturbe and Mejía, 1974). By 1984, Waymire, Gupta and Rodriguez-Iturbe (1984) carried-out analyses using a stochastic derivation of ARFs for rainfall events, which included the temporal and spatial characteristics of the rainfall events.

The two most recognised approaches to deriving ARFs, namely, the storm centred and geographically fixed approaches, has the tendency to provide inconsistent results, when compared with one another. In using a storm centred approach, the isohyets of a complete storm are analysed without considering a fixed geographical location. In the case of a geographically fixed approach, storms occurring over a fixed area or collection of rainfall stations on the catchment's surface are considered (Alexander, 2001). Bell (1976) emphasised that the essence of the geographically fixed approach is less physical and more statistical. Therefore, average areal point rainfall frequency curves were used as it best interprets the data and its values. Thus, it is quite evident that different estimates of ARFs are likely to result from different methods used to derive ARFs.

2.2.2.1 Storm Centred ARFs

Stormed centred ARFs are based on particular individual storm event(s). Storm centred ARFs are typically calculated by dividing an observed areal averaged rainfall accumulation by the maximum observed point rainfall accumulation, for the same storm. With the exception of forecasting and nowcasting, the storm centre is typically calculated after the storm event, since there is no complete accurate method of predicting where the storm centre is located within a storm, during the storm even. Probable maximum precipitation (PMP) mainly makes use of ARFs that are derived using the storm centred method. The storm centred ARF approach is rarely used outside of PMP, partially due to the fact that PMPs are strongly linked to storm type and the resulting issues that are associated with multicellular storms (Wright, Smith and Baeck, 2014).

Pavlovic *et al.* (2016) defined storm centred ARFs as ratios based and formulated by carrying out multiple analyses on individual storms. The resulting ARFs are likely to be used for the conversion between point rainfall estimates of PMP to areal rainfall estimates. This is in line with the definitions of storm centred ARFs from Wright, Smith and Baeck (2014). Although there are various challenges associated with deriving storm centred ARFs, they can be considered as an authenticity measure to assess the validity of their corresponding fixed locale counterparts.

Storm centred ARFs are affiliated with the calculation of the effective rainfall depth for individual storms as well as signify profiles of discrete storms, with data that is usually provided from a reliable source. The area in which rain falls is not predetermined as it differs for each individual storm. With storm centred ARFs, the maximum point rainfall from a rainfall event is considered the storm centre, which is a crucial factor for the derivation of ARFs. The ratio of the average areal rainfall and the maximum storm point rainfall is characterised with the aid of these values. Generally, areal rainfall depths, obtained from isohyets, are divided by the maximum point rainfall of the same storm (Gill, 2005). Storm centred ARFs are usually calculated by using Equation 1:

$$ARF = \frac{R}{P} \quad \textbf{[1]}$$

R is the sum of areal storm rainfall (in mm) enclosed by each isohyet, within which the secluded rainfall is greater than or equal to the value of the isohyet interval, and P is the maximum point rainfall, which is at the storm centre (in mm).

This research focuses on incorporating a storm centred approach due to the spatial and temporal characteristics of a storm being factored into the derivation of the ARF. A geographically fixed approach typically implies using rainfall station data, which is increasingly problematic in the hydrological field, due to the declining number of functional rainfall stations and unreliability that is associated with badly maintained rainfall stations and its data.

2.2.2.2 Geographically Fixed ARFs

Geographically fixed derived ARFs describes the relationship between point rainfall with the corresponding average areal rainfall, over a fixed area. In other words, the statistics of point and areal rainfalls is directly relayed to the derivation of the ARF, where percentage reduction is applied. As a result, this deliberates the uniform temporal and spatial distribution of rainfall for a specified area (Pietersen, Gericke and Woyessa, 2016). Geographically fixed derived ARFs are more frequently used due to the degree of difficulty that comes along with the storm centred derived ARFs. Instead of considering the maximum point values at the corresponding storm centres, this type of ARF considers different parts of different storms. Thus, these ARFs originate in rainfall statistics and are not necessarily linked to any individually recorded storms (Omolayo, 1993).

Wright, Smith and Baeck (2014).defined geographically fixed ARFs as values that are calculated by dividing the extreme estimation of the average areal rainfall through an extreme point rainfall estimation the same duration and area. This is in line with the definitions defined by Pietersen, Gericke and Woyessa (2016) and Pavlovic *et al.* (2016).

Geographically fixed ARFs are conventionally derived for a specific fixed location, from the average of annual maxima rainfall series and frequency based quantile estimates. These correlate the point precipitation depth of a specific catchment area to the average areal rainfall for that same area. Particularly, a point is chosen to be representative of the mean collective point rainfalls in the specified area. The area that is observed is dually fixed in time and space (Gill, 2005). In this case, the centre of the catchment area does not need to have the same coordinates as the centre of the storm. Thus, the ARFs values are not based on the highest point rainfall at corresponding storm area. Instead, the values of the ARFs are naturally based on various parts of different storms. Geographically fixed ARFs are typically derived from rainfall data accumulations instead of individual storms events.

Geographically fixed ARFs can be represented by Equation 1 in Section 2.2.2.1, with the exception that R is the mean of annual maximum values and P is generally the weighted mean (due to the poor spatial distribution of rain gauges) of annual maximum point rainfall estimates at gauged locations, within the specified area (Bell, 1976).

Several researchers note that there is an influence of climate and geographical location on ARFs, due to a difference in the predominant rainfall generating mechanisms (Svensson and Jones, 2010). On a global scale, a study by Omolayo (1993) suggested that ARFs associated with a duration of 1 day are generally larger using USA's method, as opposed to Australia's method. Furthermore, Asquith and Famiglietti (2000) deduced that ARFs decay more rapidly in semi-arid south-western USA (specifically Texas) than elsewhere in the country.

Although geographically fixed ARFs are popularly used in the hydrology field, it lacks the spatial variability that comes with all storm events. This ultimately leads to an overly conservative approach, as certain characteristics of storm events are completely neglected.

2.2.2.3 Annual Maxima Centred ARFs

Asquith and Famiglietti (2000) formulated and proposed the annual maxima centred method of deriving ARFs, in 2000. This approach considers an annual maxima, with the distribution of concurrent precipitation. The method is not dependent on explicit determination of spatial correlation coefficients, the prior spatial averaging of precipitation or the explicit delineation of a representative area for analysis of a particular storm event. Instead, the design of the approach makes extensive use of dense precipitation rain gauge data that is widely available across the world, for various regions. (Asquith and Famiglietti, 2000).

In order to arrive at an annual maxima centred ARF, the following steps were put in place by Asquith and Famiglietti (2000). Firstly, the ratio of the annual maxima depth to the concurrent precipitation was computed for every annual maxima within a specific database, as well as the separation distances between the two respective rain gauges. Thereafter, these ratios produced insight on separation distances and the description of the relation between criteria conditioned sample ratio values. These relations are defined by using an empirical ratio relation and fitting specific functions to the empirical relations. Thus, the expected ration is produced by a best fit line. Lastly, a user defined area with specific design criteria is used to calculate and estimate the ARFs. This sheds light on the fact that the ARFs are functions of catchment area, geographical location, shape and return period.

2.2.2.4 Methods Used in the United States of America

Infrastructure designs make use of point precipitation frequency estimates in the United States of America (USA). The area and proximity around the point precipitation estimates is limited. As such, this reduces its usefulness in many applications that demand areal precipitation frequency estimates. ARFs are highly sensitive to the method by which it is derived.

Research carried out by Pavlovic *et al.* (2016), in the USA dealt with the analysis of differences among ARFs from various geographically fixed ARF methods. The researchers defined an ARF to be a concept used in engineering design that converts point precipitation into areal precipitation, for specified durations and frequencies.

For the comparison of ARFs, Pavlovic *et al.* (2016) used one representative method from each of the main categories: empirical methods (M1), methods that analyse spatial correlation structure of rainfall (M2), methods that address temporal and spatial scaling properties of rainfall (M3), and methods inspired by extreme value theory (M4). Next Generation Radar (NEXRAD) precipitation data was used. In their research, Pavlovic *et al.* (2016) points out that the assumed relationship between precipitation depth and the radar reflectivity produces a great level of uncertainty with regard to unaltered radar precipitation estimates.

The M1 method follows an original empirical ARF method. The Weather Bureau in USA formulated several curves, for storm durations less than 24 hours and areas less than 1 000 km^2, that convert point rainfalls to areal rainfalls. As most methods that were based on empirical approaches over 50 years ago, this method disregards the influence of return period. The M2 method estimates ARFs by incorporating the spatial correlation structure of rainfall. With this, an exponential distribution for the point parent rainfall and a Gamma distribution for the areal average parent rainfall are assumed. The M3 method uses concepts of statistical self-affinity and dynamic scaling in order to arrive at an expression for the mean annual maxima that acts as a function of area and rainfall. Essentially, ARF estimates calculated from M1 are used to arrive at a general fitted expression. In addition, the M3 method disregards the influence of the return period on ARFs. Finally, for the M4 method, ARFs are derived by using a Generalised Extreme Value (GEV) that was fitted to the mean regional annual maxima series data. This was carried out to obtain precipitation frequency estimates for each combination of chosen storm durations and catchment sizes (Pavlovic *et al.*, 2016). It is evident that the USA has an extensive analysis of deriving ARFs by using the fixed area method. The methods used are highly dependent on rainfall stations but included spatial correlation structure to subsequently combat the problem of defining the spatial behaviour of a storm event.

Research conducted by Wright, Smith and Baeck (2014) in the USA on the critical examination of ARFs, argued that insufficient attention was placed on the formulations used to derive frequently used ARFs. The results portray that there exist large discrepancies between the true characteristics and properties of extreme rainfall events and the frequently used ARFs, for the specific study region. The researchers mention that using geographically fixed area method to derive ARFs can be used as a reality check for ARFs derived using a storm centred approach. By using the storm centred approach, the researchers found that the frequently used ARFs failed this reality check, and this consequently suggested important implications for flood risk estimations. Specifically, the research compared storm centred derived ARFs from a larger sample size of storms to storm centred derived ARFs for five arbitrarily chosen. This was done to ultimately determine the difference between ARFs from less extreme storms and more extreme storms with longer return periods.

The most extensively used source of ARFs in USA comes from Technical Paper 29, by the US Army Corps (Beard, 1967). Wright, Smith and Baeck (2014) point out that a principle weakness in the method Technical Paper 29 (TP-29) uses to derive ARFs is that the maximum point rainfall and maximum areal rainfall for a specified area and duration, are not from the same storm event. Furthermore, the Technical Paper 29 (TP-29) states that its storm magnitude has no influence on the ARF estimates, and in turn disregards the influence of return period (Wright, Smith and Baeck, 2014). This shows that the storm centred ARFs derived from TP-29 lacks cohesion which opens doors of uncertainty. The uncertainty potentially results from using storm characteristics from different storms for the formulation of the ARF. The ARFs tend to be higher, as the maximum areal rainfall would generally be greater than the averaged areal rainfall, while the maximum point rainfall always stays the same for the data set.

2.2.2.5 Geographically Fixed Method Used in the United Kingdom

The UK uses the geographically fixed area method (from the FSR), which does not consider the influence of return period on ARFs, as its influence was previously regarded as insignificant. For this method, a particular region is delineated where the annual maximum areal rainfall is calculated. With this, the year and point rainfall measurements at the corresponding rainfall station are recorded. Independently, at each rainfall station, the annual maximum point rainfalls for each year in the area of interest is recorded. The ARF is then calculated for a specific area and duration. This method is considered to map and simplify the US Weather Bureau method instead. It was purely used for computational and calculational efficiency. Svensson and Jones (2010) considers this method to be unorthodox, on the basis that it is an average of ratios that is safely approximating a ratio of averages.

Following Section 2.2.1.4 and 2.2.2.4, Bell's (1976) method of obtaining ARFs includes ranking an annual maximum areal rainfall series using Thiessen’s Polygon as well as ranking the annual maximum point rainfall series for each rainfall station in the fixed area of consideration. The Thiessen-weighted mean of annual maximum point precipitations of equal rank were computed to obtain a single point rainfall frequency curve, for a specific catchment area (Svensson and Jones, 2010). Thereafter, ARFs were calculated by fitting frequency distributions to point and areal rainfall series, for various return periods.

2.2.2.6 National Weather Service Method

This method falls under the M1 method of deriving ARFs in Section 2.2.2.4. It is outlined in the National Oceanic and Atmospheric Administration (NOAA) TP National Weather Services (NWS) 24. The method makes extensive use of the annual maximum two-station average rainfall statistics. The mean and standard deviation from the same points are calculated for station pairs for various durations at arbitrary distances. Each parameter in the distance-duration-space is fitted by a smoothing surface.

The method is based on the frequency analysis of the distance between two rainfall stations with the corresponding annual maxima. This way of deriving ARFs explicitly takes the influence of ARF with return period into account. This reduces the dependency for dense rain gauge networks with observations that are concurrent. The need for large and dense networks are reduced by statistics of small five-stations and station-pairs (Bell 1976). Isotropy in the spatial rainfall area was assumed due to the random locations of the station pairs and five-station network. Thus, catchments that were elongated in shape, with unidirectional rainfall, were not considered. Svensson and Jones (2010), mentions that it is questionable whether this complex methodology is justified as precipitaiton observations increase with time.

2.2.2.7 Storm Movement

Research was conducted by Bengtsson and Niemczynowicz (1986) on deriving ARFs from rain movement. The researchers took a simplified physics approach to deriving ARFs by specifically following the movement of an idealised storm across a specific area; this method closely maps the storm centred method. Data requirements for this study are limited due to the intention of the research focusing on urban catchments up to 30 km^2 with durations of up to 40 minutes. This method of deriving ARFs was called the moving storm derived ARF (M-ARF).

The derivation of M-ARFs were based on using 12 recording rain gauges in Sweden and focussed on the trajectory of convective storms. The M-ARFs were derived from rainfall observations at a fixed point location and storm speed. The main assumption made was that the velocity of movement and shape of the hyetograph does not change throughout the storm passage, over a specific area. Rainfall intensities were assumed not to change drastically over urban areas, since these areas have a limited extent. The method assumes a lateral exponential decrease in rainfall intensity that is applicable for smaller convective storms, with urban hydrology as its main area of application. Svensson and Jones (2010) mentions that this method is not applicable to larger catchment areas nor for long rainfall durations.

M-ARFs were found not to have significant dependence on a particular rain gauge hyetograph. Instead, average M-ARFs derived from hyetographs at any of the rain gauges used in the study, produced stable estimates. Bengtsson and Niemczynowicz (1986) found that the M-ARFs "*…agree well with true areal reduction factors…*" (Bengtsson and Niemczynowicz, 1986), which has the similar values all over Sweden. Synthetic storms were created and simulated to move across the catchment where hyetographs were not available (Svensson and Jones, 2010).

2.2.2.8 Review of Methods for Deriving ARFs

The relationship between areal rainfalls and point rainfalls has been observed to mainly vary with season, return period, estimation method and predominant weather type. Svensson and Jones (2010) point out that analytical methods has the tendency to categorise ARF estimations on a sound scientific basis. On the contrary, the analytical methods are typically based on assumptions that are not entirely considered as ground truth descriptions of the real rainfall process, which Svensson and Jones (2010) classifies as a *"… cause for concern and uncertainty regarding the results.*". This concern is increased by the verification of results through the limited volume of rainfall data. On the other hand, with a lower value of data requirements and computational effort, some ARF estimation methods prove to produce reasonably acceptable results in comparison to traditional ARF estimation methods.

Empirical and analytical methods may not produce areal rainfall estimates that are probabilistically correct. Obtaining an areal rainfall by applying an ARF to a T-year rainfall, may not produce an areal rainfall of equal return period. Hence, focus is put on the measurement of the discrepancy; a minor difference in results may be tolerable when it is considered in combination with its advantages. After these discrepancies are examined and addressed, it seems prudent to recommend these methods for use with rainfall frequency estimates. For any method of deriving ARFs, the underlying data has more importance than any results obtained.

2.2.3 Areal Reduction Factors in South Africa

2.2.3.1 Current ARFs

The main ARFs used for South Africa is found in the SANRAL Drainage Manual (2013). Van Wyk (1965) was the first researcher to analyse ARFs that was based on the storm centred method, for South Africa, which was conducted for smaller catchment areas of less than 800 km^2. Additionally, a small number of rainfall storm areas from the Canada and USA were analysed for comparison. Intensity duration frequency curves were based on Gumbel's theory of extremes using short duration precipitation data. As a result of focussing on smaller catchments, storms were predicted to be intense and short, producing a maximum response or peak discharge. The data used was the yearly records of 20 rainfall stations in the Pretoria region in South Africa that used maximum precipitations from 15 minutes up to 1440 minutes. Hershfield (1962) suggested a factor of 1.13 be applied to the output of the Gumbel values which were applicable in the USA based on the assumption that precipitation was the same all over the world. It was found that intensities for winter were lower than those for summer, with year-round rainfall in between. The areal distribution of rainfall for small-area storms were defined as major percentage of total volume in area to an area less than 800 km^2. For catchments ranging in area from 10 km^2 to 800 km^2, isohyetal maps for numerous storms were plotted, based on the average areal rainfall. The catchments were centred on the maximum point precipitation and the storm centre was expressed as a percentage of point precipitation. Thus, the ARFs were taken as a function of the point rainfall intensity over the storm duration at the storm centre (Van Wyk, 1965). Figure 2.2 displays the resulting depth-intensity-area envelope diagrams that was developed.

From this, it is evident that the ARFs are mainly a function of point rainfall intensity and storm area. This results from the predominant relationship between the infiltration rate of the soil and rainfall intensity and (Pietersen *et al.*, 2015). It was recommended by Van Wyk (1965) that radar data be used for a suitable depth-area analysis, which is the focus of this research.

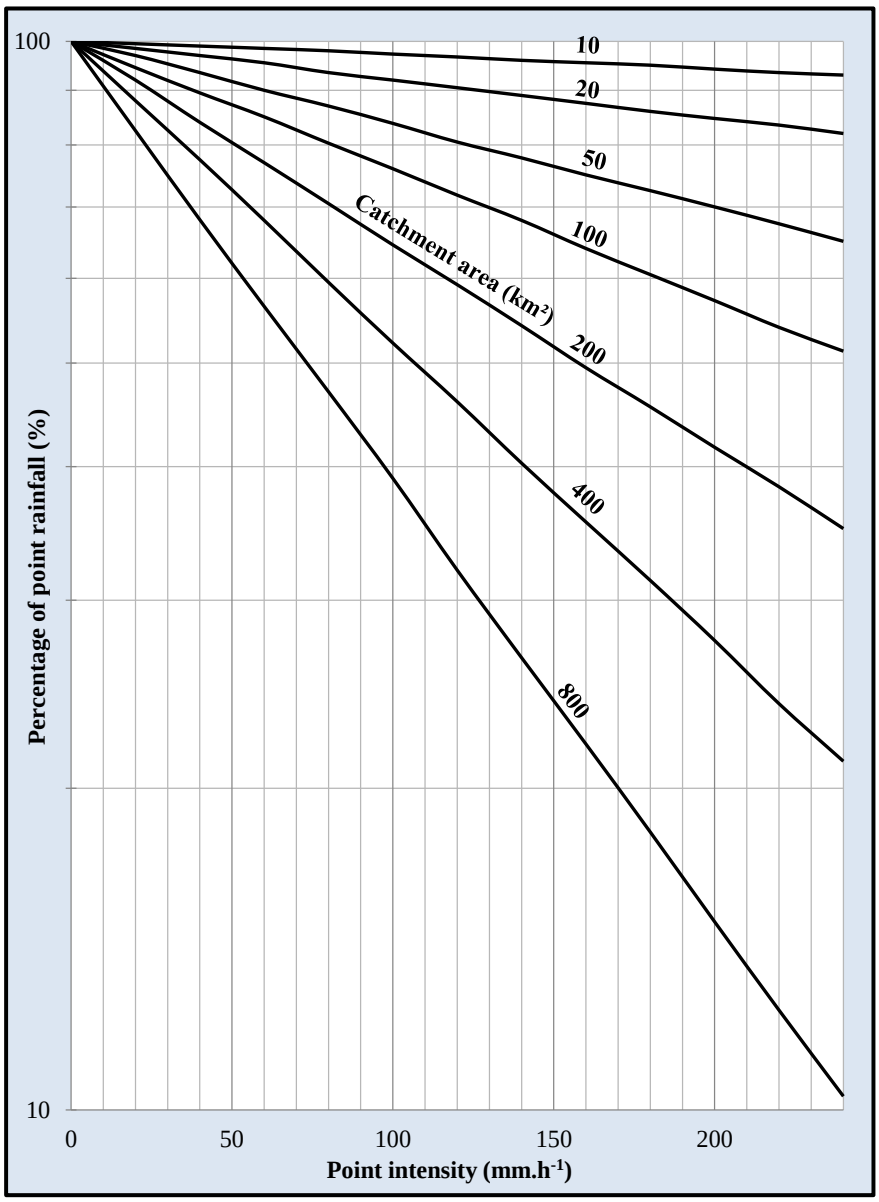

Figure 2.2: Runoff as a function of point rainfall intensity (SANRAL, 2013)

Op ten Noort and Stephenson (1982) converted the findings in Figure 2.2 into a mathematical expression using regression analysis as presented in Equation 2.

$$ARF = Exp(-0.000068iA^{0.77}) \quad [2]$$

where:

ARF = areal reduction factor for point rainfall (fraction),

A = catchment area (km²), and

i = point rainfall intensity at the storm centre (mm.h^{-1}).

Pullen, Wiederhold and Midgley (1966) produced an alternate study that focused on large-area storms with depth-area-duration analysis. The study analysed approximately 170 storms that

covered 18 delineated regions for South Africa, with catchment areas that ranged between 500 km² and 30 000 km². A formulation of isopercentile maps were used, which are smooth patterns of isometric lines that are drown among sample observations when expressed as percentages of local mean annual rainfalls. The methodology for deriving depth-area-duration curves involved the determination of maximum average precipitation depths occurring within selected time intervals throughout the total storm period, on areas encompassed by each isohyet of the total storm isohyet map. The large area storms were delineated while a sixth-degree polynomial surface was fitted to the point rainfall depths, which allowed isohyets to be plotted. For each storm, a regionalised depth-area curve was produced, at a daily interval. This resulted in co-axial diagrams that were used to estimate the rainfall that exceeded or equalled for storm durations greater than one day. The developed depth-duration-area envelope diagram is shown in Figure 2.3.

For each of the 18 regions, the average areal rainfall over increasing storm areas, with storm durations ranging from 1 to 6 days, were expressed as fractions of the maximum observed point rainfall, for storms with a large area and duration less than 24 hours. Depth-area diagrams were developed for storms that lasted 1 to 6 days in duration. Thereafter, the 1 to 24 hour storm durations were linearly extrapolated. This allowed for the rainfall associated with a specific area to expressed as a proportion of the point rainfall between 1 and 72 hours (Lambourne and Stephenson, 1986). ARFs were mainly functions of area and storm durations, since the quality of the rainfall is of great significance when compared to the number of storage areas (Pietersen *et al.*, 2015).

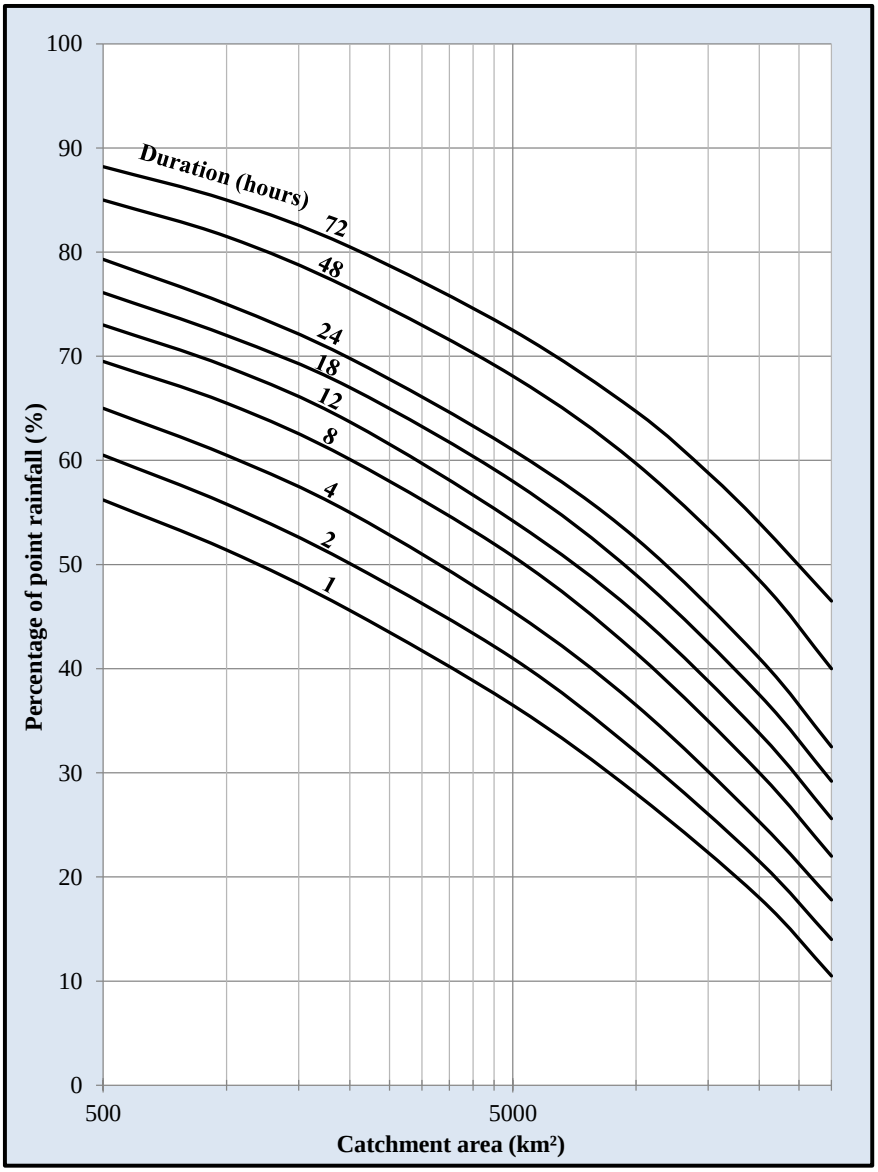

Figure 2.3: Runoff as a function of storm duration (SANRAL, 2013)

Op ten Noort and Stephenson (1982) converted Figure 2.3 to the mathematical expression using regression analysis as shown in Equation 3.

$$ARF = [1.343 - 0.09\ln(A)]T_d^{0.03A^{0.19}} \quad [3]$$

where:

ARF = areal reduction factor for point intensity (fraction),

A = catchment area (km²), and

T_d = storm duration (hours).

2.2.3.2 UK FSR

In March 1975, the United Kingdom published the Flood Studies Report (UK FSR), which contains a significant bulk of research of the analysis of available rainfall and hydrometric records, carried out in Ireland and Britain. Volume II of the FSR contains valuable information and knowledge for the field of hydrology by focusing on the estimation of rainfall depths corresponding to rainfall return periods and durations. Furthermore, the FSR provides insightful knowledge on ARFs. Cunnane and Lynn (1975) produced a review of the FSR with regard to flood estimation.

The FSR produced researched on rainfall studies that investigated point rainfall estimates, ARFs, storm profiles and estimated maximum rainfall. Point rainfall estimates were obtained by analysing rainfalls of 5-year return periods with durations of 1 hour (60 minutes) and 2 days. Growth factors along with long term rainfall and the rainfall for a 5-year return period were used to estimate the point rainfall estimates (Cunnane and Lynn, 1975).

The ARF is applied to the point rainfall of known frequency to determine the corresponding areal rainfall. The ARFs derived in the UK FSR is provided in Table 2.1, with recommended ARF values for areas up to of 30 000 km^2 and durations of up to 25 days. The ARF was found to not vary significantly with return period or geographical location. On the other hand, the FSR shows that the ARF does increase for a specific area with an increase in duration; the ARF diminishes with an increase in area, for a specific duration. The results displayed in Table 2.1 are in accordance with experience, from which it would be predicted that rain with a longer storm duration would have greater areal uniformity, while short duration rainfall might not be very uniform, as reflected in the smaller ARF's.

Table 2.1: ARF with Duration and Area (adapted from Cunnane and Lynn (1975))

Duration, D	Area, A (km^2)									
	1	5	10	30	100	300	1000	3000	10000	30000
1 min	0.76	0.61	0.52	0.4	0.27	-	-	-	-	-
2 min	0.84	0.72	0.65	0.53	0.39	-	-	-	-	-
5 min	0.9	0.82	0.76	0.63	0.51	0.38	-	-	-	-
10 min	0.93	0.87	0.83	0.73	0.59	0.47	0.32	-	-	-
15 min	0.94	0.84	0.83	0.77	0.64	0.53	0.39	0.29	-	-
30 min	0.93	0.91	0.89	0.82	0.72	0.62	0.51	0.41	0.31	-
60 min	0.96	0.93	0.91	0.86	0.72	0.71	0.62	0.53	0.44	0.35
2h	0.97	0.95	0.93	0.9	0.84	0.78	0.73	0.65	0.55	0.47
3h	0.97	0.96	0.94	0.91	0.87	0.83	0.78	0.71	0.62	0.54
6h	0.98	0.97	0.96	0.93	0.9	0.87	0.83	0.79	0.73	0.67
24h	0.99	0.98	0.97	0.96	0.94	0.92	0.89	0.86	0.83	0.8
48h	-	0.99	0.98	0.97	0.96	0.94	0.91	0.88	0.86	0.82
96h	-	-	0.99	0.98	0.97	0.96	0.93	0.91	0.88	0.85
192h	-	-	-	0.99	0.98	0.97	0.95	0.92	0.9	0.87
25 days	-	-	-	-	0.99	0.98	0.97	0.95	0.93	0.91

Bell (1976) conducted a study on ARFs in rainfall frequency estimations. Following Section 2.2.1.4, Bell (1976) considers the certainty that comes with the assumption of the return period having a negligible influence on ARFs. The method used for deriving ARFs were reassessed and questioned. Bell (1976) re-examined these ARFs by fitting frequency distribution curves for the areal and point maximum rainfall series. The ARF was taken as the ratio between the areal rainfall and point rainfall values for equivalent return periods. Bell (1976) found that ARF for 1- and 2-hour durations both decreased with longer return periods. In turn, this contradicts the values provided in the FSR.

2.2.3.3 Review of ARFs for South Africa

Recently, Pietersen *et al.* (2015) carried out a review of the current methods for estimating ARFs used in South Africa, with a preliminary focus on the identification of new methods. The main objectives of this study included a national and international comparison of ARF estimation methods, with an emphasis on the oddities in these methods, along with the assessment of graphical and numerical ARF estimation methods, using typical input variables (such as catchment area, time of concentration, duration and rainfall intensity). The overarching theme was that the ARFs currently implemented in South Africa are outdated with a need for renewal. The review study investigated at the ARFs currently presented in the SANRAL Drainage Manual (2013).

Pietersen *et al.* (2015) discussed the two storm centred methods, as discussed in Section 2.2.3.1, and compared to their numerical estimated counterparts, formed by Op ten Noort and Stephenson (1982). For the geographically fixed method, Alexander (1980), who produced ARFs for South Africa based on the UK FSR, was reviewed. It was found that these ARFs were only applicable when assuming uniform spatial and temporal rainfall distribution over a catchment. In addition, Alexander (1980) had produced a numerical relationship for his graphical results, which included the concentration time of a storm event.

The research continued to produce a case study, to apply the review ARF estimation methods; firstly, by using standard input variables, and secondly, by applying these ARF estimations to a pilot study area. For the standard input variable phase, it was found that the ARFs decreased for an increase in catchment area with significant differences that presented the presence of inconsistencies between results from the graphical and numerical methods. Pietersen *et al.* (2015) pointed out that Van Wyk (1965) and Pullen, Wiederhold and Midgley (1966) methods are not appropriate for estimation of average areal rainfall from point rainfalls. In doing so, the incorrect assumption is made that extreme areal rainfall and extreme point rainfall are produced by identical rainfall types or for the same rainfall event. For the case of the pilot study area, it was found that the geographically fixed numerical ARF estimation methods were more consistent, with the exclusion of the influence of return period. Pietersen *et al.* (2015) points out that ARFs should be derived from local rainfall data as opposed to the UK FSR transposed data, due to the variation observed from areal rainfall characteristics in South African catchments. Furthermore, it was suggested that the current ARFs for South Africa need to be updated by making use of longer rainfall records. The variation of ARF with return period and rainfall-producing mechanisms was suggested for further research. Finally, Bell's (1976) method was recommended for use in practice due to its geographically fixed approach which encompasses an unofficial national conventional method.

2.3 Radars

2.3.1 Weather Radars in South Africa

Following Section 2.3.1, Terblanche, Pegram and Mittermaier (2001) researched the development of the weather radar for South Africa. There are various types of radars that exist in the world, each suited for its specialising functions. Figure 2.4 displays the waves and frequency ranges that radars operate in and are typically named after (Wolff, 2002).

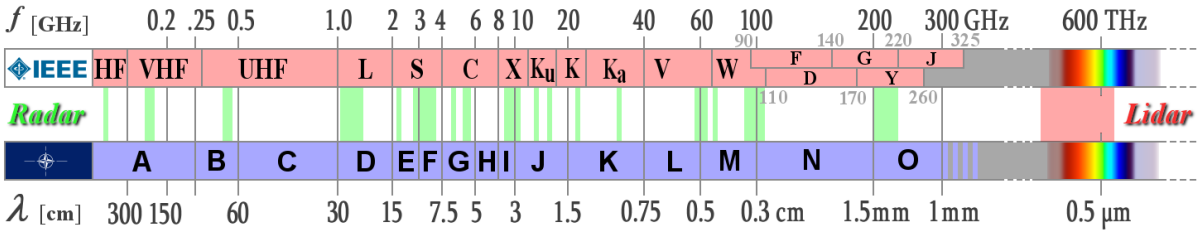

Figure 2.4: Waves and Frequency Ranges that are used by Radars (Wolff, 2002)

In 2002, the South African Weather Bureau (SAWB), now called the South African Weather Service (SAWS), owned ten C-band Enterprise radars of different ages. At this time, Doppler facilities were installed for the newer radar systems. The radars were installed in Bloemfontein, Cape Town, Port Elizabeth, Durban, East London, Bethlehem, De Aar, Irene, Ermelo and Pietersberg, as shown in Figure 2.5. The Water Resource Commission (WRC) owned a Pacer C-band radar located near Tzaneen and an MRL-5 dual wavelength (X-and S-band) radar that was used for research, near Bethlehem. The Pacer radar was used in the Northern Province to exclusively support the rainfall enhancement programme. The spacing of the radars shown in Figure 2.5, resulted from the need for rain and storm intensity surveillance at the regional offices of SAWB, with no intention of hydrological application in mind. Terblanche, Pegram and Mittermaier (2001) point out that the spacing of the radars are not ideal for observing stratiform rainfall, due to the relative shallowness of these systems. The radar beam would generally overshoot the echo top at long ranges, for these instances. Furthermore, convective rainfall systems have deeper vertical dimensions that allow them to be monitored at larger ranges. The radar sites are said to be well selected for the radar horizon that determines beam blockage. However, some beam blockage occurs at the Tzaneen and Bethlehem C-band radars, at low elevations.

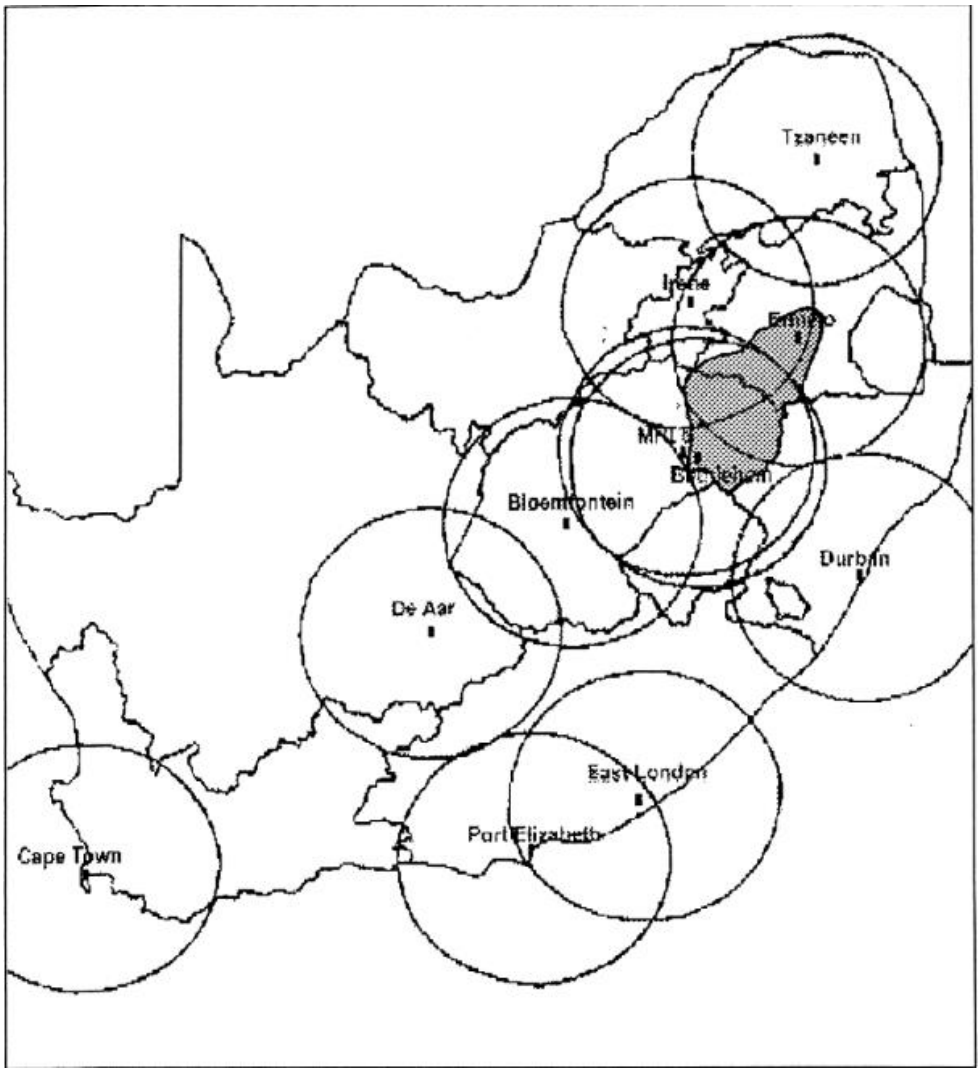

Figure 2.5: The South African Weather Radar Infrastructure, with Circles that represent 200 km data collection range (Terblanche, Pegram and Mittermaier, 2001)

A PC-based radar data acquisition and antenna control system (RDAS) was created to ensure flexibility, with regards to data collection, from the various models and types of radars used. RDAS software was expanded to integrate routines that assists the calibration of a radar as well as to stabilise uniformity in the way any calculations and procedures were carried out. This provided the hydrological readers with large volumes of technical detail. The procedure eliminated manual and error prone calculations. The result was a receiver slope with an electronic file that contained calibration information used in the operation of the radar, and consequently formed part of the calibration history for a specific radar. Calibration checks were carried out consistently and was found to be "*…remarkably stable.*" (Terblanche, Pegram and Mittermaier, 2001).

RDAS was improved to facilitate the data processing and calibration from the X- and S-band radars, after the arrival of the MRL-5 in 1994. A continuous power supply, with a microwave link installed for real-time data transfer to Bethlehem, was generated to the system to facilitate 24-hour operations. Thus, for 24-hour volume scan operations, the MRL-5 was deemed a reliable system.

The customary averaging of the logarithmic output was replaced by an efficient processing algorithm. The logarithmic output was corrected using a 2.5 dB averaging bias. The algorithm, created by Terblanche (1996), was called ‘displace’. The function carries out pair-wise averaging on digitised logarithmic receiver samples, using averaging lookup values that are functionally dependent on the difference between the pair and the receiver transfer function that is to be simulated. In this way, a true unbiased average of received power is obtained when simulating a quadratic receiver. This eliminates the underestimation that occurs in areas of steep reflectivity gradients when using the customary averaging technique.

The algorithm was further developed to achieve more accurate interpolations for the conversation between Cartesian coordinates and spherical coordinate volume scanned radar data. This technique was found to be twice as computationally efficient as conventional interpolation techniques. Constant Altitude Plan Position Indicator (CAPPI), a coordinate file type that is an output from the ‘displace’ algorithm, simplified the merging of information from several radars. This is a requirement for the TITAN software, which plays a crucial role in the South African weather radar representation and data manipulation system (Terblanche, Pegram and Mittermaier, 2001).

2.3.2 Current Radar Network for South Africa

Table 2.2 provides the date that each radar was commissioned, along with its operational frequency and capabilities. The current radar network in South Africa is displayed in Figure 2.6. In comparison with Figure 2.5, Figure 2.6 shows the current operational radar network, produced by Becker and Pegram (2014). The white rings represent S-band frequency radars, and the green, the C-band frequency radars. The smaller rings (as from Figure 2.5) represent a range of 200 km, with the larger rings covering a range of 300 km. Blue dots indicate radars that make use of Doppler capabilities, with the red dots showing the lack thereof. The turquoise dot represents Doppler and Dual-Polarisation capabilities.

Table 2.2: SAWS Radar Network (Adapted from (Becker and Pegram, 2014))

Radar	Date Commissioned	Frequency Band	Capabilities
Bethlehem	March 2010	S-band (10 cm)	Doppler and Dual-Pol
Bloemfontein	July 2011	S-band (10 cm)	Doppler
Cape Town	< 1998	C-band (5 cm)	Reflectivity Only
Cape Town Int. Airport	Not Yet Active	X-band (3 cm)	Doppler and Dual-Pol
De Aar	< 1998	C-band (5 cm)	Reflectivity Only
Durban	May 2011	S-band (10 cm)	Doppler
East-London	May 2011	S-band (10 cm)	Doppler
Ermelo	November 2010	S-band (10 cm)	Doppler
George	January 2012	S-band (10 cm)	Doppler
Irene	January 2010	S-band (10 cm)	Doppler
OR Tambo Int. Airport	Not Yet Active	X-band (3 cm)	Doppler and Dual-Pol
Ottosdal	November 2010	S-band (10 cm)	Doppler
Mthatha	March 2010	S-band (10 cm)	Doppler
Polokwane	November 2010	S-band (10 cm)	Doppler
Port-Elizabeth	< 1998	C-band (5 cm)	Reflectivity Only
Skukuza	February 2007	S-band (10 cm)	Reflectivity Only

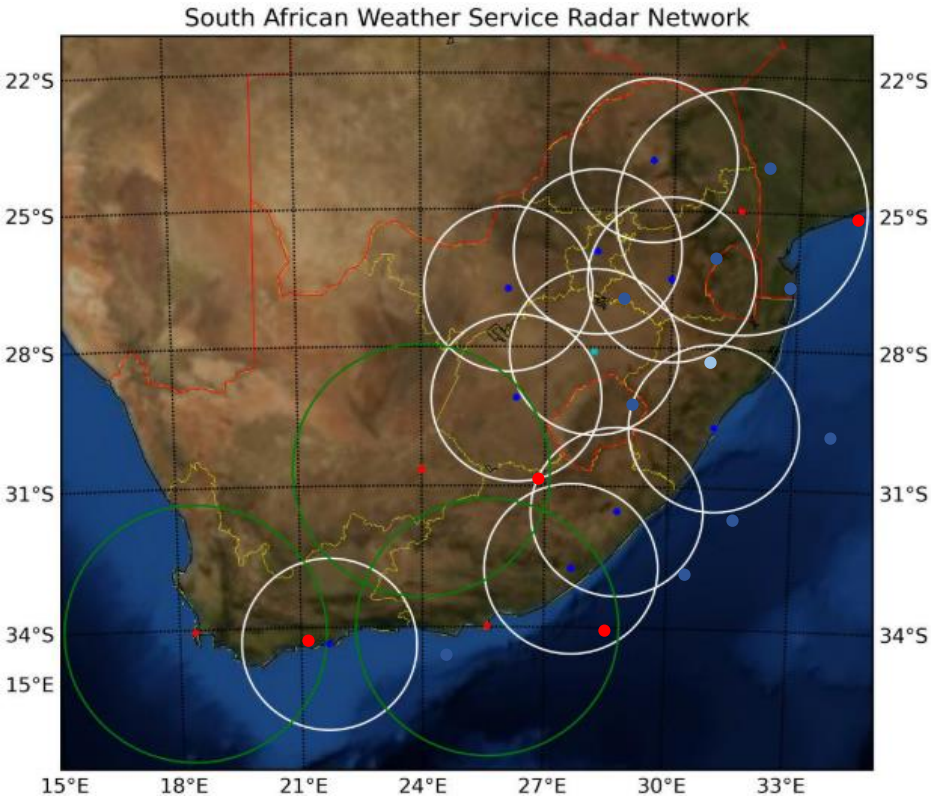

Figure 2.6: Current Radar Network employed by SAWS (Becker and Pegram, 2014)

2.3.3 Radar Reflectivity Problems

Radar reflectivity measurements must be carefully corrected and extracted before rainfall can be estimated. Beam blocking, anomalous propagation hail and bright band are a few of the errors that contribute to incorrect, and consequently inaccurate, precipitation estimates. These are discussed in more detail in the following sections.

2.3.3.1 Beam Blocking

When a radar beam meets a fixed object (for example, a mountain or skyscraper), it constitutes to beam blocking. Beam blocking tends to be a significant source of error within precipitation estimation. Generally, two types of beam blocking occur. Partial beam blocking occurs when the apex or upper segment of a fix object is within range of the beam, causing power losses and severe underestimation of precipitation estimations. The second type is called total beam blocking, in which a fixed object comes into the full range of the beam. This causes full power blocking with no precipitation estimations to be read beyond the range. Thus, this makes beam blocking extremely dependent on the surround topography of its location (Becker and Pegram, 2014).

2.3.3.2 Bright Band

Bright band occurs when observations of a uniform band of higher reflectivities are captured just beneath the zero-degree isotherm (at freezing level). Higher reflectivities are a result of several characteristics of electromagnetic waves and hydrometers within the atmosphere. These include the differences of ice and water with regards to their reflective properties, density above and below the melting level and terminal velocity. This phenomenon is observed in more organised stratiform precipitation, where a clear distinction in particles between different layers in the atmosphere is present. When particles precipitate from a cloud and the ice particles move through the melting layer, they start to melt from the outside inward (Becker and Pegram, 2014).

2.3.3.3 Ground Clutter

Ground clutter appears when the main beam intersects the ground. This causes an echo that is returned to the radar. The targets typically consist of mountains and tall structures in the immediate area, close proximity of the radar. Mostly, the object causing ground clutter is easily identified. Usually, a radar clutter map is used to identify and delete ground clutter from a weather radar display (Becker and Pegram, 2014).

2.3.3.4 Anomalous Propagation

Anomalous Propagation (AP) is defined as the extended detection of ground targets. It usually occurs in clear weather conditions with the presence of a temperature inversion, or whenever the water vapour content of the atmosphere is at relatively high levels. This results in a more refracted radar beam, as opposed to one obtained in normal atmospheric conditions. In extreme cases, this can cause the beam to curve toward the surface of the Earth (Becker and Pegram, 2014).

2.3.4 Radar Data for Research in Hydrology

Weather radars provide quantitative precipitation estimates with a high temporal and spatial resolution. With this, adjustments need to be applied to these estimates due to gross errors, such as beam attenuation, that are caused by variability of the drop size distribution and those caused by strong precipitation and a non-uniform profile of reflectivity.

On average, South Africa receives less than 500 mm of precipitation annually and is considered to be a semi-arid country. Large-scale flood events are often brought on by prolonged periods of drought. Convective storms produce a large percentage of the annual rainfall and this adds to the potential to cause severe storm related damages, specifically local flash floods. The topic of radar data has become more and more ‘popular’ over the years, especially within hydrology. From flash flood warning systems, to ARFs, radar data is proving its true potential in its ability to add knowledge and significant research to the hydrological field. On a global scale, radars have been extensively used in research, and radars, have become more refined and streamlined in order to obtain outputs that are useful for further analyses. On a national scale, radars are proving to be useful toward South African hydrology. Researchers like Terblanche, Pegram and Mittermaier (2001) could be considered the ‘forefront’ runners on producing research for the use of radar data in South Africa. SAWS is also integrating the use of radars for hydrology.

Terblanche, Pegram and Mittermaier (2001) point out that the South African Weather Bureau (now called South African Weather Service, or SAWS) is the custodian for the compilation of rainfall data as part of its climate database. However, daily records of rainfall data from rain gauges has decreased from 4500 to 1750 active gauges in about 55 years, with about 600 gauges producing daily recordings. This adds the urgency to improve South Africa’s ability to observe rainfall events over large areas in close to real-time during flood events. In addition, there is a need for improvement on the spatial resolution of rainfall measurements that can improve the accuracy of catchment rainfall estimates under convective climatic conditions. This points to radar data as a possible alternative.

The UK, USA and several other European countries have already successfully produced hydrological applications that has integrated weather radar data, such as water resource management and flood warning systems. In South Africa, limited resources are available as it is a largely developing country.

From 1970 to 1990, South African radar meteorological research was limited to studies and activities that fixed on improving the understanding of severe storms, natural precipitation processes and the possibility of creating a viable rainfall enhancement technique. Storm dynamics, cloud microphysics and hail for severe storm studies were the priority studies at the Council for Scientific and Industrial Research (CSIR). In the early 1990s, this program was terminated, and two C-band radars and an S-band Doppler radar was constructed and operated in the Johannesburg and Pretoria regions, which resulted in multiple Doppler studies. Simultaneous rainfall enhancement research was carried out in Nelspruit. Thereafter, rapid progress was made towards developing 'new' cloud seeding technology for the rainfall enhancement. At this point the emphasis on radar research moved away from the radar-based comparison between natural and seeded storms in randomised seeding experiments, toward quantitative measurements of areal rainfall. (Terblanche, Pegram and Mittermaier, 2001).

Terblanche, Pegram and Mittermaier (2001) researched the use of weather radars as a research and operational tool for hydrology in South Africa. In short, RDAS for control of radar antennae, processing and digitising outputs from the radar's receiver into useful reflectivity, was developed. A 'displace' processing method for the elimination of digitised receiver averaging errors in areas of steep reflectivity gradients was developed. Furthermore, development for the performance of upgrades and testing procedures to ensure sustained radar operations and high-quality radar data was carried out. Finally, the introduction of Thunderstorm Identification Tracking and Nowcasting (TITAN) real-time storm analysis and tracking system was presented for use in South Africa. This is discussed in more detail in Chapter 3.

2.3.5 Radar Data for the use of ARFs

The derivation of ARFs have been described in Section 2.2, with nearly every empirical derivation making use of rain gauge data, with some methods using radar data. Radar data has become available and numerous authors have investigated its use in hydrology as an alternative to using ground observation based data (Stewart, 1989; Terblanche, Pegram and Mittermaier, 2001; Allen and DeGaetano, 2005b; Sinclair and Pegram, 2005; Wright, Smith and Baeck, 2014).

Svensson and Jones (2010) mentions that radar data provides an improved spatial coverage of rainfall events, in comparison with dense rain gauge networks. On the other hand, records obtained from radars tend to be short particularly for fine spatial resolution. In addition, quantitative measurements are poor in comparison with rain gauge data, which can be overcome by incorporating rain gauge data with radar data.

2.3.5.1 Rain Gauges

Rain gauges are the most widely used data source when it comes to deriving ARFs. At any given location, rain gauges are generally considered to provide the most accurate precipitation information, with certain limitations. These limitations include under-catch, due to erratic behaviour of the mechanical aspects of the rain gauge and wind, and instrumental errors, during intense rainfall. Furthermore, interpolation of areal rainfall from point rainfall is considerably sensitive to the interpolation method that is used. This is due to the high spatial variability of precipitation and presents a significant challenge for ARF calculations, particularly at sub-daily durations (Pavlovic *et al.*, 2016).

Multiple studies have been carried out on the joint use of rain gauge and radar data. Stewart (1989) described the analysis of spatial variability of rainfall, considering the joint use of rain gauge and radar data, for North West England, UK. A fixed area ARF derivation approach was implemented for extreme rainfall events with durations of 1 hour to 8 days, within an area of 100 000 km^2. A similar methodology to Bell (1976) was put in place, where ARFs were derived directly from frequency curves. Due to the limitations of the record of radar data, the calculation of ARFs were carried out directly for 1 to 8-day durations, ranging in areas of 25 to 10 000 km^2, from which average areal values were computed. It was found that ARFs increased with duration for a given area, and decreased with area for a given duration, in line with findings from several other studies (Bell, 1976). These ARFs were compared to ARFs produced in the FSR and showed that the FSR contained conservative ARF values. Furthermore, ARFs decreased with return period; there was no strong tendency for ARFs to vary with location for the study area. The study concluded that more confidence is placed on ARFs obtained for smaller areas than for larger areas.

2.3.5.2 Storm Centres

Convective cells, from a storm event, are dynamic objects that comes with the difficulty of tracking using conventional approaches, due to their rapid change in shape. Algorithms for the identification of storm centres within radar data has been developed over time, following two approaches. The first being correlation tracking algorithms that provide velocity and direction information for larger area events, and the second being cell identification and tracking algorithms that provide location information for isolated cells.

A study carried out by Picus *et al.* (2008) focused on tracking storm centres in radar data for short term weather prediction, using a mean-shift method with integral image computation. The mean-shift algorithm identifies the high density of modes within a complex feature. For the identification of each mode, the mean-shift algorithm requires an iterative computation of area integrals. It was concluded that the mean-shift algorithm was able to only correctly track small storms.

Following Section 2.2.1.5, Kim *et al.* (2019) identified that storm centres were based on the assumption that extreme events could be captured by referring to the pixels of a radar image, on the basis that the accumulated rainfall volume with a given duration exceeds a specific threshold over the entire record of the six-year period. Storm centres that corresponded spatially and temporally with extreme storms types, were identified. An assumption was made that the extreme storms contained at least one of the extreme pixels that have rainfall depth greater than the rainfall associated with the10-year return period, and less than a 200 year return period. With the now identified storm centre, an analysis was carried out on each storm, to eliminate instances of overlap in time. The study showed that the spatial and temporal correspondence of each storm centre was of great importance because ARFs are primarily used to reflect the characteristics of extreme storms in designing flood defence systems.

2.3.5.3 Precipitation Arrays

Olivara *et al.* (2006) calculated ARFs using NEXRAD precipitation estimates, using the storm centred method. The study was carried out in Texas over and area of 685 000 km^2. The storms analysed were assumed to be elliptical in shape and of different aspects and ratios. The methodology included using the annual maximum precipitation depth for one hour for each cell within the precipitation array, producing a grid of annual maxima precipitation values for 1, 3, 6, 12 and 24 hr durations. Following this, threshold precipitation values were applied for each storm duration: 20 mm for 1 hour, 25 mm for 3 hours, 30 mm for 6 hours. 30 mm for 12 hours and 40 mm for 24 hours. The research concluded that ARFs are dependent on geographic region and precipitation depth, which is associated with storm frequency for specific durations. The ARFs calculated were lower when compared to other US studies.

2.3.5.4 Other Countries

Following Section 2.2.2.4, Wright, Smith and Baeck (2014) derived ARFs from a 10-year, high resolution radar with a bias corrected data record for a Hydro-NEXRAD system. The research made use of a mean-field bias correction of the 10-year record at a daily scale using rain gauges within the study region, Charlotte, USA. ARFs were calculated for 1, 3, 6 and 12-hour durations for a threshold area of 3 600 km^2, using the storm centred approach. The researchers found the ARFs calculated from the study is less than the ARFs in TP-29. With longer durations, the ARFs tend to approach ARFs presented in TP-29. It was highlighted that longer-duration ARFs compared well with the ARFs found in TP-29. This resulted from the storms that produced high point accumulations for long durations which have the tendency to additionally produce high areal rainfall accumulations for longer durations. However, storms that produced high point accumulations for short durations, did not necessarily produce high accumulations for short durations, over larger catchment areas. The mean AFR's for tropical and non-tropical storms are significantly less than the ARFs presented in TP-29 for all durations. The researchers bring to light that there is a tendency toward multicellular storm structure for longer-duration storms that are based on the number of ARFs that do not uniformly decrease with storm area. In addition, ARFs were found to decay more rapidly with area for the storms that were selected based on the size and shape of the catchment used for the study (Wright, Smith and Baeck, 2014).

Wright, Smith and Baeck (2014) concluded that storm type has a significant effect on the derivation of storm centred ARFs, within the study area: Charlotte, North Carolina. The rainfall from tropical storms had the tendency to be longer in duration and spatially larger than rainfall from organised storm systems. Therefore, tropical storms decay less rapidly with increasing in storm area. The study used radar precipitation data, which the authors provided as an alternative for improving ARF estimates based on the principle that radar data captures a wide range of storm behaviour that can be readily used to characterise rainfall spatial variability. Furthermore, the variability has the potential to be incorporated into flood risk estimates and design storms.

Pavlovic *et al.* (2016) used NEXRAD gridded precipitation data with rain gauge data to determine ARFs for Oklahoma, USA. The predominant source of uncertainty with unaltered radar precipitation values is the assumed relationship between precipitation amount and the reflectivity. This typically varies, based on precipitation type. The precipitation detected by the radar could potentially evaporate before reaching the ground or move large distances downwind, since precipitation is sensed well above ground surface. More uncertainty ascends from radar technology itself. Conversely, radar data has the potential to be useful for calculating the statistics of extreme events, and spatial pooling can typically be used to compensate for short radar records.

Following the study carried out by Pavlovic *et al.* (2016) , ARFs estimates were compared for the M1 through M4 methods, as discussed in Section 2.2.2.4. ARFs were calculated from the averages of the annual maximum series data and compared to the US Weather Bureau ARF estimates. The researchers found that for longer durations, the ARFs were similar for all the storm areas. However, the differences became more emphasised as the duration decreased. All four methods were classified as conservative with regards to the US Weather Bureau across all storm durations and areas considered. This notion lies more in line with the TP-29 estimates, and consequently, does not follow the conclusions stated by Wright, Smith and Baeck (2014). This could be due to the methodologies (storm centre vs geographically fixed) to arrive at these ARF estimates. Furthermore, the average recurrence interval's (ARI's) influence was tested on the ARF estimates and it was reported that there was a clear separation of ARFs with longer ARIs, in line with the findings of Bell (1976). The dependency of ARI on ARF was found to be more pronounced for shorter durations.

Bacchi and Ranzi (1996) obtained ARFs using a stochastic derivation of storm intensity, based on the analysis of crossing properties of the rainfall process aggregated in time and space for Italy. Thus, the storm centred approach was mapped. The data used within the study included radar images with a time resolution of 15 minutes. This data was verified with corresponding rain gauge data for 17 stations, which produced satisfactory results. The researchers point out that radar data is more efficient than common rain gauge networks as radars host the ability to capture spatial distributions and internal structure of storms. The main findings of the research included an observation that the ARFs decay according to a power function with respect to area, as well as a weak decay of the ARFs with respect to the return period, in urban areas.

Lombardo, Napolitano and Russo (2006) researched the use of radar reflectivity for estimation of ARFs. The study consisted of analysing ARFs using radar reflectivity maps that were collected with a Polar 55C weather radar, which is a C-band Doppler dual polarised coherent weather radar with polarisation agility. This radar measures the most used horizontally reflectivity factor (Z_h), the differential phase shift and the differential reflectivity. These measurements are obtained by averaging 64 pulses with a range-bin resolution of 75 m, and threshold of 120 km away from the radar location. The conversion of reflectivity to rainfall intensity (R) was based on a non-linear regression analysis, shown in Equation 5:

$$R = 7.27 \cdot 10^{-2} Z_h^{0.62} \quad \textbf{[4]}$$

An approach different to the geographically fixed or storm centred method was followed; a scaling law was used and obtained by the ratio between the radar rain rate estimates over an area ranging from 1 km^2 to 900 km^2 and the radar rain rate estimates over 1 km^2. Similar results as reported by Bell (1976) and Wright, Smith and Baeck (2014) were reported; a higher storm duration produced a higher the ARF, for selected areas as well as the larger the area, the higher the ARF for selected durations. These results were found to be more applicable to floodplain management as well as in the design of urban drainage systems, for basins 200 – 900 km^2 in area, with storm rainfalls that are typically associated with 25 to 50 year return periods and 1 to 2 hour storm concentration times: estimated ARF values ranging from 0.1 to 0.3.

The spatial interpolation of rain gauge data assists in arriving at extreme areal rainfall depths. A low spatial density of rain gauge networks often hampers reliable estimations of extreme areal rainfall depths. Overeem *et al.* (2010) investigated extreme value modelling of areal rainfall obtained using a weather radar. An 11-year radar rainfall data set, in the Netherlands, was used to abstract annual maximum rainfall depths with storm areas ranging from 6 to 1700 km^2 for storm durations of 15 min to 24 hours. A General Extreme Value distribution was fitted to the annual maxima for each storm area and duration, separately. With this, areal rainfall depth-duration-frequency curves were estimated and ARFs calculated. The ARFs for the study were compared to the ARFs produced in the FSR; it was concluded that the difference in ARFs of rain gauge data and rain data estimated through radar pixels, is small for a duration of 24 hours. Adjustment factors were applied to the ARFs in the FSR which produced ARFs for short durations and had strong correlation with ARFs produced in the Overeem *et al.*(2010) study. Figure 2.7 displays the radar-based ARFs and reveals an indicative influence of the return period. For areas up to 500 km^2, ARFs decay significantly with storm area, for both long and short durations. These results are indicative of rare rainfall events that have relatively high spatial gradients.

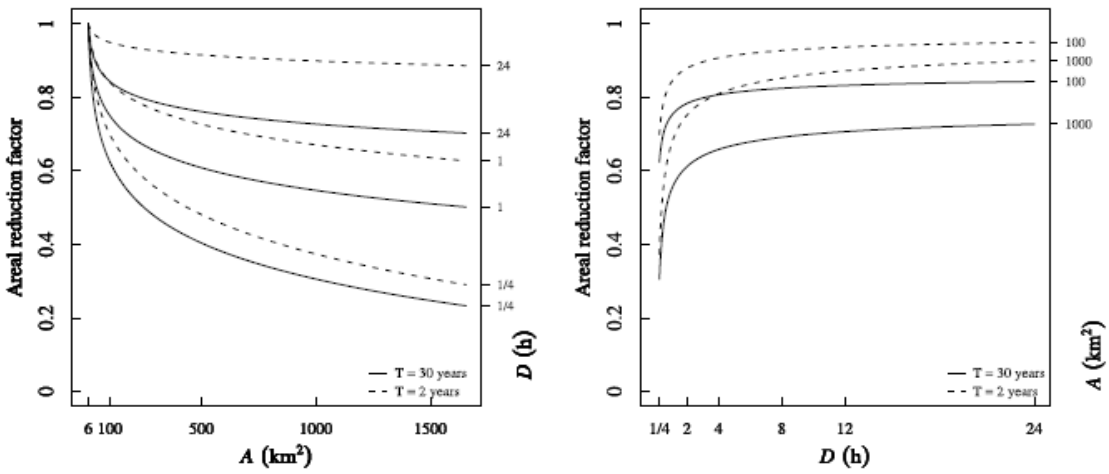

Figure 2.7: Radar-based ARFs plotted against area size (left) and duration (right) (Overeem et al. (2010))

Following Section 2.2.1.5, Kim *et al.* (2019) analysed the effect of numerous storm characteristics on ARFs. The characteristics considered were the mean, maximum, coefficient of variation and variance of the pixel radar rainfall estimates within a storm. It was found that an increase of the storm mean rainfall was associated with an increase in ARF estimate, for most areas and storm durations. This results from ARFs being a direct function of storm average areal rainfall. The increase of the maximum storm areal rainfall was associated with an increase in ARF estimates for shorter durations and larger areas, with an opposing trend for smaller areas and longer durations. An increase in rainfall variance generally lead to a decrease of ARF values due to the spatial variation of certain storms (like convective storms) having the tendency to produce smaller ARFs in comparison to storms that have little spatial variability (like frontal storms). The coefficient of variation was a means to test the pure effect of the spatial variability of rainfall, regardless of mean storm areal rainfall. It was found that the increase in the coefficient of variance strongly correlates with a decrease in ARF values. This signified the most consistent factor affecting the ARF amongst the other storm characteristics.

2.4 Summary

The ARF is an essential engineering parameter with an essential role for the design of hydraulic structures. This requires knowledge of the depth of rain that is likely to occur over a specific area for a certain time period. Point rainfalls are only symbolic for a limited area with larger storms having an areal average rainfall depth much smaller than the maximum point rainfall. The derivation and estimation of ARFs is directly concerned with the relationship between areal rainfalls and point rainfalls.

There are various factors that influence the derivation and estimation of ARFs. Climate, storm area and duration and rainfall intensity are considered the main variables that influences the derivation of ARFs, all with an interdependency on one another. With the various rainfall processes, convective and frontal rainfall regions are well suited for analysis and derivation of ARFs, on a global scale. In terms of return period, many studies show that there tends to be a general decrease in ARF with an increase in return period; essentially, research is showing that the effect of return period on ARFs, should not be neglected.

The two main methods, storm centred and geographically fixed method, of deriving ARFs are said to produce inconsistent results. For South Africa, the current ARFs being implemented were both derived using rainfall stations. The storms used in the analyses lack adequate spatial resolution, which could affect ARFs. The geographically fixed method only analyses parts of different storms, whereas the storm centred method analysis all types of storm, regardless of storm or catchment area. It was further mentioned that either method could validate the findings or derivation for the remaining method.

The use of radars within hydrology has become more popular recently. Radars provide the ability to reproduce storm events for further extensive analyses. These storm events are high in temporal and spatial resolution. However, reflectivity errors are considered to be a major setback when using radars and radar data. The reflectivity errors mainly affect the precipitation estimation. In terms of ARFs, radars have been used extensively on a global scale. Radars tend to produce the most reliable results when incorporating rain gauge data as a means of calibration. Comparatively, radars and radar data have not been incorporated into hydrology nationally, as it has been incorporated internationally. Thus, using radars and its data to derive and estimate ARFs for South Africa, is a means of combating this notion.

3 METHODOLOGY

3.1 Introduction

The methodology of arriving at ARFs using radar imagery is discussed in this section. An overview of the research plan is provided, which consists of explaining the methods of obtaining radar data. Thereafter, the execution of 'converting' radar imagery to ARFs is explained by utilising ArcGIS and Excel. This methodology is validated through obtaining ARFs using Precipitation Arrays.

3.2 Research Plan

Figure 3.1 displays the steps followed in this research. First, research was carried out, in order to observe the need and suitability for the research in the hydrological field on a global and national scale, which included conducting an extensive literature review (Chapter 2). Thereafter, organisations and companies that could produce radar data were approached. After the radar data was obtained, a conversion tool was applied in order to convert the data into a GIS compatible format. Thereafter, an extensive methodology was executed in ArcGIS to calculate ARFs.

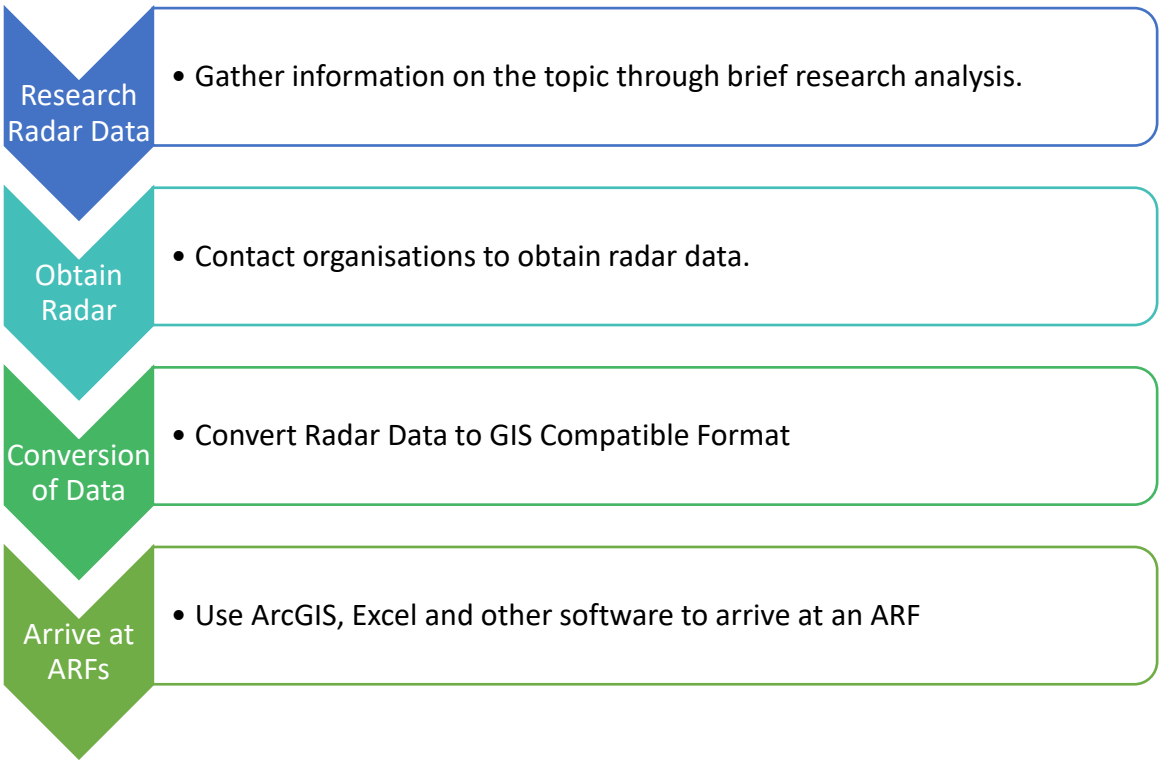

Figure 3.1: Broad Research Plan to Arrive at End Results

3.3 Obtaining Radar Data

Radar data was obtained from SAWS. The following procedure was carried out in order to obtain radar data:

1. Hourly rainfall data from automatic weather station (AWS) was requested, for a two-year period from 1 Jan 2016 at 00:00 to 31 December 2017 23:00. This was needed to identify major storm events to be investigated further.
2. The hourly data was used to gather 3- and 24-hourly rainfall accumulations from the automatic weather station. The top fifty storms were selected, in terms of rainfall accumulation, for each accumulation period. These storms were dated.
3. A request was sent to SAWS for radar images of the top 50 storms, referenced from the Irene AWS readings.
4. Storms were received and a methodology for analysis, was put in place. Each radar image contained a mosaic of all the rainfall occurring across South Africa for the specified date and time accumulation. This implies that storms across the entire country could be analysed from the mosaic, and not just for storm events occurring close to the Irene AWS.

3.4 Analysis of Radar Data to Arrive at an ARF

An extensive process was carried out to produce AFRs from the MDV file format. The chart in Figure 3.2 describes this process. The first step was to install TITAN, in order to visualize the obtained data. The conversion software would then be applied to make the radar file compatible in GIS. ArcGIS would then be used for any further analyses.

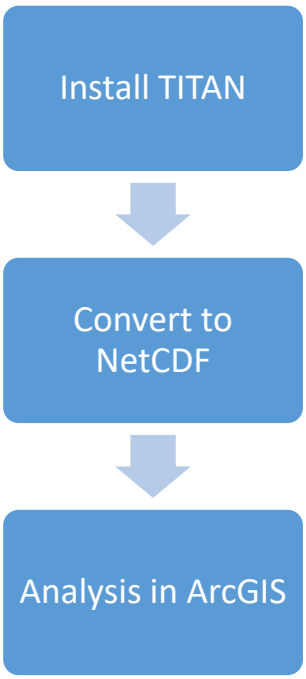

Figure 3.2: Broad Methodology to arrive at ARFs

Approximately 120 storm files in MDV format, were received from SAWS. Once converted to netcdf file type, it was found that 97 storms were suitable for analysis, as shown in Table 3.1. The suitability and selection of each storm for analysis was arbitrary but based on the following criteria, for each netcdf file:

- Minimal radar reflectivity issues visibly present in each file, as mentioned in Section 3.5.3
- Single cellular storm: the gridded pixel cells surrounding the maximum point rainfall cells were lower than the maximum point rainfall cell.
- No noticeable missing cells, or 'gaps' within a storm
- Storms closer to the Irene AWS were given preference in terms of selection. If a more suitable storm was found closer to the coast, it was selected for analysis

Due to the selection criteria, all storms were not analysed close to the Irene AWS. The Irene AWS was only used to reference storm events. Table 3.1 contains a summary of the number of storms used for analysis, for each storm duration.

Table 3.1: Summary of Storms Analysed

Storm Duration	Number of Storms used for Analysis	Number of Frontal Storms	Number of Convective Storms
1 Hour	32	12	20
3 Hour	33	4	29
24 Hour	32	13	19
Total	**97**	**29**	**68**

3.5 TITAN Software

The National Centre for Atmospheric Research (NCAR) created and developed TITAN software system in the USA by Dixon and Wiener (1993). TITAN was introduced in 1995 and was developed using previously implemented South African software. TITAN is a storm tracking system that operates in real-time and permits its users to analyse storm properties and its time evolution. Additionally, TITAN produces fields including Vertically Integrated Liquid, which is often used in accumulated rainfall estimates, projected storm size and movement changes and sever storm identification. The combination of TITAN and RDAS, in using the locally developed processing techniques, is successfully used in the analysis of data from radars around the world. TITAN makes use of a specific data format for all its generated and input products known as Meteorological Data Volume (MDV). MDV is specifically suited for gridded two- and three-dimensional meteorological data. From 2001, this data format has become the commonality between satellite, radar and other data and its derived products in South Africa.

3.5.1 Meteorological Data Volume

In 1990s, the Research Applications Laboratory (RAL) at NCAR developed the Meteorological Data Volume format for gridded data. RAL used several gridded data formats at the time. A single gridded data type for internal use was created for the simplification of these data systems. MDV has since advanced as a data format unique to NCAR and RAL. It is described as an efficient format for gridded data, with efficient internal compression capability and suffice meta-data support that allows for designated decompression of single planes from single data fields (Dixon, 2006).

Two and three dimensional gridded data are well suited to be stored by the MDV data file type. Each MDV data set contains data for a single time period. Retrieval and time searching are handled by a naming convention that is based on the times of storm events. Multiple data fields can be managed in a single file through the capabilities provided by the MDV file format. Furthermore, the MDV format is expandable in that it gives the MDV user access and space capabilities to define optional generic ‘chunk’ data. Additional data set information that is not appropriate for storage in the MDV data or header fields can be attached to the chunk data (Dixon, 2006).

Figure 3.3 displays the layout of the data set for the MDV format, with the header lengths given in bytes. All the MDV header information appears at the top of the file. Thereafter, chunk and field data appear. Offsets to the field header array, chunk header array and ‘Vlevel’ header array are all contained in the master header file. Third dimensional data (such as radar elevation angles and Cartesian plane heights) is stored in the Vlevel headers. The chunk headers contain file offsets to the chunk data.

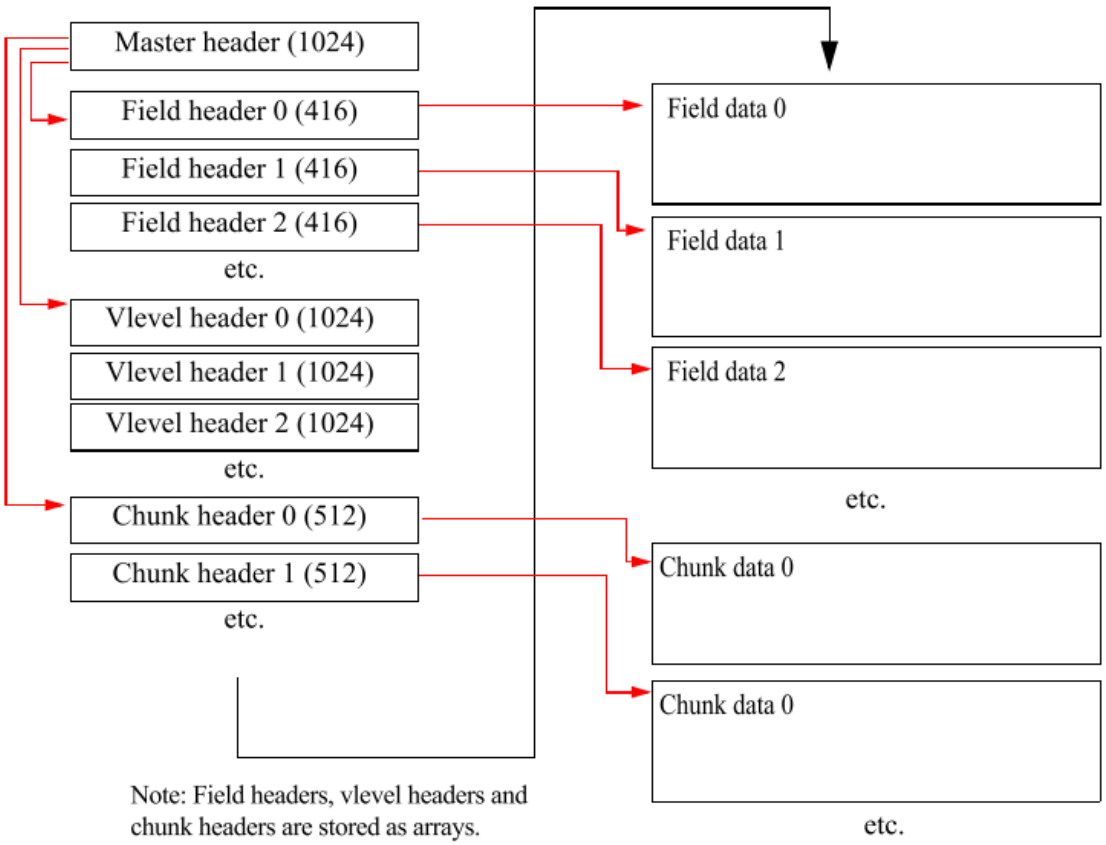

Figure 3.3: MDV Data Set Structure Organisation (Dixon, 2006).

The MDV file naming convention is essential for the retrieval of specific MDV files. Specifically, time is considered an important attribute for meteorological data. Thus, each MDV file contains data for a sing time period. MDV files are named according to the time of data stored within the file. Internationally, UTC times are used. However, since the use of TITAN is well integrated with the South Africa Weather Services (SAWS), GMT (+2) is used. Times applicable for the naming convention include:

- valid time – the time at which the radar observation occurred
- generate time – the time at which a model was executed, or a forecast generated
- forecast time – the time at which a forecast is considered valid
- lead time – time difference between forecast and generated time for a forecast time

For this research, MDV valid times were used, since storms that already occurred have been analysed. Thus, the file name is as follows:

“`data_dir/yyyymmdd/hhmmss.mdv`”

The "yyyymmdd" implies the folder in which the data is stored, with "data_dir" being the directory for the storage of all MDV files. The "yyyy", indicates the year, "mm", the month and "dd", the date. The actual file is stored as a timestamp "hhmmss.mdv", with "hh", indicating the hour of 24-hour digital time of the observation, "mm" the minutes and "ss", the seconds. As an example, a storm captured on the 25 November 1995 at 06:30 AM would be in the following location, with the following file name:

"data_dir/19951125/063000.mdv"

Considering that the files are merely accumulations for specific durations, the timestamp for each file name indicates the end time of accumulation. For example, a 3-hour storm with the file name "160000.mdv" would have the accumulated rainfall from 14:00:01 to 16:00:00.

More of the MDV Interface Control Document is available at https://www.eol.ucar.edu/system/files/MDV_format_ICD.pdf .

3.5.2 TITAN

The data provided from SAWS was in MDV format, which is extensively described in Section 3.5.1. TITAN was installed following the installation guide found on https://ral.ucar.edu/projects/titan/docs/ . TITAN is known for being a specialised software tool that is used by weather experts. This research aims to make radar data more usable for hydrologists in South Africa. A conversion tool developed by De Waal (2018) for TITAN creates a network common data form (netcdf) that is compatible in GIS systems. The software code is found in APPENDIX A. Figure 3.4 shows TITAN displaying a 1-hour storm event that occurred on 2018/04/11 at 16:00. This resulted from the execution of the "start_all" function. The legend (toward the right of Figure 3.4) illustrates intervals of precipitation.

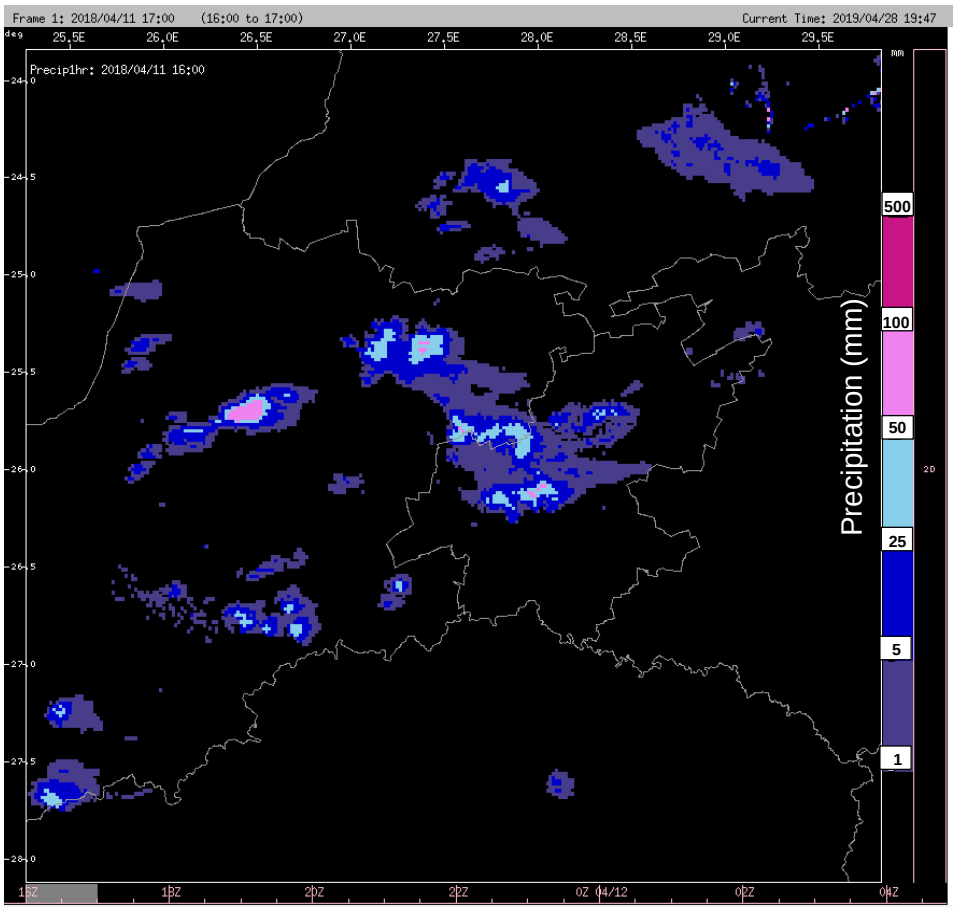

Figure 3.4: One-hour storm rainfall event in TITAN (MDV format).

3.5.3 Converting Radar Reflectivity to Rainfall

After corrections for reflectivity errors are applied, the conversion of the reflectivity to rainfall values can be done. The Marshall-Palmer relationship is one of the most commonly used relationships that is applicable to stratiform precipitation as well as radar derived precipitation. The relationship was derived by comparing Drop Size Distributions and radar reflectivity measurement from numerous precipitation events. The relationship is expressed in Equation 6:

$$Z = 200 \cdot R^{1.6} \quad \textbf{[5]}$$

Z is in mm^6mm^{-3} and R in mmh^{-1}. This research makes use of this relationship by default, as it is received from SAWS with the relationship already applied.

3.5.4 Summary of Radar Information for this Study

Individual radar images are merged into one field to produce a mosaic field for the whole of South Africa. This is done by means of TITAN composing scripts. The standard radar reflectivity measurements from the mosaic field and for each 6-minure radar scan is used in the standard Marshall-Palmer relationship, described in Section 3.5.3, to calculate the rainfall rate. Thereafter, TITAN scripts are used to accumulate the 6-minute rainfall rates, to produce an hourly rainfall. The same procedure is applied for the 3- and 24-hourly periods.

Minor ground clutter, attenuation and occultation corrections were carried out on the raw radar reflectivity data that was used to arrive at precipitation data. Many artefacts on the radar is said to be a challenge to remove. However, there are corrections for scenarios like this built into TITAN. Bright band and anomalous propagation corrections were needed to be calculated separately. However, most of SAWS radars are S-band, which implies little attenuation and RLAN interference.

With regards to precipitation estimates, no bias corrections were performed on the radar rainfall data. Since the data is estimates of rainfall based on radar reflectivity, it is possible to overestimate or underestimate rainfall values. However, the rainfall data received directly from SAWS is assumed to be reliable for this research as it makes use of the storm centred method of deriving ARFs. Thus, the only errors that may produce incorrect ARFs are errors that affect both the calculation of the areal rainfall and the maximum point precipitation. From a theoretical point of view, if the reflectivity is overestimated, the areal rainfall is consequently overestimated as well as the point of maximum rainfall. Once the areal rainfall is divided by the point rainfall, it 'cancels' out any errors that are brought upon by the reflectivity errors.

Becker and Pegram (2014) researched the accuracy of precipitation estimates, comparing TITAN precipitation estimates with rainfall station data. The analysis carried out by these researchers were more interactive and extensive with the Irene radar, producing a more scientifically sound and reliable conclusion: reliable accuracy of radar rainfall estimation. The results are presented in Table 3.2. It shows a slight tendency of overestimation of rainfall, due to the bias being greater than 1. Thus, the conclusion from the research carried out by Becker and Pegram (2014) was suitable enough for further analysis. Their research mentions the following:

"The S-band radar at Irene produces high quality reflectivity data that is free from RLAN interference and less effected by attenuation, particularly over short ranges from the radar. This is favourable for precipitation estimates. Ground clutter from the reflectivity data has been removed as well as possible by the Doppler filter." - (Becker and Pegram, 2014).

Table 3.2: Scores from Contingency Tables (Adapted from (Becker and Pegram, 2014))

	Scores (1 mm)	Scores (5 mm)	Scores (10 mm)
Accuracy	0.973	0.99	0.995
Bias	1.6	1.719	1.766

3.6 Converting to NETCDF

An MDV conversion function was formulated to convert the MDV files to netcdf files, which is compatible in most GIS systems. This was done as TITAN, the programme that hosts MDV files, is less suited for the research than typical GIS software (e.g. ArcMap, QGIS, etc.). By converting this to a netcdf file type, it becomes more accessible and convenient for data interpretation.

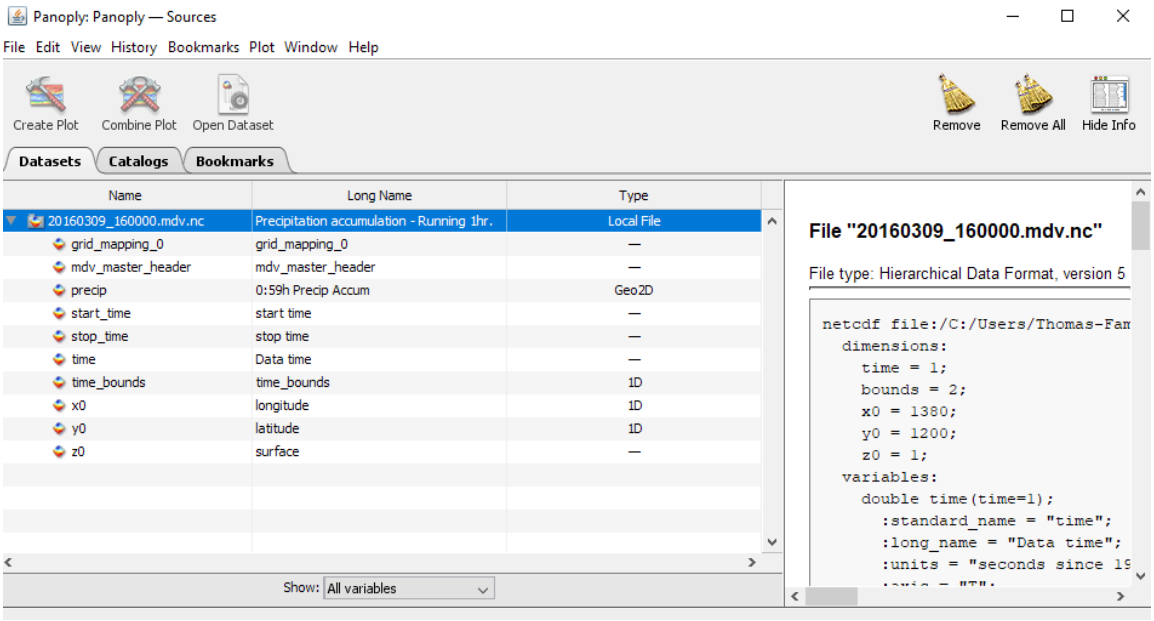

Figure 3.5: A netcdf File with 10 Arrays of Data

The netcdf file type is defined as a set of interfaces for array-oriented data access. The netcdf files for this study contain a total of 10 arrays. This is displayed in Figure 3.5, under the column “Name”. The description for each file is displayed under the “Long Name” column. The software used is called Panoply and is further discussed in Section 3.8. Note that the “precip” array, under the “Name” column, has a long name of “0:59 Precip Accum”. This is merely just the label. The “start_time” array contains the start time, which is at 15:00:01, and the “stop_time” contains the time at which the accumulation ends, which is at 16:00:00 (for the netcdf file used in Figure 3.5).

The MdvConvert function acts as a key component for the conversion from MDV to netcdf. Various parameters need to be kept the same when it comes to file conversion, such as georeferences, size and shape of the data. The gridded precipitation values within the MDV file are particularly important as they are the essential to the derivation of ARFs. The following is considered and integrated into the MdvConvert function as "`TRUE`", found in APPENDIX A:

- "`_latest_data_info_`" was written for the output files
- "`apply_threshold_to_field_values`" limits the values (in this case precipitation) in specified fields between the "`min_threshold`" and "`max_threshold`" values
- "`remap_pole_at_north`" is flag indicating stereographic occurs over the North Pole
- "`ncf_set_global_attributes`" an option to set specific global attributes to the output netcdf file. Mainly includes strings as attributes
- "`ncf_compress_data`" acts as an option to compress field data
- "`ncf_output_latlon_arrays`" the latitude and longitude arrays of grid are in the output file

The storm event displayed in Figure 3.4 is in MDV format. Thus, after applying the conversion tool, a netcdf file was readily available to be used in software called ArcGIS. The following code was executed in TITAN, to convert the files from MDV to netcdf, for the file displayed in Figure 3.4:

"`MdvConvert -params MdvConvert.1hr -f /home/titan5/projDir/data/mdv/precip/1hr/20180411/160000`"

3.7 Analysis in ArcGIS

After conversion of the MDV to netcdf, the file was imported into a GIS software system known as ArcGIS. The following example was used for this section: a 1hr storm occurring on 9/03/2016, starting at 15:00:01 and ending at 16:00:00. The methodology for this storm is thoroughly explained and is applied for every netcdf storm file. Thus, following procedure was put in place to arrive at Excel input values:

1. ArcGIS was set up to have a Projected Coordinate System, with the characteristics displayed in Figure 3.6.

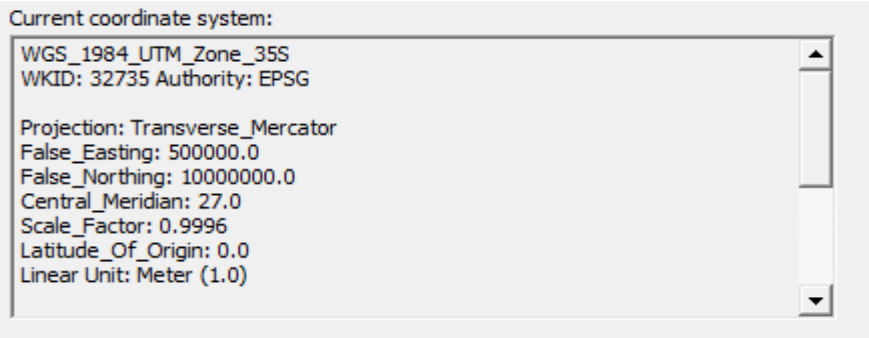

Figure 3.6: Projection Coordinate System in ArcGIS

2. The netcdf file was imported in ArcGIS as a raster layer with the settings displayed in Figure 3.7. The netcdf layer uses the same projected coordinate system as in 1.

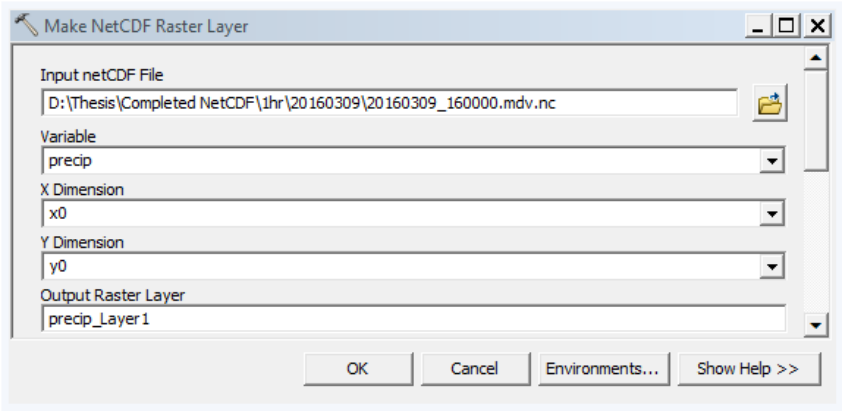

Figure 3.7: Importing netcdf File into ArcGIS

3. The netcdf file, now considered a raster, needed to be re-classed into isohyets. The 'Reclassify' function in ArcGIS is able to do this with the settings displayed in Figure 3.9. Isohyet intervals of 5 mm were chosen, for accuracy purposes. The 'Old values' in Figure 3.9 represent the boundaries of each isohyet rainfall interval. The 'New values' represent the label of each isohyet. For example, the new raster file would consist of all point precipitation values between 0 and 5 mm, as '1'; a point rainfall value of 2.5 and 7 mm would now be identified as '1' and '2' respectively, for the new reclassed layer.

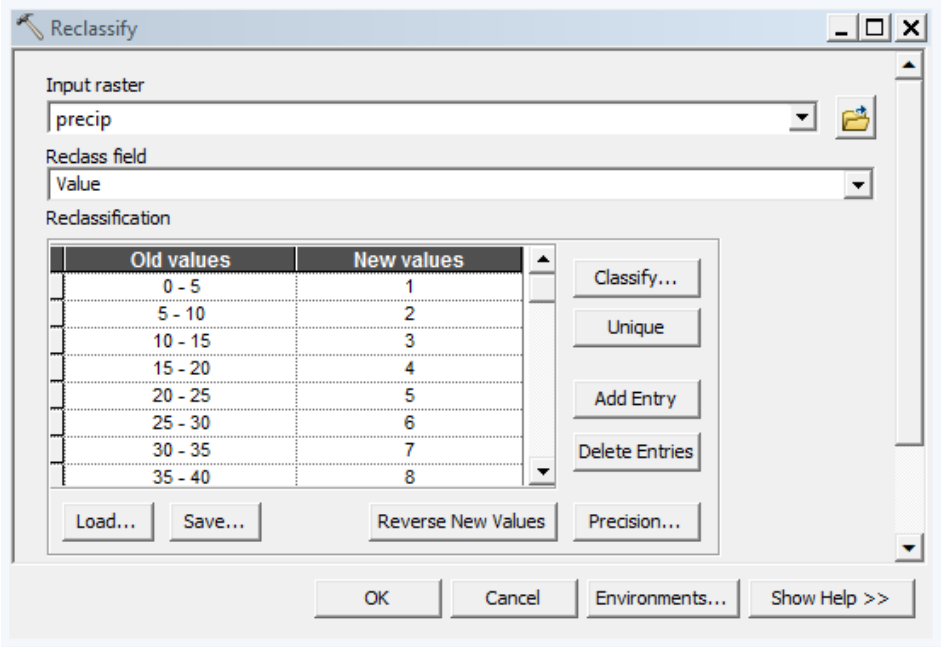

Figure 3.9: Reclassify Parameters used in ArcGIS

4. From the reclassified raster layer, a single cellular storm is selected. This is done by drawing a polygon around the storm. The single cellular storm is extracted using the raster processing function called 'Clip', which uses a polygon as the clipping extent. The single sell storm is displayed in Figure 3.8.

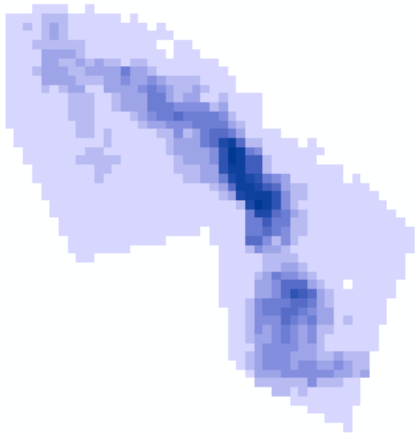

Figure 3.8: Single Cell Storm in ArcGIS

5. The ‘Zonal Statistics as Table’ function was used to gather information of the single cell storm in 4. Figure 3.10 illustrates the settings used to arrive at a table of information of the single cellular storm.

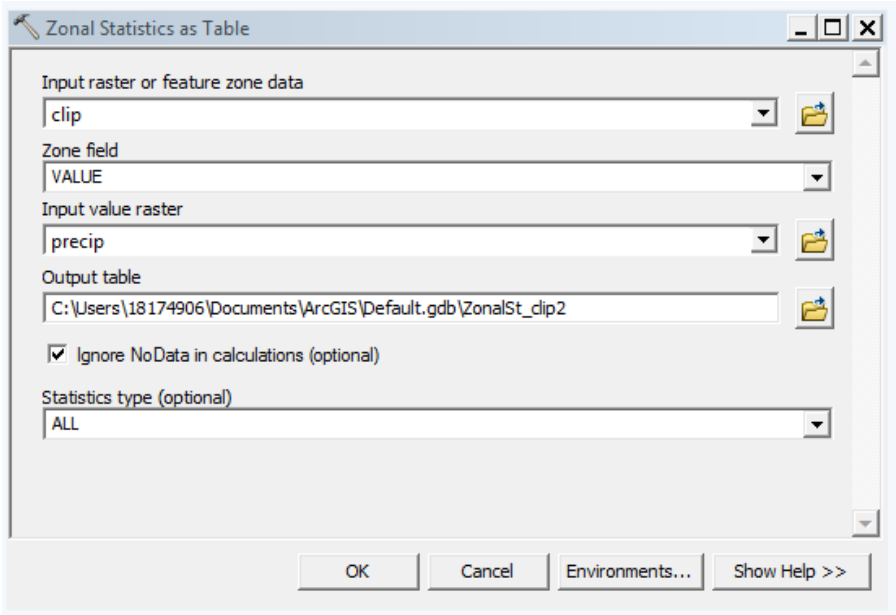

Figure 3.10: Zonal Statistics as Table Function Settings in ArcGIS

6. The Zonal Statistics Table output is shown in Figure 3.11. The heading ‘VALUE’ represents the re-classed interval, ‘COUNT’ represents the number of cells within the re-classed interval, ‘AREA’ represents the area of cells for each interval and the rest of the column headings are descriptive statistics for each interval. The maximum point precipitation is found by the highest value in the ‘MAX’ column.

Table

ztbl

Rowid	VALUE	COUNT	AREA	MIN	MAX	RANGE	MEAN	STD	SUM
1	1	676	2063440157.739167	0	5	5	1.671598	1.418702	1130
2	2	148	451759087.789048	5.5	10	4.5	7.496622	1.399199	1109.5
3	3	112	341871742.110631	10.5	15	4.5	12.522321	1.257812	1402.5
4	4	62	189250428.668385	13	20	7	17.282258	1.645181	1071.5
5	5	44	134306755.829177	20.5	25	4.5	22.522727	1.360792	991
6	6	21	64100951.645743	25.5	30	4.5	27.595238	1.240383	579.5
7	7	7	21366983.881914	30.5	35	4.5	33	1.732051	231
8	8	7	21366983.881914	35.5	39.5	4	37.285714	1.687287	261
9	9	8	24419410.150759	40.5	45	4.5	42.625	1.595893	341
10	10	12	36629115.226139	45.5	50	4.5	47.208333	1.435536	566.5
11	11	3	9157278.806535	52	53.5	1.5	53	0.707107	159

0 (0 out of 11 Selected)

ztbl

Figure 3.11: Zonal Statistics as Table Output

7. The values in Figure 3.11 are exported to Excel, where the data is extracted and the ARF calculated.

8. The maximum point intensity was calculated for each storm event. This was done by dividing the maximum point rainfall by the storm duration.
9. The final step was to calculate the ARF in Excel. The areal rainfall, in Table 3.3 was obtained following the isohyetal method, where the following is valid:

$$R_i = \frac{(I_{i-1}+I_i)}{2} \cdot \frac{A_i}{A_T} \quad \textbf{[6]}$$

Where R_i Rainfall for current interval

I_i Current rainfall interval boundary

I_{i-1} Previous rainfall interval boundary

A_i Current interval area

A_T Total area

Table 3.3: Calculation of ARF from Zonal Statistics

Interval (mm)		VALUE ID	COUNT	Area km²	Rainfall (mm)	ARF	Max Point Rainfall (mm)
20	25	5	44	134.31	9.71		
25	30	6	21	64.10	5.66		
30	35	7	7	21.37	2.23		
35	40	8	7	21.37	2.57	**57.27%**	**53.5**
40	45	9	8	24.42	3.33		
45	50	10	12	36.63	5.59		
50	55	11	3	9.16	1.54		
			Total	**311.35**	**30.64**		

A threshold of 20 mm for 1-hour, 25 mm for 3 -hour and 40 mm for 24-hour storm durations were suggested and implemented by Olivera *et al.* (2006), in Section 2.3.5.3. Thus, 'VALUE' ID 1 – 4 (0 – 20 mm) is ignored, as this is a 1hr storm. This is also convenient as it assists in classing single cellular storms. Figure 3.14 displays the threshold value of the precipitation array of rainfall, in Excel. Thus, the ARF is calculated using Equation 1, with the areal rainfall as 30.64 mm and a maximum point precipitation of 53.5 mm. The ARF is calculated to be 57.27%, as displayed in Table 3.3.

3.8 Validation of ArcGIS Outputs

The netcdf files were also used to abstract precipitation arrays. Panoply (available from https://www.giss.nasa.gov/tools/panoply/download/) is a software application that plots geo-referenced arrays from netcdf files. Panoply was extensively used to abstract the precipitation arrays from the netcdf files for analysis in Excel. Using the same case study storm in Section 3.7 (1hr storm on 9/3/2016 from 15:00:01 to 16:00:00), the following methodology was carried out to arrive at the storm area, areal rainfall and ARF in order to validate the storm outputs, and consequently, the functionality, of ArcGIS:

1. The netcdf file was imported into the Panoply application. This is shown in Figure 3.5.
2. The storm event was plotted using the “Combine Plot” functionality in Panoply. The settings for the execution of the function is displayed in Figure 3.12.

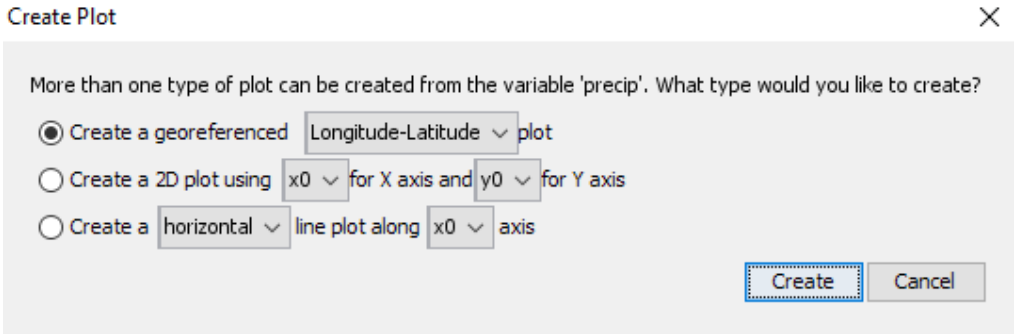

Figure 3.12: Settings for the "Combine Plot" Function in Panoply

3. The storm within the netcdf file was plotted in panoply. This plot was compared to the storm plotted in ArcGIS, to check whether the storms matched in terms of coordinates and location. The plot is displayed in Figure 3.13.

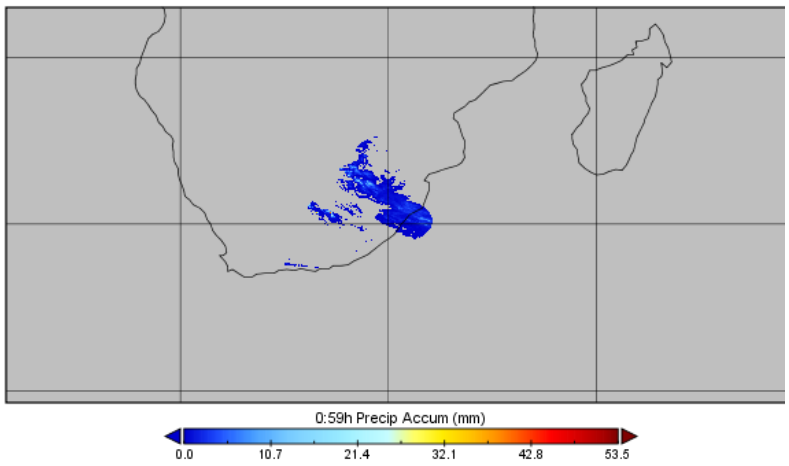

Figure 3.13: Storm Event Displayed in Panoply

4. The precipitation array for this storm event, labelled “precip” in Figure 3.5, was exported as a “.csv” file, for analysis in Excel. The data within the “.csv” file was organized using the “Text to Columns” function in Excel.
5. The precipitation array was assigned a colour scale using the “Conditional Formatting” function in Excel. This assisted in delineating the same storm event as in ArcGIS. The same threshold values, as mentioned in Section 2.3.5.3 and Section 3.7, were applied to the precipitation array. Figure 3.14 displays the gridded precipitation accumulations for the storm event.

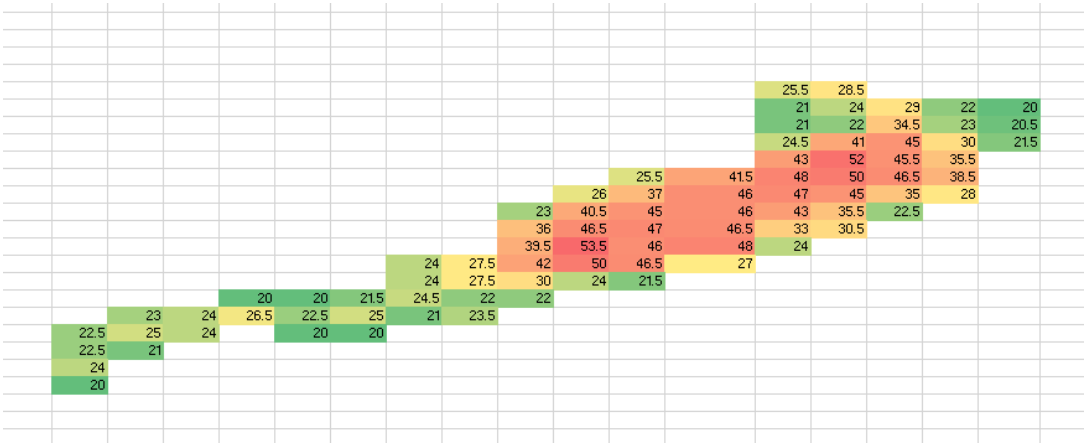

Figure 3.14: Precipitation Array in Excel

6. The precipitation values were classed into isohyetal intervals of 5 mm, for the calculation of storm area and isohyetal rainfall, similar to Step 3 in Section 3.7. This is displayed in Table 3.4.
7. The area for each storm was obtained by calculating the area of one cell (or pixel). The resolution for each cell is 1 minute, which is equivalent to 0.0167 degrees (1/60). The length of a degree was found using an online degree to length converter at http://www.csgnetwork.com/degreelenllavcalc.html. It was found that 0.0167 degrees latitude, at -25.91 degrees (latitude of Irene AWS), was equivalent to 1.847 km in length, and 0.0167 degrees longitude, at 28.21 degrees (longitude of Irene AWS), 1.599 km in length. The cell area (CA_1) was thus equivalent to the product of these lengths, resulting in an area of 2.95 km^2 (1.847 x 1.599). The area for each interval was calculated by multiplying the Cell Count in each interval with CA_1, for example: interval 1 has 36 cells that lie between 20 and 25 mm. The area would be calculated by multiplying 36 with CA_1, resulting in an interval area of 106.36 km^2 (36 x 2.95). Finally, the total storm area was calculated by summing the area of each interval (see Table 3.4).

Table 3.4: ARF Calculation for Precipitation Array in Excel

Interval Label	Cell Count in Interval	Interval (mm)		Max Point Rainfall (mm)	Area (km^2)	Isohyetal Rainfall (mm)	Areal Average Rainfall (mm)	ARF Isohyetal Method
1	36	20	25		106.36	9.53		
2	12	25	30		35.45	3.88		
3	5	30	35		14.77	1.91		
4	7	35	40	**53.5**	20.68	3.09	**31.62**	**60.31%**
5	6	40	45		17.73	3.00		
6	15	45	50		44.32	8.38		
7	4	50	55		11.82	2.47		
Total	**85**	-	-	-	**251.131**	**32.26**		

8. The areal rainfall was calculated using two methods: isohyetal method and the average method. The isohyetal rainfall was calculated the same as Step 9 in Section 3.7. The average areal rainfall was obtained by using Equation 8. Equation 8 consisted of summing the point rainfalls represented by each cell for the entire storm area. A total cellular rainfall of 2 687.70 mm was obtained. The summation of all point rainfalls was then divided by the total number of point rainfalls for the storm, which was 85 cells. This resulted in an average areal rainfall of 31.62 mm (2 687.70 / 85).

$$Average\ Areal\ Rainfall = \frac{\sum Point\ Rainfall\ in\ each\ Cell}{Number\ of\ Cells} \quad [8]$$

9. Finally, the ARFs was calculated using Equation 1. This was achieved by using the isohyetal areal rainfall estimation as the areal precipitation, which was 32.26 mm from Table 3.4, with the maximum point precipitation, which was 53.5 mm, resulting in an ARF of 60.31% (32.26 / 53.5).

3.9 Analysis of Results

The analysis of the radar derived variables and other rainfall values were carried out by multiple regression analyses. Figure 3.15 describes the process as to how the analysis of the results were carried out.

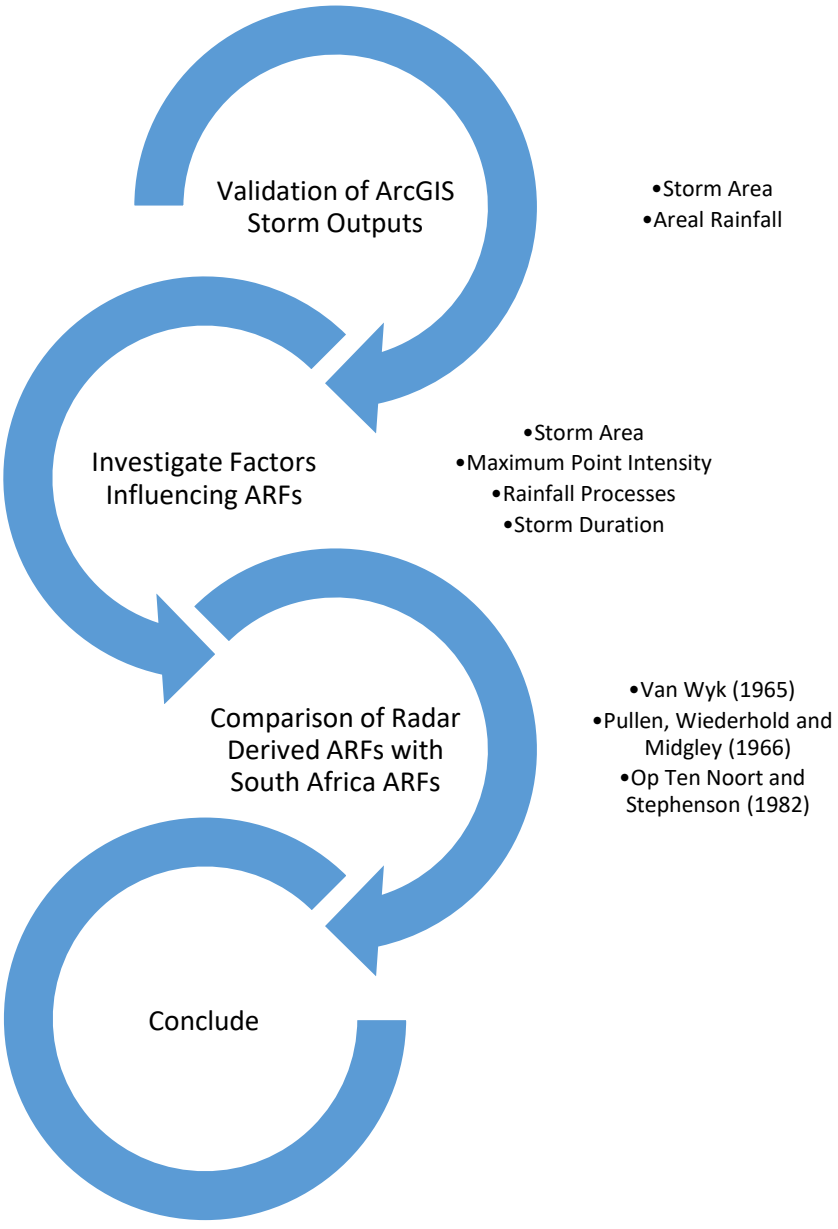

Figure 3.15: Process of Analysis

To evaluate and illustrate the results between the approaches used within this research, the difference between two specific variables were calculated for each individual storm. An average difference was also calculated. These calculations are displayed in Table 3.5. The “Difference Equation” in Table 3.5 was carried out on each individual storm, whereas the average difference and cumulative difference considers all storm events.

Table 3.5: Difference Equations

Variable 1 (V1)	Variable 2 (V2)	Difference Equation	Average Difference Equation	Cumulative Difference
ArcGIS Storm Area	Precipitation Array Storm Area	V1 – V2	$\frac{\sum(V1 - V2)}{Number\ of\ Storms}$	$\sum(V1 - V2)$
ArcGIS Isohyetal Areal Rainfall	Precipitation Array Isohyetal Areal Rainfall			
Precipitation Array Isohyetal Rainfall	Precipitation Array Average Areal Rainfall			
ArcGIS ARF	Precipitation Array ARF			
Radar Derived ARF	Van Wyk (1965) ARF			
Radar Derived ARF	Op Ten Noort and Stephenson (1966) ARF Equation 2			
Radar Derived ARF	Pullen, Wiederhold and Midgley (1966) ARF			
Radar Derived ARF	Op Ten Noort and Stephenson (1966) ARF Equation 3			

3.10 Summary

The research plan, as presented in Section 3.2, encapsulates the core processes that were executed in order to arrive at the results. The radar data was requested and referenced using the hourly rainfall from Irene AWS, which is the closest weather station to the Irene radar. The data was then obtained from the service provider, SAWS, and a methodology put in place.

The main methodology includes using ArcGIS to arrive at ARFs. First, the MDV files were converted to GIS compatible netcdf files, using conversion software. The radar files in ArcGIS were reclassed and clipped to produce a table of statistics of each storm where the storm area, maximum precipitation and other statistical information was obtained. Using this information, the areal rainfall for each storm was calculated using the isohyetal method. The isohyetal areal rainfall was divided by the maximum point precipitation in order to arrive at ARFs using ArcGIS.

Precipitation Arrays were used to arrive at ARFs, in order to validate the functionality and methodology of obtaining ARFs using ArcGIS. The Precipitation Array within each netcdf file was abstracted. The area of one cell was calculated in order to calculate the total storm areas (by counting the number of cells for each storm), as well as the isohyetal areal rainfall. The average areal rainfall was also calculated in order to validate the isohyetal rainfall. The ARFs for the Precipitation Arrays were calculated in the same way the ArcGIS ARFs were obtained: by diving the isohyetal areal rainfall by the maximum point rainfall.

A methodology for the analyses of the results was set out. This included using regression analyses and Difference Equations for the comparison of ARFs.

4 RESULTS AND ANALYSIS

4.1 Introduction

This section contains the results obtained from carrying out the methodology in Chapter 3. First, the validation of ArcGIS derived ARFs through Precipitation Arrays, was carried out. Thereafter, the influence of storm area, maximum point rainfall intensity, rainfall process and storm duration with the ARFs obtained from ArcGIS, was analysed. Finally, the ArcGIS derived ARFs were compared with the current ARFs implemented in South Africa. All results and data used in this section is found in Appendix B.

4.2 Validation of ArcGIS Derived ARFs

ArcGIS was used to calculate the storm area, areal rainfall using isohyetal method and the maximum point rainfall. The validation of the functionality and efficiency within ArcGIS was carried out by analysing the Precipitation Arrays from the same respective storm that was analysed in ArcGIS. The validation procedure was carried out on all 97 storms analysed in ArcGIS. Storm outputs obtained from using Precipitation Arrays are considered 'reliable', as an extensively controlled methodology that includes manual calculations of all the storm outputs, is followed.

Using ArcGIS to derive ARFs is considered efficient as it exclusively makes use of calculating outputs using various functions within ArcGIS itself, as mentioned in Section 3.7. Producing the same ArcGIS outputs (storm area, areal rainfall using isohyetal method and the maximum point rainfall) as when using Precipitation Arrays was necessary, as it would be indicative of the accuracy, efficiency and reliability of using ArcGIS to calculate ARFs. The comparison between the outputs obtained from ArcGIS and Precipitation Arrays were not categorised based on any criteria. In other words, the storm area derived from ArcGIS was merely compared to the storm area calculated from the Precipitation Arrays; the comparison of the storm areas was not carried out for each storm duration or any other criteria. Also, the maximum point precipitation value and rainfall region are the same in ArcGIS and the Precipitation Arrays.

4.2.1 Storm Area

The calculation of the storm area was carried out in ArcGIS by obtaining a Zonal Statistics Table, as described in Section 3.7. The ArcGIS storm area validation was done through the calculation of storm area using the precipitation array data, as described in Section 3.8. This data is found in Table B.1 (columns 6 and 7).

Figure 4.1 illustrates the relationship between the storm area calculated using ArcGIS and the storm area calculated using the Precipitation Array data. The coefficient of determination, or R^2 value, measures the variance of the dependent variable for the regression model. A higher R^2 value indicates that the model traces close to the actual values. On the other hand, the correlation coefficient, or r-value, measures how strongly two variables are related. An r-value closer to 1 indicates linear proportionality and conversely, an r-value closer to -1, indicates inverse proportionality. The p-value indicates the significance of the results obtained from the comparison. Thus, after carrying out a regression analysis, an R^2 value of 0.9861 for the storm areas is indicative of reliable areas calculated in ArcGIS when compared to the Precipitation Array data. Furthermore, a p-value of approximately 0 was obtained, indicating significant results.

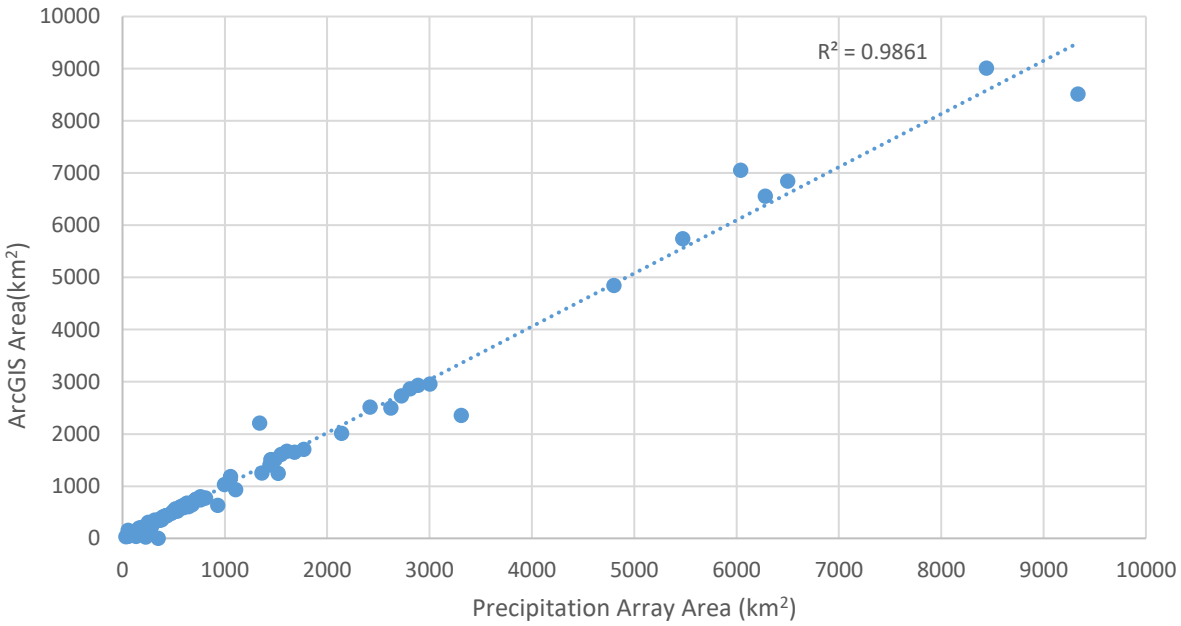

Figure 4.1: Storm Area Comparison

For the difference calculations, the Precipitation Array storm area was always subtracted from the ArcGIS storm area, as shown in Table 4.1. Thus, a positive difference indicates that using a Precipitation Array yielded a larger storm area than ArcGIS, and vice versa. The largest storm area calculated from ArcGIS and Precipitation Arrays was 9013.18 km^2 and 9 333.21 km^2, respectively. Interestingly, these storm areas were not from the same storm. The maximum storm area difference was 1 018.25 km^2, obtained from a 1-hour storm. On the other hand, the smallest storm area difference was -949.49 km^2, obtained from a 24-hour storm duration. A cumulative difference of 754.34 km^2 was calculated from all the storm areas, and an average difference of 7.78 km^2 was found. Table 4.1 also shows the maximum increase and decrease in storm area from the Precipitation Array to ArcGIS storm areas. A maximum increase in storm area of 192.73% and maximum decrease 99.12% was calculated. On average, ArcGIS overestimated storm areas by 0.23%.

Table 4.1: Difference Summary of Storm Outputs: Storm Area

Storm Output	Output Calculation	Minimum Difference	Maximum Difference	Cumulative Difference	Average Difference
Storm Area	$(ArcGIS\ Output - Precip.Array)$	-949.49 km^2	1018.25 km^2	754.34 km^2	7.78 km^2
Change in Storm Area (Increase/ Decrease)	$\frac{(ArcGIS\ Output - Precip.Array)}{Precip.Array}$	Decrease of 99.12%	Increase of 192.73%	Cumulative increase of 22%	Average increase of 0.23%

Table 4.2 displays the distribution of the overestimation and underestimation of storm areas calculated using ArcGIS. A total of 56 storms had storm areas that were overestimated, and 41 storms were underestimated, with reference to storm areas obtained from Precipitation Arrays. Storm areas obtained by using ArcGIS were mainly overestimated for the 1 and 3 hour storms, and mainly underestimated for the 24 hour storm durations. Considering that a positive average difference, increase, and more overestimation of storm area was achieved, ArcGIS has a tendency of slightly overestimating the storm area. However, this can be considered negligible as the average difference is close to 0 km^2 and increase, 0%.

Table 4.2: Estimation Distribution of Storm Areas for ArcGIS

Storm Duration (hours)	Number of Storms Overestimated in Storm Area	Number of Storms Underestimated in Storm Area
1	18	14
3	25	8
24	13	19
Total	**56**	**41**

From Figure 4.1, for smaller storm areas, Precipitation Arrays and ArcGIS produce nearly identical storm areas. For larger storm areas, ArcGIS tends to slightly overestimate the area. Considering a high R^2 and r-value with a negligible average storm area difference, and increase/decrease, using the storm area obtained from ArcGIS is considered suitable for further use in analyses.

4.2.2 Areal Rainfall

The Precipitation Arrays were used to calculate the areal rainfall using the isohyetal and average method, found in Table B.1 (columns 3 and 4). The average areal rainfall estimation method was considered in order to validate isohyetal rainfall method solely for the Precipitation Array output. Thus, the average method was not carried out in ArcGIS. The difference in value between the isohyetal and average method was always calculated by subtracting the average areal rainfall from the isohyetal areal rainfall, as shown in Table 4.3. A minimum difference of -2.50 mm and a maximum difference of 0.11 mm was found. An average difference of -0.35 mm was obtained. A maximum increase in areal rainfall, from isohyetal to average areal rainfall, was calculated to be 0.38%, with an average decrease of 0.88%. These results indicate that, on average, isohyetal areal rainfall method yielded slightly larger areal rainfall than the average areal rainfall method.

Table 4.3: Difference Summary of Storm Outputs: Areal Rainfall Methods

Storm Output	Output Calculation	Minimum Difference	Maximum Difference	Cumulative Difference	Average Difference
Precipitation Array Areal Rainfall	$(Isohyetal - Average\ Areal)$	-2.50 mm	0.11 mm	-33.80 mm	-0.35 mm
Change in Areal Rainfall (Increase/ Decrease)	$\frac{(Isohyetal - Average\ Areal)}{Isohyetal}$	Decrease of -4.57%	Increase of 0.38%	Cumulative decrease of 84.94%	Average Decrease of 0.88%

Figure 4.2 shows that the average areal rainfall and the isohyetal rainfall approximately produces the same areal rainfalls, as the R^2 value is 0.9995 with a strong linear correlation. The p-value was calculated to be approximately 0, indicating a high significance. With highly favourable statistical outputs and correlation, it was found that isohyetal rainfall was suitable for the use of deriving ARFs. Furthermore, the isohyetal method of estimating areal was chosen over the average method as the isohyetal method was used by Van Wyk (1965) to arrive at ARFs for South Africa. This becomes favourable when comparing the radar derived ARFs with Van Wyk's (1965) ARFs for South Africa. Adding to this, the isohyetal method also produces slightly higher areal rainfalls than the average method, which could be considered more conservative within engineering practice.

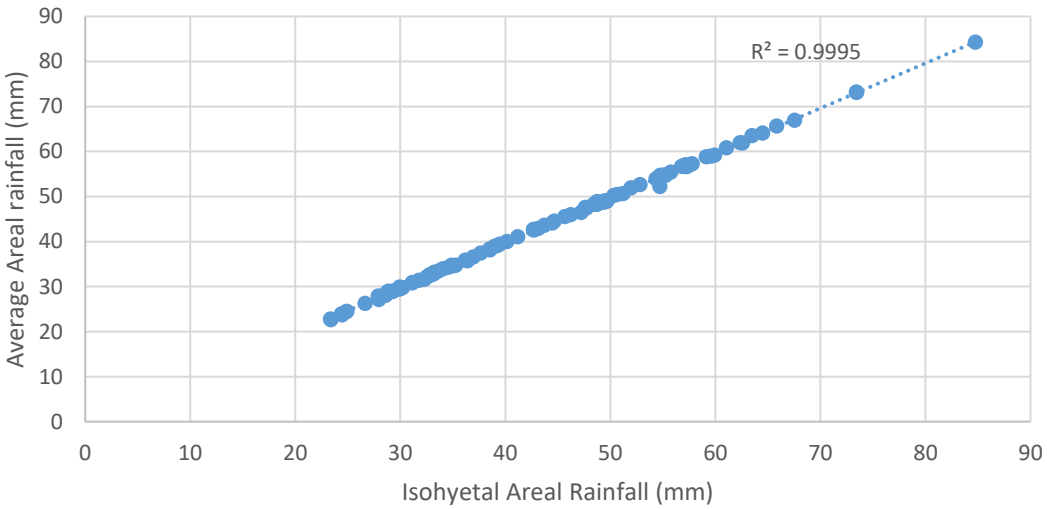

Figure 4.2: Average Areal Rainfall vs Isohyetal Rainfall

Next, the areal rainfall was calculated using the isohyetal method for the Precipitation Arrays and within ArcGIS, for comparison. This method is highly dependent on the isohyetal interval size and pixel count for each interval. Figure 4.3 displays the relationship between the isohyetal areal rainfall calculated from ArcGIS, found in Table B.1 (column 5) and the Precipitation Arrays. Figure 4.3 illustrates that the isohyetal rainfall calculated from the ArcGIS is nearly identical to the isohyetal rainfall obtained from Precipitation Arrays, across all storms analysed.

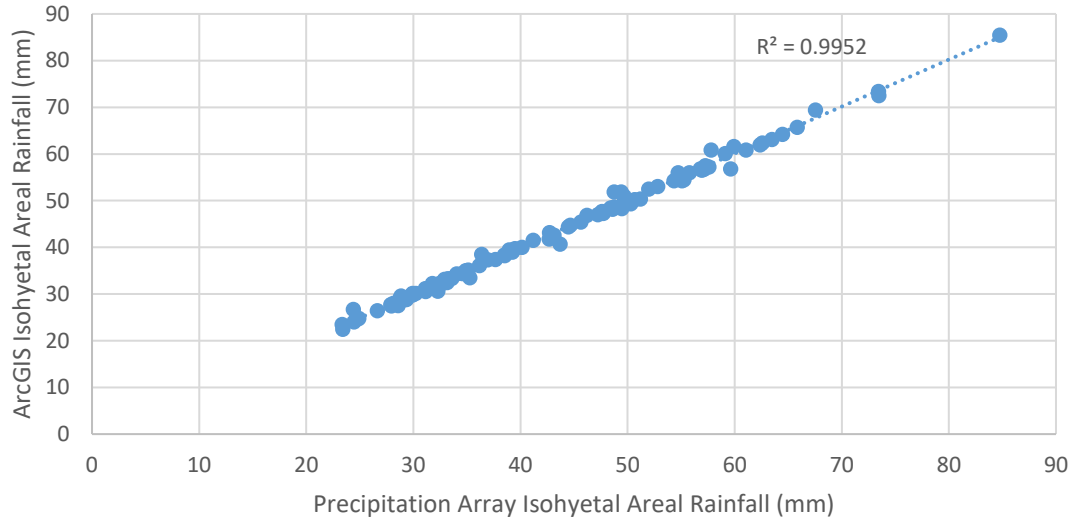

Figure 4.3: Areal Rainfall Comparison for Precipitation Arrays and ArcGIS

Table 4.4 shows the difference in value between isohyetal rainfall calculated using Precipitation Array data, and ArcGIS. It was found that the maximum difference between the isohyetal areal rainfall calculated from the Precipitation Arrays and in ArcGIS was 3.18 mm and the minimum difference was -2.99 mm. An average difference of 0 mm, across all storms, was obtained indicating that ArcGIS produces an isohyetal rainfall similar to what an isohyetal areal rainfall obtained from using Precipitation Arrays. The greatest decrease from the isohyetal areal rainfall using Precipitation Arrays to ArcGIS, was 6.85%, with the greatest increase of 9.60%. An average decrease in isohyetal areal rainfall of 0.05% was obtained.

Table 4.4: Difference Summary of Storm Outputs: Areal Rainfall

Storm Output	Output Calculation	Minimum Difference	Maximum Difference	Cumulative Difference	Average Difference
Isohyetal Areal Rainfall	$(ArcGIS - Precip.Array)$	-2.99 mm	3.18 mm	0.13 mm	0.00 mm
Change in Isohyetal Rainfall (Increase/ Decrease)	$\frac{(ArcGIS - Precip.Array)}{Precip.Array}$	Decrease of 6.85%	Increase of 9.60%	Cumulative Decrease of 4.40%	Average Decrease of 0.05%

After carrying out a regression analysis, an R^2 value of 0.9952 and an r-value of 0.9731 was obtained. A p-value of approximately 0 was obtained, indicating significant results. With this knowledge, and the low average decrease of 0.05%, the isohyetal areal rainfall calculated in ArcGIS was considered suitable for further analysis based on the highly favourable statistical correlation outputs.

4.2.3 ARFs Derived from Precipitation Arrays and ArcGIS

A comparison of the ARFs produced from the storm outputs obtained from Precipitation Arrays and ArcGIS, found in Table B.1 (columns 11 and 12), was carried out. The calculation of the ARF includes dividing the isohyetal areal rainfall by the maximum point rainfall for each storm. Thus, the Precipitation Array and ArcGIS uses the same maximum point rainfall for the calculation of ARFs, but different isohyetal areal rainfalls.Table 4.5 Table 4.5 displays the difference calculations that were carried out for ARFs obtained using Precipitation Arrays and ArcGIS. A maximum difference of 3.83%, and a minimum difference of -6.72% was calculated. An average difference of -0.12% was calculated. The positive difference suggests that, on average, Precipitation Array yielded slightly larger ARFs. This was expected as a greater areal rainfalls produces greater ARFs. When comparing this to isohyetal areal rainfall in Section 4.2.2, an average difference of 0 was calculated. The R^2 value of 0.9896 and r-value of 0.9948 makes it evident that there exists strong correlation between these two variables. Furthermore, a p-value of approximately 0, is indicative of high significance.

Table 4.5: Difference Summary of Storm Outputs: ARF

Storm Output	Difference Equation	Minimum Difference	Maximum Difference	Cumulative Difference	Average Difference
ARF	(ArcGIS ARF) – (Precipitation Array ARF)	-6.72%	3.83%	-11.75%	-0.12%

Figure 4.4 illustrates the relationships between the Precipitation Array derived ARFs and the ArcGIS derived ARFs. The graph shows that there is strong linear correlation between the ARFs. The R^2 value and r-value for the storm area, isohyetal areal rainfall and ARFs estimation between the Precipitation Array and ArcGIS are all greater than 0.9, along with p-values less than 0.05. This shows that there is high correlation between estimating ARFs using Precipitation Arrays and ArcGIS. Thus, with these statistical parameters, it was found that the ArcGIS methodology to arrive at ARFs is reliable and efficient through the validation of deriving ARFs using Precipitation Arrays.

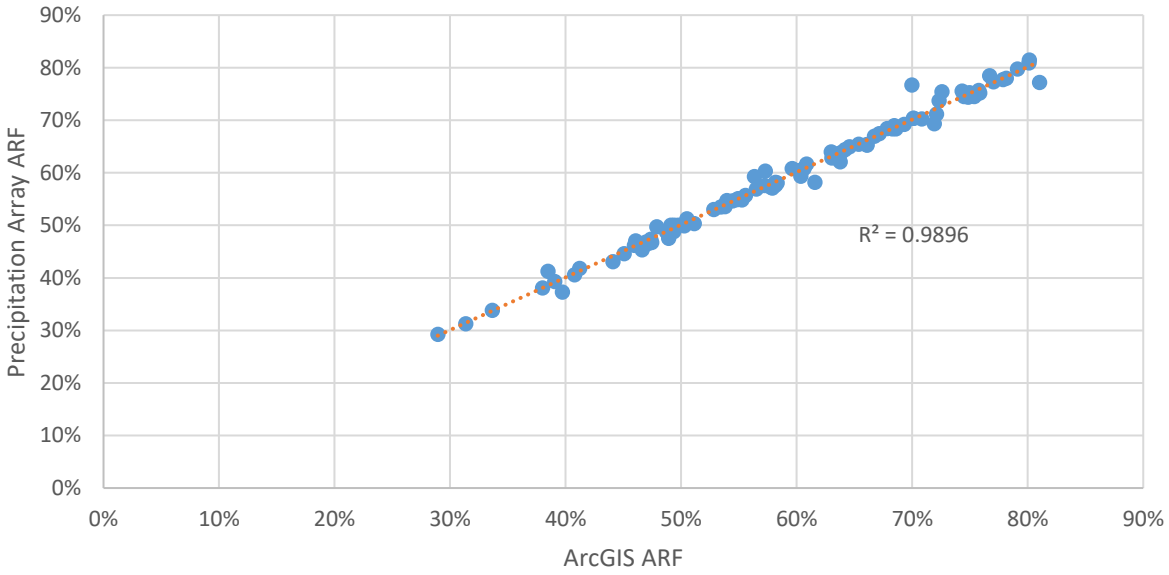

Figure 4.4: ARFs obtained using Precipitation Arrays and ArcGIS

4.3. Factors Influencing ARFs

This section contains the analysis of the statistical correlation between various factors that could affect the radar derived ARFs. In Section 4.2, it was found that using ArcGIS to arrive at ARFs is considered reliable and efficient. Therefore, in this section, the radar derived ARFs are based on the ARFs obtained using ArcGIS, as presented in Table B.1 (column 12), Appendix B, using the ArcGIS isohyetal areal rainfall.

ARFs produced in South Africa by Van Wyk (1965) and Pullen, Wiederhold and Midgley (1966) considers ARFs to be estimated based on point precipitation, storm area and duration. In Section 2.2.1, the influences affecting ARFs are discussed. Similarly, this section consists of detail on the influence of the radar derived ARFs with storm area, areal rainfall, rainfall processes, maximum point rainfall and storm duration. Storm duration was used as a means of categorising the ARFs for each statistical analysis.

4.2.4 ARFs with Storm Area

On a global scale, the storm area is rarely used as the only variable to determine an ARF. The literature from Chapter 2, specifically with regards to the AFRs derived in South Africa by Van Wyk (1965) and Pullen, Wiederhold and Midgley (1966), shows that the storm area is a significant variable to consider when deriving ARFs. The data used in this section is presented in Table B.1 (columns 7 and 12).

Figure 4.5 illustrates the relationship between the storm area and radar derived ARFs for 1-hour storm duration. The regression analysis showed a logarithmic trend best fits the data. Figure 4.5 shows that storm areas that are less than 1 000 km^2 produce ARFs that are more scattered, in terms of correlation. This could result from the variability of smaller storms being mainly a function of storm area and point rainfall intensity (Alexander, 2001). For storm areas greater than 1 000 km^2 the ARFs resulting from larger storm areas tend to follow trend line as. This could possibly result from larger storms being functions of storm area and duration (Alexander, 2001). An R^2 and r-value of 0.3792 and -0.6158 was obtained, respectively. A p-value of approximately 0 was found. The R^2 value indicates weak fit of the data, due to the scatter of storm areas less than 1 000 km^2. The r-value and p-value indicate satisfactory inverse correlation and high significance. A regression analysis was also carried out by separating the data for into storm areas less than 1 000 km^2 and greater than 1 000 km^2.

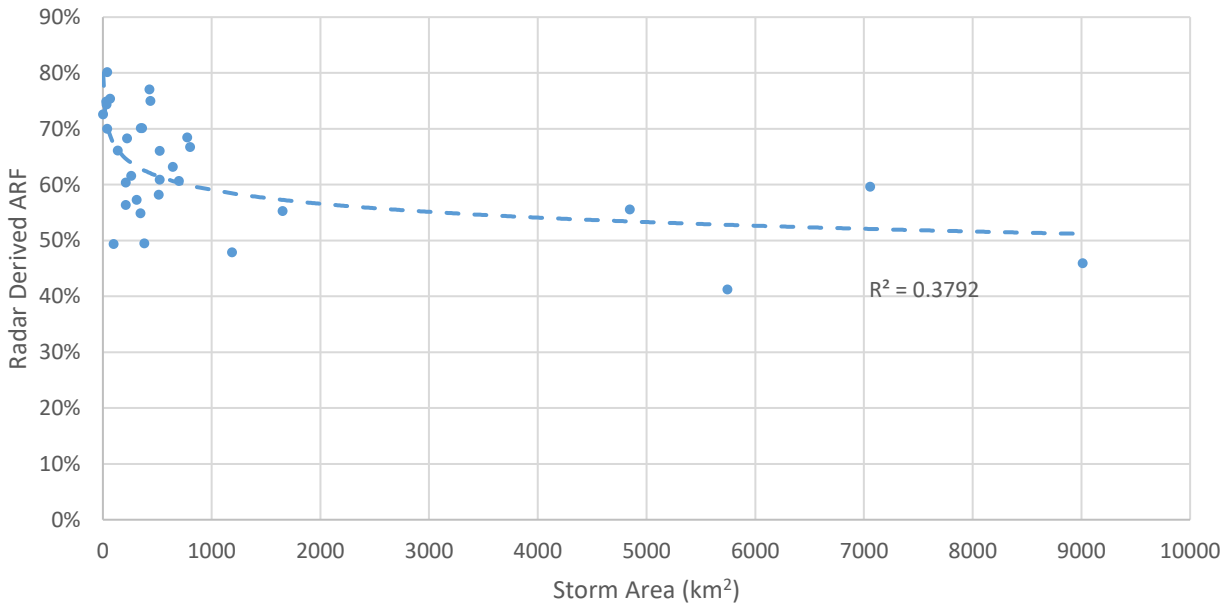

Figure 4.5: ARF with Storm Area for 1 Hour Storm Duration

Figure 4.6 displays the relationship between the storm area and the 3-hour storm duration radar derived ARFs. The regression analysis showed that a logarithmic trend best fits the data. The R^2 value of 0.4733 indicates that for all the 3-hour storms, the fit it is more appropriate than for the 1-hour storm duration ARFs in Figure 4.5. This could result from the difference in storm durations. It is evident that the storms with a storm area of less than 1 000 km^2 produce ARFs that are more scattered, which is in line with the 1-hour storm duration ARFs (Alexander, 2001). From Figure 4.6, there is a tendency for the ARFs to fit the regression line as the storm area increases. Thus, also attaining to the notion that ARFs for storm areas greater than 1 000 km^2, are mainly functions of storm area and storm duration (Alexander, 2001). An r-value of -0.6880 was obtained. A p-value of approximately 0 was found. The R^2 value indicates slightly weak fit of the data that is due to the scatter of the ARFs for smaller storm areas. The r-value and p-value indicate good inverse correlation and high significance.

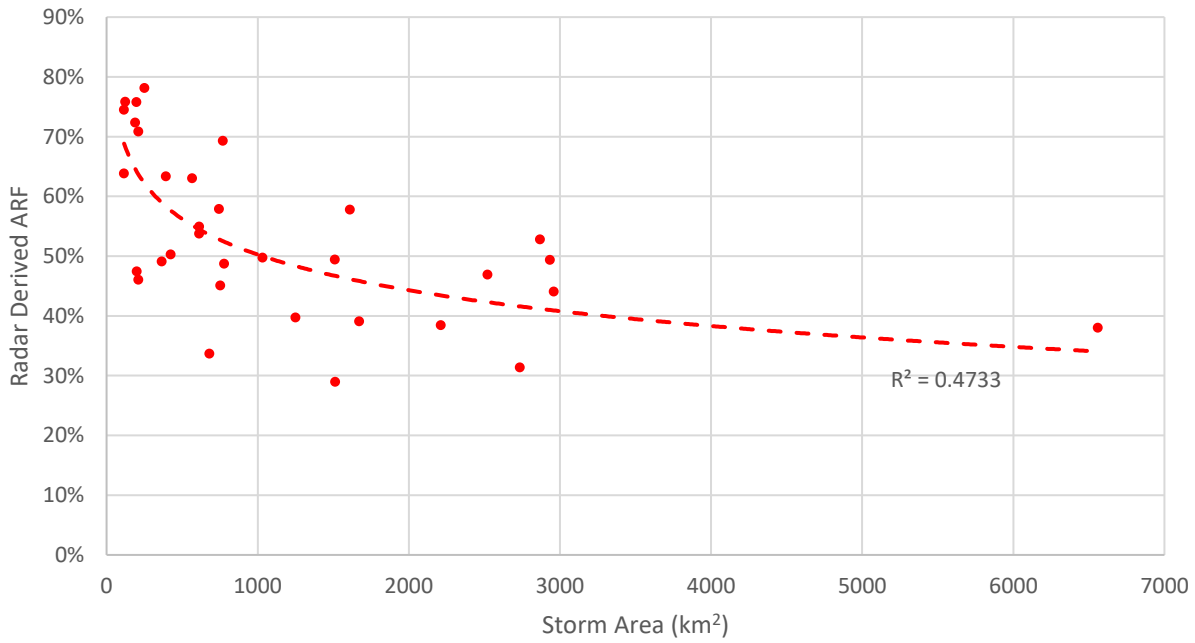

Figure 4.6: ARF with Storm Area for 3 Hour Storm Duration

Figure 4.7 illustrates the relationship between the storm area and the 24-hour storm duration radar derived ARFs. The regression analysis showed that a logarithmic trend best fits the data. The R^2 value of 0.1738 indicates that the data does not fit the trend line well. For storms less than 1 000 km^2 the 24-hour storm duration produced scattered ARFs, in line with the trends observed from the 1- and 3-hour storm duration ARFs and the observation made by Alexander (2001). Fewer storms larger than 3 000 km^2 were analysed for the 24-hour storm events, than for the 1- and 3-hour storm events. However, in Figure 4.7, the storms with a storm area larger than 3 000 km^2 the ARFs tend to fit the trend line better. An r-value of -0.4169 was obtained. A p-value of 0.018 was calculated. The R^2 value indicates weak fit of the data that is due to the scatter of the ARFs obtained for the 24-hour storms. The r-value indicates less than average inverse correlation exists, and the p-value indicates high significance.

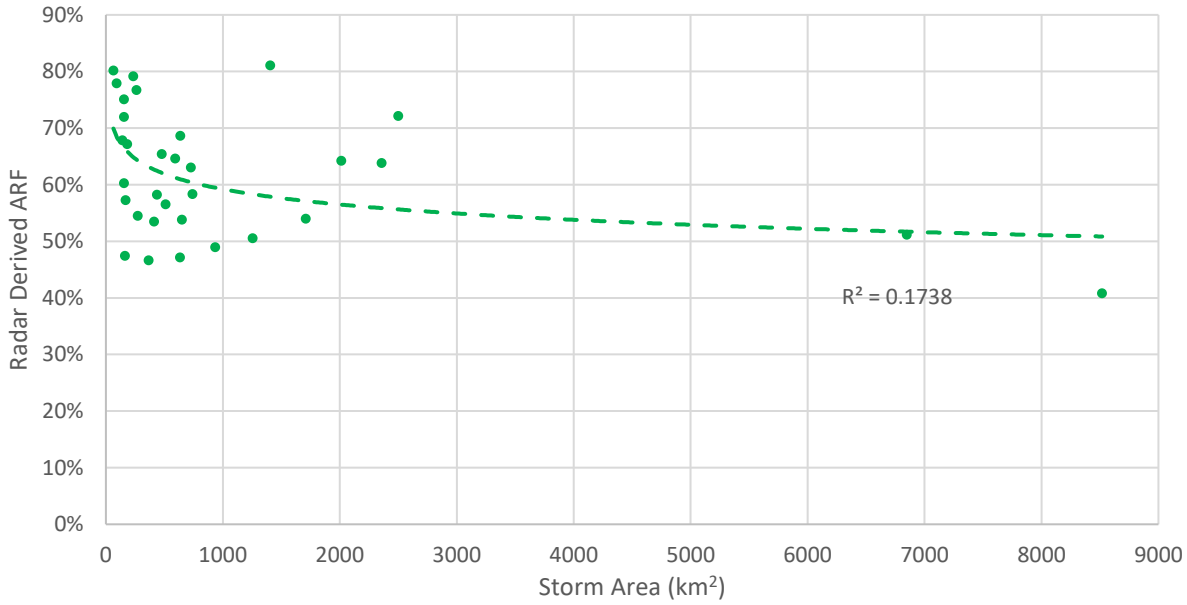

Figure 4.7: ARF with Storm Area for 24 Hour Storm Duration

Figure 4.8 illustrates the correlation between ARFs and storm areas for all storm durations (1, 3 and 24 hour). The regression analysis showed that a logarithmic trend best fits the data. The R^2 value of 0.3269 suggests a weak fit of the data with regards to the trend line but the r-value of -0.5718 indicates that there is good inverse correlation between the two variables. For all storm durations, it is evident that as the storm area increases, the ARFs decrease. In addition, storm areas less than 2 000 km^2 tend produce more scattered ARFs and storm areas larger than 2 000 km^2 tend to fit the trend line better.

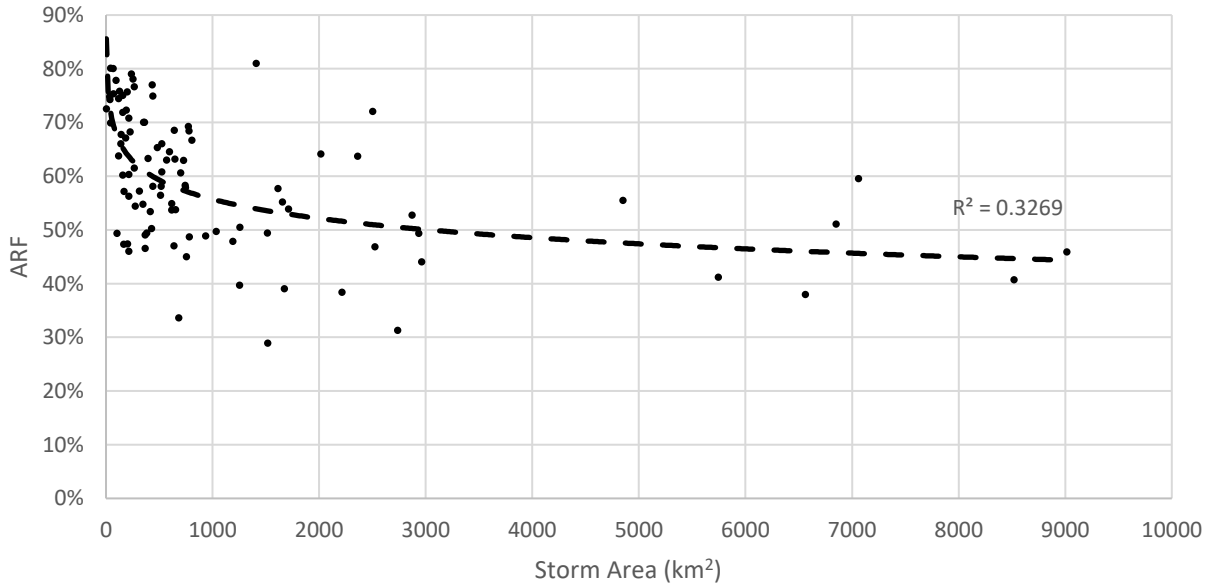

Figure 4.8: ARF with Storm Area for Any Storm Duration

Considering all the statistics obtained from the regression analyses, it was found that storm area does have a significant influence on radar derived ARFs. When compared with storm durations, it was found that the 3-hour storm durations produced the best relationship between storm area and radar derived ARFs. With this, the storm duration with the storm area has a significant relationship. More so, the storm duration with the storm area, shows stronger correlation for the 1- and 3-hour storm durations, and weaker correlation for the 24-hour storm durations.

4.2.5 ARFs with Maximum Point Intensity

This section contains analysis that contains the work of Van Wyk (1965), as the ARFs derived by Van Wyk (1965) mainly incorporates storm area and point rainfall intensity, which is found in Table B.1 (columns 7 and 9).

Figure 4.9 displays the relationship between maximum point rainfall intensity and the radar derived ARFs. The maximum point rainfall intensities were categorised based on storm duration (1, 3 and 24 hour). Through the regression analysis, it was found that a logarithmic trend best fits all data sets. The 1- and 3-hour storm events fits the logarithmic trend line significantly better than the 24-hour storm events. This results from the way in which the maximum point rainfall intensity is calculated (Section 3.9); a higher storm duration results in a smaller maximum point rainfall intensity, and vice versa. For the 1-hour storm duration storms, the maximum point rainfall intensity appropriately fits the trend line, with a high R^2 value of 0.7892, and contains strong inverse correlation, with an r-value of -0.8884, with the corresponding ARFs. This also holds true for the maximum point rainfall intensities produced from the 3- and 24-hour duration storm events and the corresponding ARFs. An appropriate data trend line fit results from the R^2 values of 0.8878 and 0.8363, for the 3- and 24-hour storm events respectively, and strong inverse correlation resulting from the r-values of -0.9422 and 0.9145 respectively. When statistically analysing the storm by disregarding the influence of storm duration (not categorising the data based on storm duration), a low R^2 value of 0.1029 and an r-value of -0.3208 was obtained, as shown by the black dotted line in Figure 4.9. These statistical parameters show that by not categorising the storm events based on storm duration for statistical analyses, a display of weaker fit and correlation between the maximum point rainfall intensity and the corresponding ARFs, is present. Although, the r-value indicates a slight inverse proportional relationship, a p-value of 0.001 suggests high significance. Thus, a strong inverse proportional relationship exists for each storm duration when comparing the maximum point rainfall intensity with ARFs; as the maximum point rainfall intensity increases logarithmically, the ARF decreases linearly.

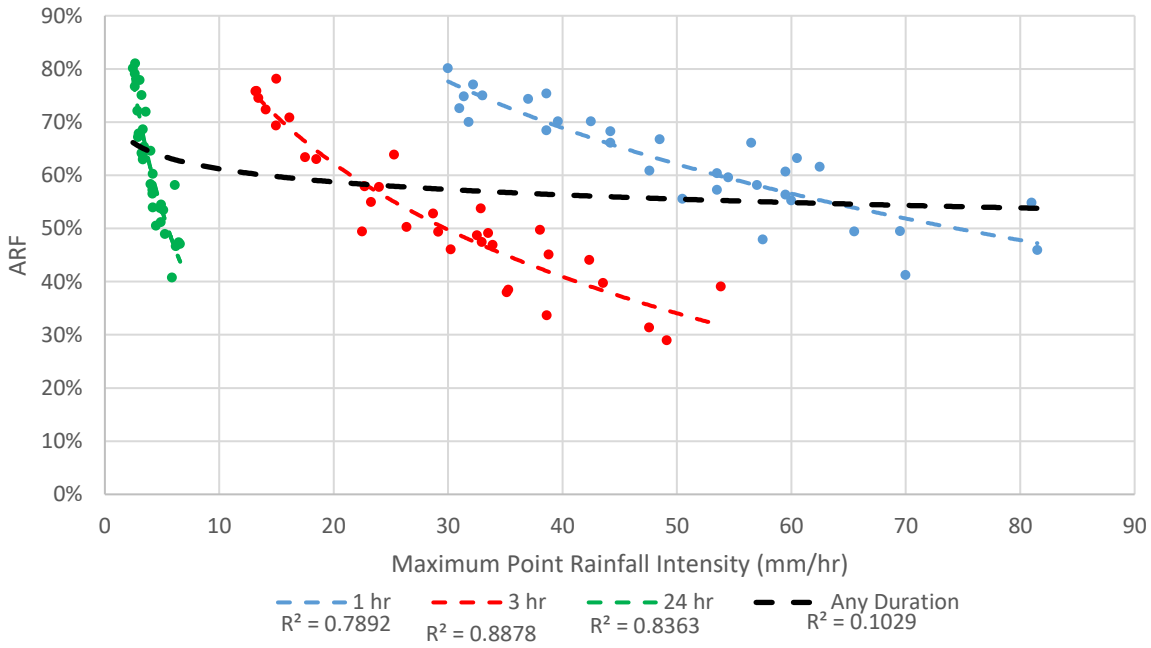

Figure 4.9: ARF with Maximum Point Rainfall Intensity

Figure 4.10 displays the relationship between the maximum point rainfall (and not maximum point rainfall intensity) with the corresponding ARFs. The maximum point rainfalls were not categorised based on storm durations as the relationship between the maximum point rainfalls and ARFs and the relationship between the maximum point rainfall intensities and ARFs are equivalent, for the same storm durations. These relationships are equivalent because the conversion calculation from maximum point rainfall to maximum point rainfall intensity is constant. Thus, the following relationship exists between the ARF and maximum point rainfall for each storm duration: as the maximum point rainfall increases logarithmically, the ARF decreases linearly. When considering the relationship between maximum point rainfall and ARFs, disregarding the influence of storm duration, an R^2 value of 0.5587, r-value of -0.7475 and p-value of approximately 0 was obtained. This shows that when disregarding the influence of storm duration, better correlation exists between maximum point rainfall and ARFs, than maximum point rainfall intensity and ARFs. Thus, this suggests that the data fits satisfactorily with the trend line, contains high significance and that there is good inverse proportional correlation between maximum point rainfall and ARFs, when disregarding the influence of storm duration.

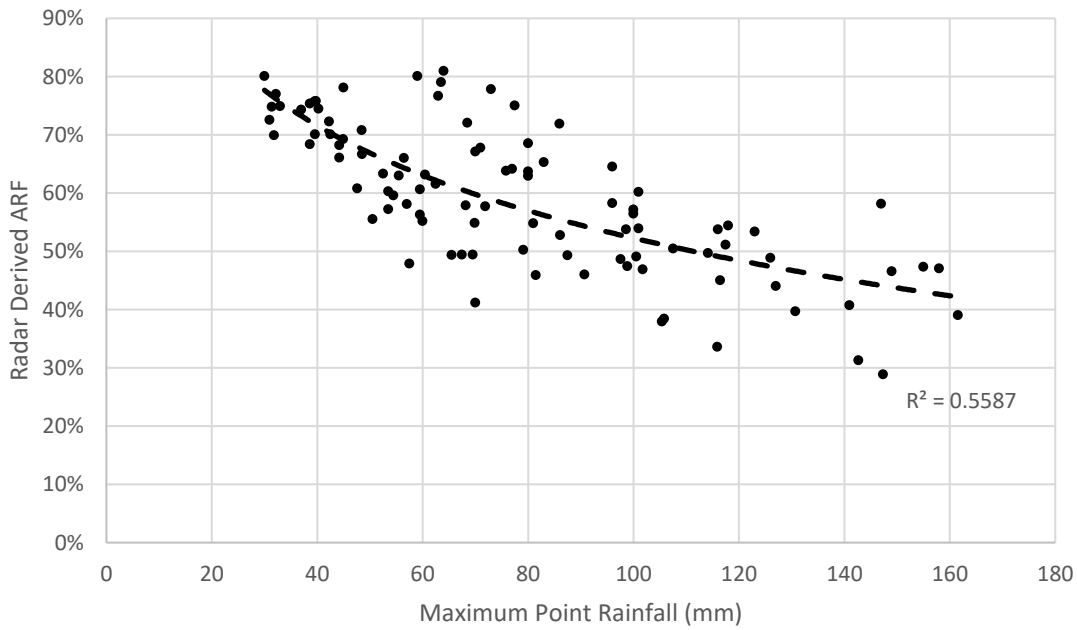

Figure 4.10: ARF with Maximum Point Rainfall

4.2.6 ARFs for Different Rainfall Processes

The rainfall processes considered in this study only focuses on convective and frontal rainfall regions. In Section 2.2.1.3, the various rainfall processes are described with their influences on the derivation of ARFs. Furthermore, Section 2.2.1.3 states that in convective regions, ARFs may be lower due to thunderstorms with rapid changing rainfall intensities. On the other hand, frontal rainfall regions may produce higher ARFs as these ARFs are considered to be more representative of the actual rainfall process. The distribution of convective and frontal rainfall events used for statistical analyses is found in Table 3.1, Section 3.4. The results obtained and displayed in Figure 4.11 showed that convective rainfall regions produced slightly higher ARFs than AFRs produced in frontal rainfall regions. It is important to note that the number of convective storms analysed is not the same as the number of frontal storms analysed. Thus, the results obtained does not truly contradict the notion that ARFs for frontal regions are lower than ARFs for convective region, as many more factors need to be controlled. However, this study conforms to the limitations presented in Section 1.5, which does not accommodate various controlled factors. These controlled factors could include constant storm area, duration and maximum point intensity for storms analysed in frontal and convective regions.

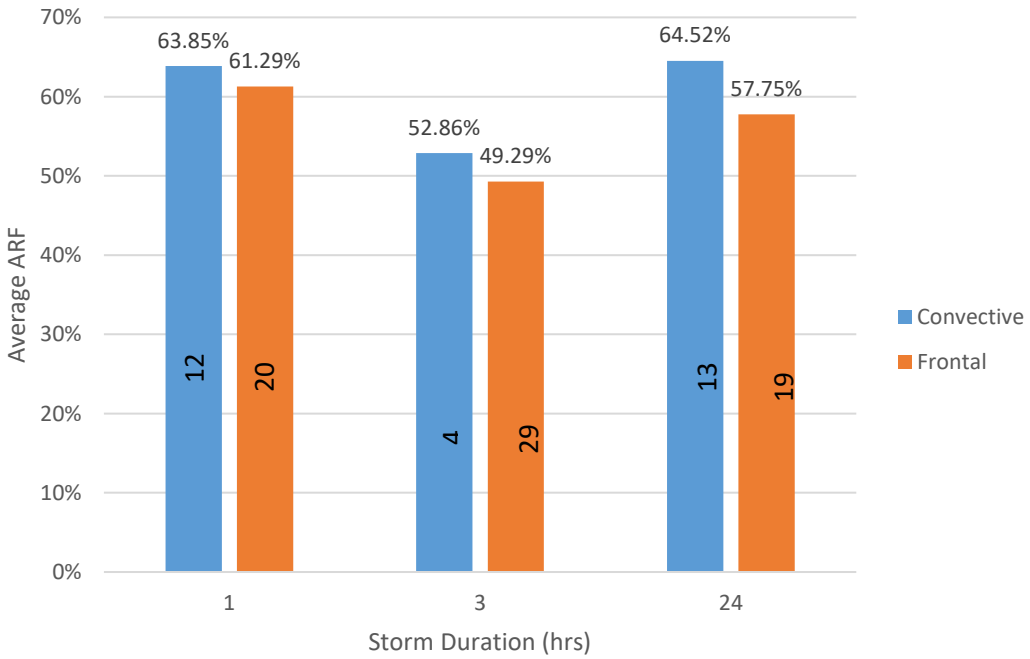

Figure 4.11: ARFs for Convective and Frontal Rainfall Regions

Although the difference in AFRs for the two rainfall regions is minimal and the results obtained are not configured with consistent and fair variables, it was found that the rainfall region/process does have an effect on ARFs derived from radar imagery.

4.2.7 ARFs with Storm Duration

The ARF was analysed for each storm duration, which was bound by the limitations mentioned in Section 1.5. Figure 4.12 displays the ARFs obtained for all storm durations with the respective ARF average. On average, the ARFs decrease from the 1-hour storm duration to the 3-hour storm durations. This is expected as ARFs typically decrease with an increase in storm duration (Figure 2.3, Kim *et al.* (2019)). On the other hand, there is a slight increase in terms of the averages of ARFs from the 3-hour storm duration to the 24-hour storm duration. Table 4.6 displays the average of the storm area, radar derived ARF and standard deviation of ARFs for each storm duration. The average storm area for the 3-hour storm events are the highest. This is in line with the conclusion made in Section 4.2.4, and Figures 2.2 and 2.3: the higher the storm area, the lower the ARF. However, the 24-hour storm events host the lowest storm area average, but not the highest ARF average.

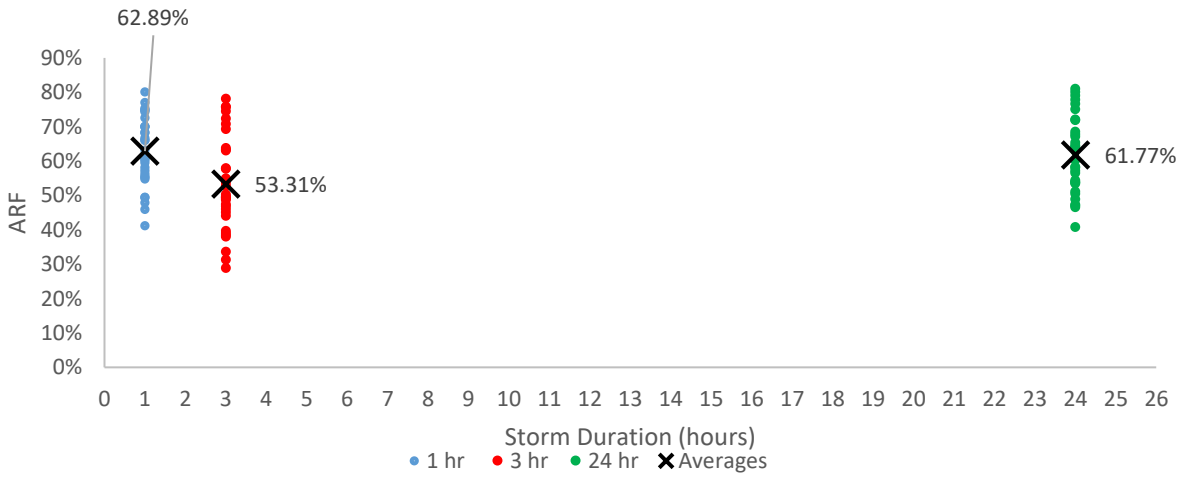

Figure 4.12: ARF for Various Storm Durations

The standard deviation for the 1 hour storms is the lowest, indicating that the data is the least spread out. The 24 hour storm events had a lower standard deviation than the 3 hour storm events, indicating that the ARFs from the 24 hour storm events are more spread out than that of the 3 hour storm events. The rise in average ARF from 3 hour to 24 hour storm events could be explained by the number of storms with corresponding ARFs of storm areas less than 1 000 km^2. Since more storms with storm areas less than 1 000 km^2 were produced from the 24 hour storm events than the 3 hour storm events, a higher average ARF was produced. This results from higher ARFs which are calculated for smaller storm areas (Figures 2.2 and 2.3). This implies that more storms with a larger area were calculated for the 3 hour storms, which decreased the ARF average, as larger storm areas produce smaller ARFs.

Table 4.6: Storm Average

Storm Duration (Hours)	Average Storm Area (km^2)	Average ARF	Standard Deviation of ARFs	Number of Storms with Storm Areas < 1000 km	Number of Storms with Storm Areas > 1000 km
1	1186.26	62.89%	9.94%	26	6
3	1203.30	53.31%	13.73%	20	13
24	1118.24	61.77%	11.13%	24	8
Any Duration	**1169.62**	**59.26%**	**12.38%**	**70**	**27**

Upon further analysis, it was found necessary to group the ARF for each storm duration, based on storm area: 200, 500, 1 000 and 10 000 km^2, shown in Figure 4.13. Figure 4.13 can be paired with Table 4.7. From literature (Figure 2.3), the ARF should increase for a decrease in storm area and an increase in storm duration. In essence, the predicted results should portray an increase in ARF for an increase in storm duration, on each graph in Figure 4.13, as the graphs already represent increasing storm area categories. Figure 4.13 (a) shows a rise in ARF from 1 hour to 3-hour storm events, and then a decline from the 3- to 24-hour storm events is observed. Figure 4.13 (b), (c) and (d), a decrease in ARF average from the 1 hour to 3 hour storm events and increase in ARF average from the 3 to 24 hour storm events. The expected trend is seen in Figure 4.13 (a), from 1 to 3 hour storm events, and Figure 4.13 (b), (c) and (d) from 3 to 24 hour storm events.

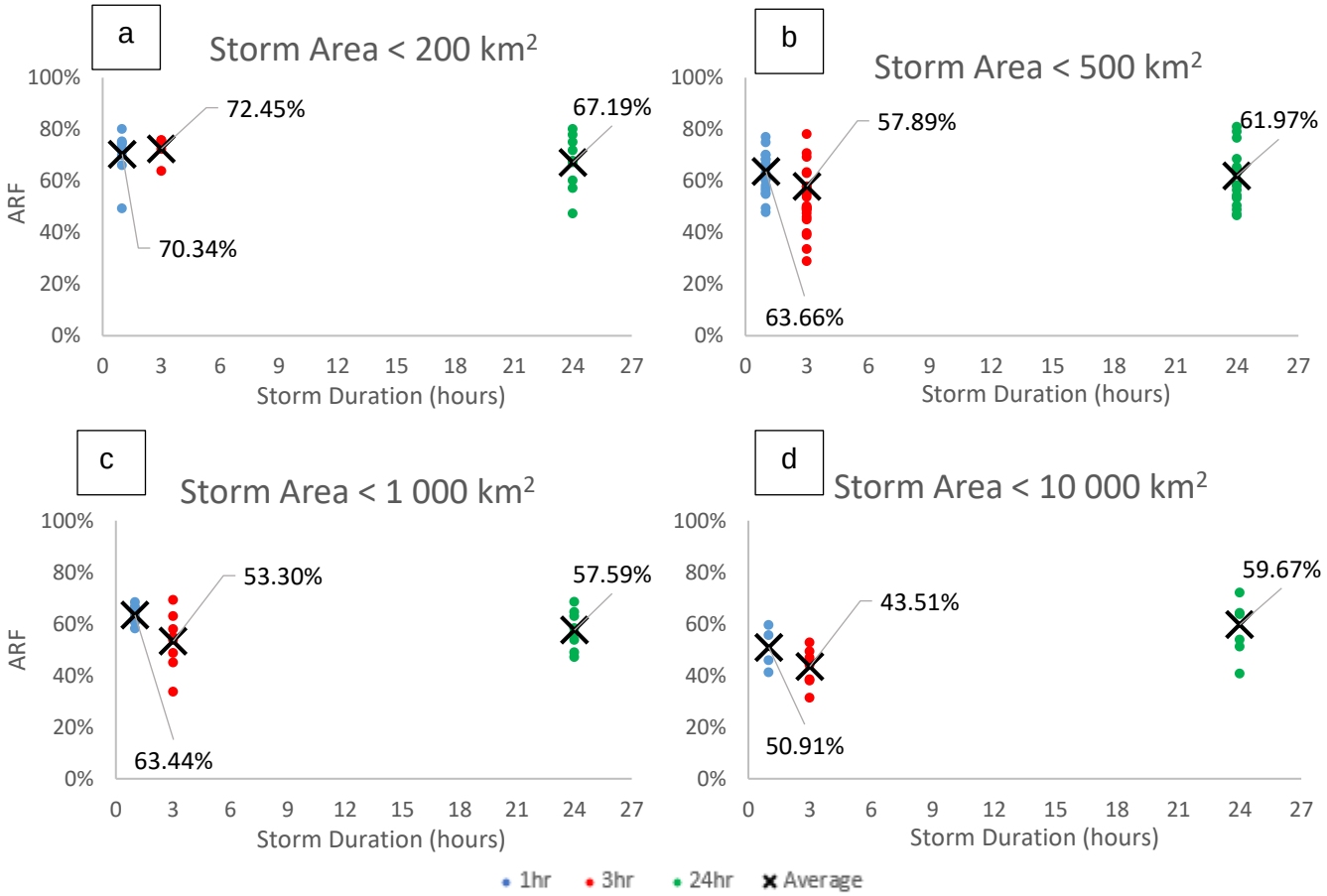

Figure 4.13: Average ARFs per Storm Duration, Categorised based on Storm Area

The results that do not follow the trend can be explained by the storm area averages displayed in Table 4.7. The variability of the storm area averages, within each storm area category, explains the variability of the resulting average ARF. Thus, storm duration with storm area have a significant influence of the derivation of ARFs.

Table 4.7: Average Storm Area for each Storm Duration

Storm Duration (hours)	< 200 km²	<500 km²	<1 000 km²	<10 000 km²
1	56.47	320.27	640.14	4917.46
3	148.96	293.91	690.23	2414.23
24	142.11	351.90	678.40	3326.76

4.3 Comparison of ARFs

Van Wyk (1965) suggested that the ARFs produced from his study be validated using radar technology. This section compares the radar based ARFs that were derived from ArcGIS with ARFs that are currently implemented in South Africa, i.e. ARFs derived by Van Wyk (1965) and Pullen, Wiederhold and Midgley (1966) using a storm centred approach, and Op ten Noort and Stephenson (1982).

The storm centred ARFs currently implemented in South Africa are separated into two categories based on the storm criteria: catchments less than 800 km^2; and catchments greater than 800 km^2 but less than 30 000 km^2. Thus, for the comparison of ARFs, the radar derived ARFs were separated into the two categories based on the same criteria.

4.3.1 Current ARFs for Small Catchments

The radar derived ARFs were compared to Van Wyk's (1965) ARFs for catchments less than 800 km^2, following Section 2.2.3. The dataset for Van Wyk (1965) was obtained using the radar derived maximum point intensity and storm area to arrive at each ARF, for each storm. The ARFs were also tested with Op ten Noort and Stephenson's (1982) (OTN) Equation 2. A graphic illustration is displayed in Figure 4.14. All the data used in this section is contained in Table B.2.

Table 4.8: Difference of Radar Derived ARFs with Smaller Catchment ARFs in South Africa

Comparison	Storm Area Range	Difference Equation	Minimum Difference	Maximum Difference	Average Difference	No of storms with Difference < 0%
Van Wyk	< 800 km^2	(Van Wyk ARF) - (Radar Derived ARF)	-2.55	50.17%	24.12%	3
OTN Equation 2	< 800 km^2	(Radar Derived ARF) – (OTN ARF)	-56.13%	45.65%	0.55%	29

A regression analysis was carried out on the Van Wyk (1965) ARFs with the radar derived ARFs. An R^2 value of 0.1217 and r-value of 0.3489 was obtained, indicating weak correlation between the two variables. Upon further analysis, it was found, on average that Van Wyk's (1965) storm centred derived ARFs were, on average, 24.12% higher than the radar derived ARFs, as displayed in Table 4.8. This was expected as Van Wyk's (1965) method of deriving storm centred ARFs included using rain gauges, which produces ARF with poor spatial resolution (Sinclair and Pegram, 2005). Figure 4.14 contains a reference line called “Perfect Correlation”. The “Perfect Correlation” line graphically illustrates the deviation of the comparison between the radar derived ARFs with ARFs in South Africa, from having perfect correlation. In other words, the perfect correlation line would exist if all the radar derived ARFs were the same as Van Wyk’s (1965) ARFs, by using storm area and maximum point intensity as the storm inputs. Regarding Op ten Noort and Stephenson's (1982) Equation 2, it was found that using the equation to calculate AFRs, produced ARFs that were, on average, only 0.55% higher than the radar derived ARFs. Figure 4.14 shows that the trendline of Op ten Noort and Stephenson's (1982) ARFs almost identically matches the “Perfect Correlation” line. Although the trend lines are almost identical, an r-value of 0.4030 was obtained, indicating weak correlation. In other words, both data sets contain trend lines that fits their respective data sets similarly, however, there still exists weak correlation between the two data sets. Comparing the average difference in ARFs from Van Wyk (1965) and Op ten Noort and Stephenson's (1982), it is clear that using Op ten Noort and Stephenson's (1982) Equation 2 produces ARFs closer to the radar derived ARFs. Figure 4.14 shows the deviation of the results from perfect correlation with Van Wyk’s (1965) ARFs.

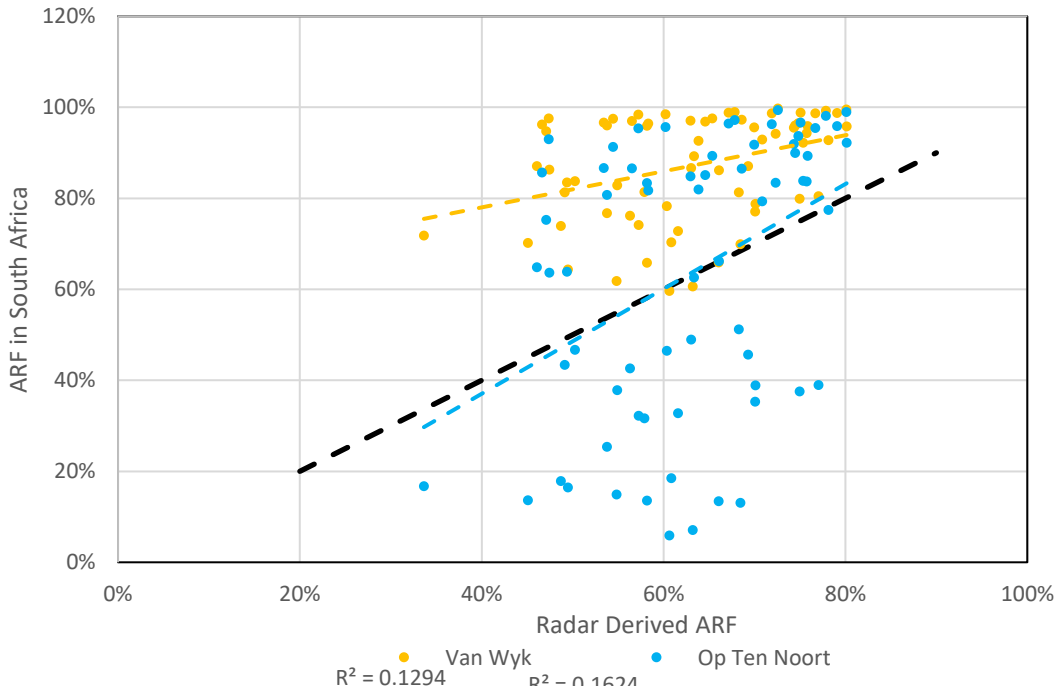

Figure 4.14: Statistical Comparison for Smaller Catchment Areas

A regression analysis was carried out on the ARFs produced by Op ten Noort and Stephenson's (1982) Equation 2 and Van Wyk (1965), which made use of radar storm outputs found in Table B.2 (columns 8 and 10). This was carried out in order to validate the high correlation present between the two ARF data sets, as mentioned by Op ten Noort and Stephenson's (1982). An R^2 value of 0.9486 and r-value of 0.9740 was obtained, indicating and confirming that there exists high correlation between the two ARF data sets used for this research.

Figure 4.15 displays the current ARFs implemented in South Africa.

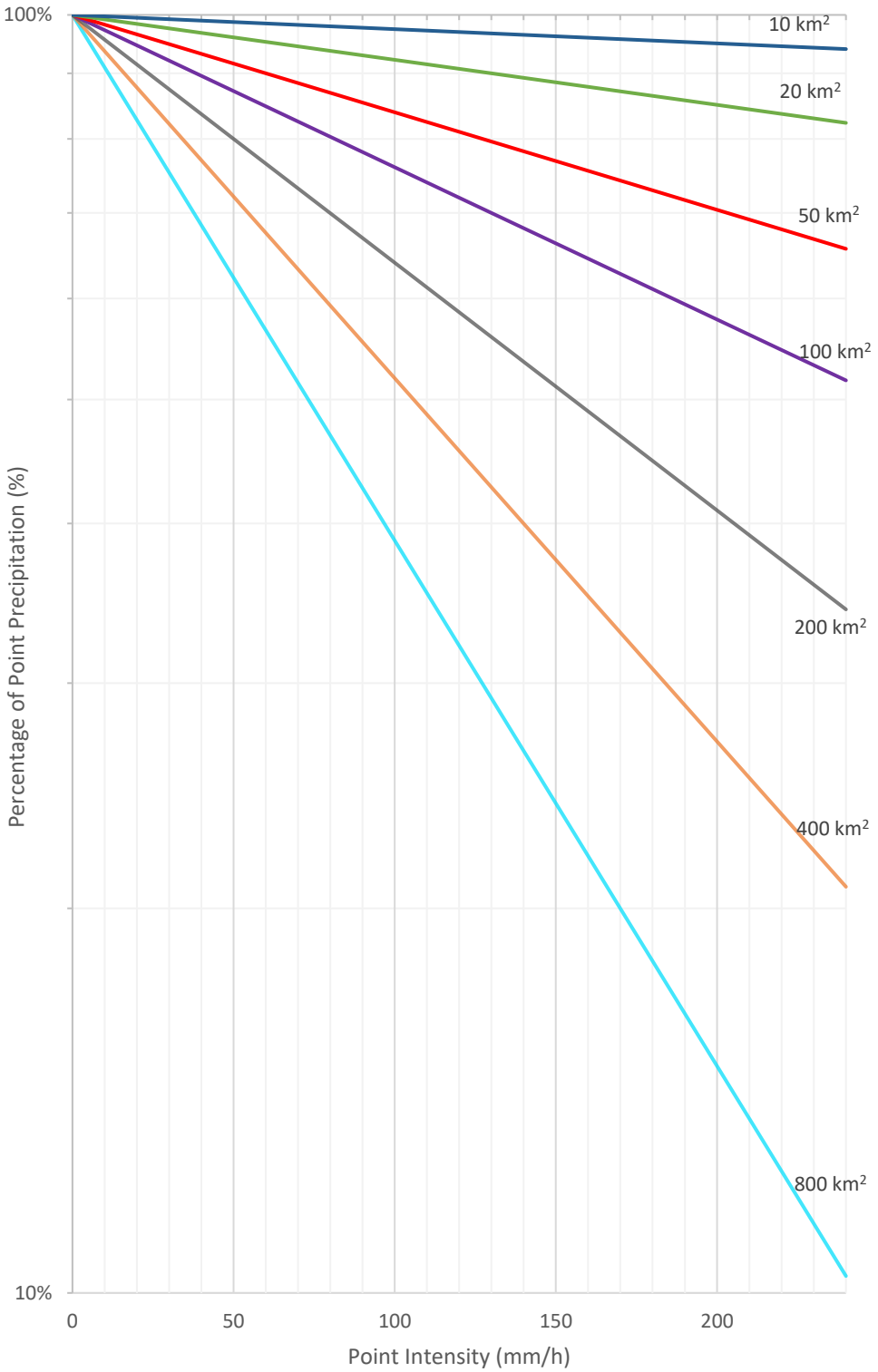

Figure 4.15: Adaption of Van Wyk's (1965) ARFs in South Africa

Figure 4.16 graphically illustrates the comparison between the radar derived ARFs, and ARFs currently used in South Africa. The data shows that the highest point intensity analysed was 81 mm/h. Thus, Figure 4.16 only compares the radar derived ARFs with ARFs in South Africa up to 81 mm/h. These can be considered “low point intensity storms”, for comparison purposes. The storms were grouped into the seven following storm area boundaries: 0 – 15, 15 -35, 35 – 75, 75 – 150, 150 – 300, 300 – 600 and 600 – 800 km^2, which matched the storm areas set out by Van Wyk (1965): 10, 20, 50, 100, 200, 400 and 800 km^2. Trend lines were then calculated for each data set. Only one storm event conformed to the 0 – 15 km^2 boundary. The ARF for that particular storm was found to be significantly lower than Van Wyk’s (1965) ARF. The radar based storm events in the storm categories of 20, 50 and 100 km^2, in Figure 4.16 (b), (c) and (d), were found to be all lower than Van Wyk’s (1965) ARFs, with similar gradients.

For radar derived ARFs in the 200 km^2 category, Figure 4.16 (e), lower ARFs were obtained for lower rainfall intensities. However, as the rainfall intensity increased, the difference between the ARFs decreased slightly. A similar trend was followed for the radar derived ARFs in the 400 and 800 km^2 categories, Figure 4.16 (f) and (g): lower radar derived ARFs obtained up until a rainfall intensity of 80 and 70 mm/h, respectively. From Figure 4.16 (a), (b), (c) and (d), it can be stated that most of the radar derived ARFs were lower than Van Wyk’s (1965), for storm areas less than 200 km^2, for lower point intensity storm events. As for storms events with storm areas greater than 200 km^2, a certain point rainfall intensity threshold exists where the radar derived ARFs starts to exceed ARFs as predicted by Van Wyk (1965), which constitutes a significant variation.

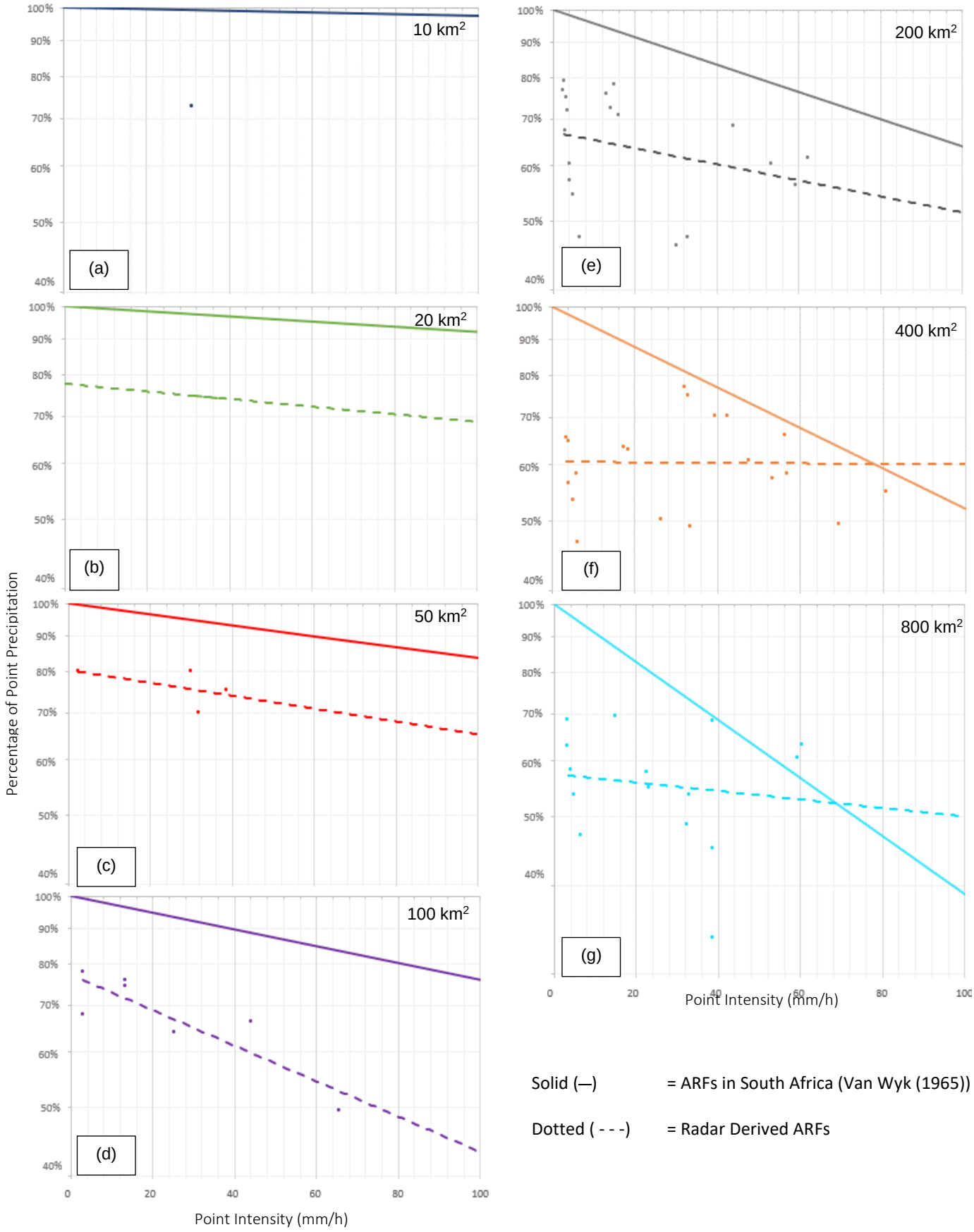

Figure 4.16: Comparison of ARFs for Smaller Catchments

4.3.2 Current ARFs for Larger Catchments

The radar derived ARFs were compared to Pullen, Wiederhold and Midgley's (1966) ARFs for catchments greater than 800 km^2 but less than 30 000 km^2. The dataset for Pullen, Wiederhold and Midgley's (1966) was obtained using the radar derived storm area and duration to arrive at each ARF, for each storm. The radar derived ARFs were also tested with Op ten Noort and Stephenson's (1982) Equation 3. A graphic illustration of the results is presented in Figure 4.17. The data used in this section is contained in Table B.3.

A regression analysis was carried out on Pullen, Wiederhold and Midgley's (1966) ARFs with radar derived ARFs. An R^2 value of 0.1066 and r-value of 0.3265 was achieved, indicating weak correlation between the two variables. In comparison, the radar derived ARFs correlated better with ARFs produced by Pullen, Wiederhold and Midgley (1966) than with the ARFs produced by Van Wyk (1965), despite that the correlation coefficients are small. Upon further analysis, Pullen, Wiederhold and Midgley's (1966) storm centred derived ARFs were, on average, only 3.61% higher than the radar derived ARFs. This is presented in Table 4.9.

Table 4.9: Difference of Radar Derived ARFs with Smaller Catchment ARFs in South Africa

Comparison	Storm Area Range	Difference Equation	Minimum Difference	Maximum Difference	Average Difference	No of storms with Difference < 0%
Wiederhold	> 800 km^2	(Radar Derived ARF) – (Wiederhold ARF)	-33.55%	33.94%	3.61%	11
OTN Equation 3	> 800 km^2	(Radar Derived ARF) – (OTN ARF)	-5.05%	56.15%	29.52%	1

Figure 4.17 contains a reference line called “Perfect Correlation”. The “Perfect Correlation” line graphically illustrates the deviation of the comparison between the radar derived ARFs with ARFs in South Africa, from having perfect correlation. In other words, the perfect correlation line would exist if all the radar derived ARFs were the same as ARFs Pullen, Wiederhold and Midgley's (1966), by using storm area and duration as the storm inputs. Regarding Op ten Noort and Stephenson's (1982) Equation 3, it was found that using the equation to calculate AFRs, produced ARFs that were 29.52%, on average, higher than the radar derived ARFs. This is displayed in Table 4.9. Comparing the average difference in ARFs from Pullen, Wiederhold and Midgley (1966) and Op ten Noort and Stephenson's (1982) from Table 4.9, it is clear than using Pullen, Wiederhold and Midgley's (1966) method to produce ARFs would obtain results that are closer in correlation to the radar derived ARFs.

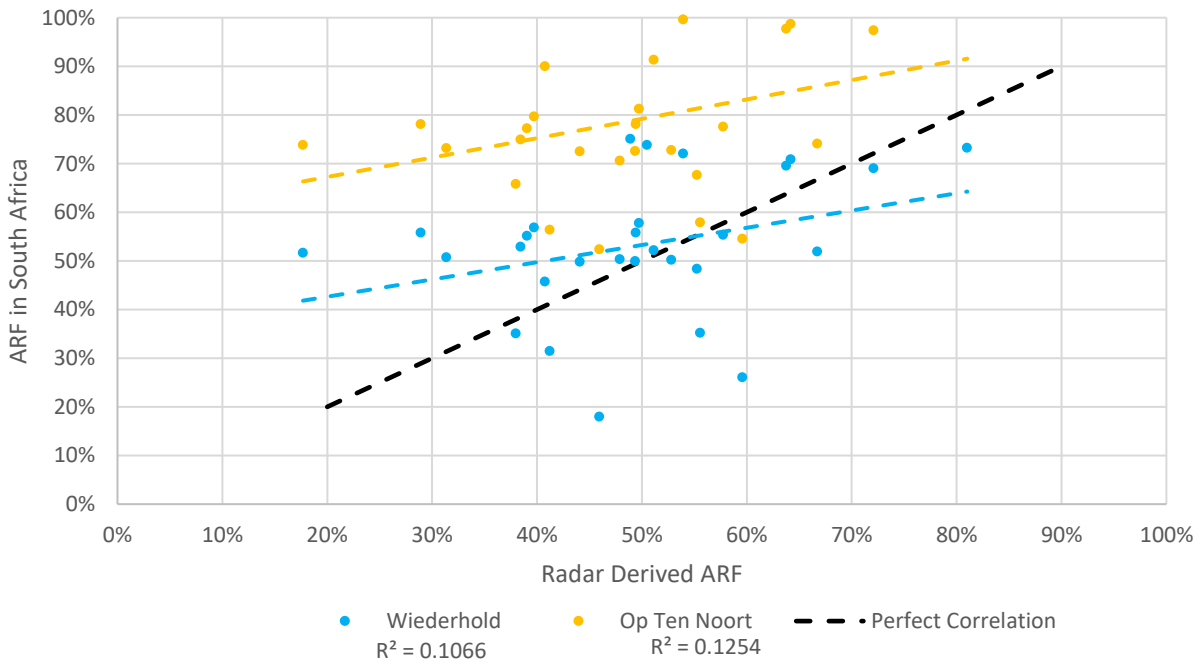

Figure 4.17: Statistical ARF Comparison for Larger Catchment Areas

A regression analysis was carried out on the ARFs produced by Op ten Noort and Stephenson's (1982) Equation 3 and Pullen, Wiederhold and Midgley's (1966), which made use of using the radar storm outputs found in Table B.3 (columns 8 and 10). This was carried out in order to validate the high correlation present between the two ARF data sets, as mentioned by Op ten Noort and Stephenson's (1982). An R^2 value of 0.8591 and r-value of 0.9269 was obtained, indicating and confirming that there exists high correlation between the two ARF data sets used for this research.

Figure 4.18 displays the comparison of the radar derived ARF with Pullen, Wiederhold and Midgley's (1966) ARFs currently implemented in South Africa. The radar derived ARFs were categorised based on storm durations: 1, 3 and 24 hours. Trend lines were then produced for each storm duration. Figure 4.18 illustrates that 1-hour radar-based storm events overestimates the ARF for all storm areas. The ARFs for 3- and 24-hour radar based storm events are underestimated up until a storm area of approximately 6 250 and 7 500 km^2, respectively. From this, it can be said that radar derived ARFs are overestimated for storm durations under 1-hour, and overestimates ARFs for storms greater than 1 hour, up until a certain storm area threshold, compared to Pullen, Wiederhold and Midgley's (1966) ARFs that are currently implemented in South Africa.

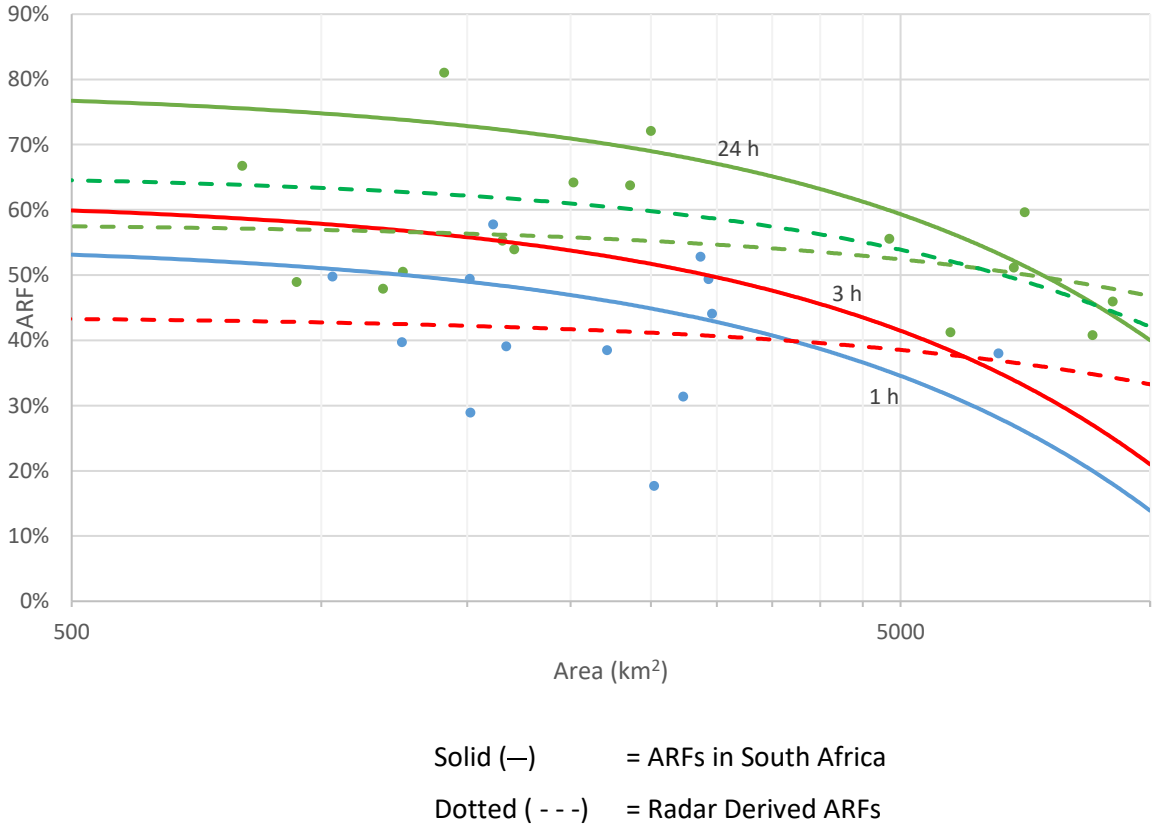

Figure 4.18: Comparison of ARFs for Larger Catchments

4.4 Summary

The main methodology consisted of using ArcGIS to obtain storm areas and isohyetal rainfall and consequently the calculation of the ARF. This was validated through the manual calculation of using Precipitation Arrays to calculate ARFs. It was found that the ArcGIS methodology to obtain the following outputs: storm area, isohyetal rainfall and rainfall intensities, was reliable based on the validation of using Precipitation Arrays to arrive at the same outputs. Regression analyses indicated high correlation between ARFs obtained using both methodologies.

Continuing the analysis with the ArcGIS outputs, it was found that storm area and maximum point intensity generally have an influence on the ARF; an increase in storm area or maximum point intensity, produced lower ARFs. There was an insignificant influence of the rainfall process on ARF. Furthermore, it was found that storm duration on ARFs produced inconsistent results.

The radar derived ARFs were compared to ARFs currently implemented in South Africa. An overestimation of the ARFs currently implemented in South Africa for both smaller and larger catchment areas were found, in comparison with radar derived ARFs. Additionally, radar derived ARFs were lower than those calculated by using Op ten Noort and Stephenson's (1982) formulas.

Considering the findings presented in this section, it is clear that the use of radar data has some potential to test the validity of ARFs currently used in South Africa. The high spatial and temporal resolution, response time, weather casting and historic record of radar data could possibly account for some of the overly conservative parameters used in hydrological application for South Africa. From this, it shows that the potential of using radar data could produce a significant impact within hydrology. The main potential obstacle hindering the use of radar data results from large uncertainties and correlation of radar produced results with traditional deemed reliable methods that have been used up to date.

5 CONCLUSION

An areal reduction factor is defined as a factor that is applied to point rainfall depths to convert these rainfall depths to an average rainfall over a specific catchment area. There are two main methods currently used to derive an ARF: the storm centred method, which considers the area of a specific storm, and the geographically fixed method, which considers rainfall occurring over a specific fixed location. For South Africa, the ARFs currently implemented were derived and estimated by Van Wyk (1965) and Pullen, Wiederhold and Midgley (1966), using the storm centred method. The storms used in these analyses lack adequate spatial resolution, which could significantly affect the derivation of ARFs. Thus, radar data was tested as an alternative, as it hosts the ability to produce high spatial and temporal resolution storms for analysis. Furthermore, radars consider the internal structure and behaviour of storms.

The South African Weather Services provided radar imagery, in an MDV file format, that was used for analysis. The MDV files were converted to netcdf files for analysis in ArcGIS. An extensive methodology was put in place, following the storm centred method, to derive ARFs. Storm outputs obtained in ArcGIS were validated through the use of Precipitation Arrays.

The radar derived ARFs in ArcGIS for 1-, 3- and 24-hour storm durations were statistically analysed using multiple regression analyses. Firstly, it was found that an inverse proportional relationship exists between the ARF and the respective storm area. An inverse proportional relationship exists between the maximum point rainfall intensity with the respective ARF, for each storm duration. When disregarding the influence of storm duration, little correlation was found. Secondly, higher ARFs were obtained for convective rainfall regions than for frontal rainfall regions. The influence of storm duration on ARFs contained no significant correlation. However, when comparing the influence of storm duration with storm area on ARFs, a potentially significant influence exists. Thirdly, the radar derived ARFs were lower than ARFs in South Africa, by Van Wyk (1965), for storm areas less than 200 km^2 for smaller catchments. Using Op ten Noort and Stephenson's (1982) Equation 2 produced ARFs that were, on average, slightly higher than the radar derived ARFs. For larger catchments, it was found that radar derived ARFs were lower than ARFs in South Africa for storm durations of more than 1 hour. The radar derived ARFs for the 1 hour storm events were found to be overestimated. Using Op ten Noort and Stephenson's (1982) Equation 3 produced ARFs that were, on average, significantly higher than the radar derived ARFs. Finally, the comparison of radar derived ARFs and the ARFs currently implemented in South Africa, suggest that there could be value in reproducing ARFs for South Africa, considering the significant evolution of data capturing since 1965, using advanced technology (such as radars).

The ARFs determined using radar data are generally lower than those derived by conventional methods. This suggests than the current methods may yield ARFs that are conservative. Radars provide more detailed information for the analyses of storms when compared to using traditional analysis methods. Although radars are known for their large uncertainties and convoluted bias applications, radars expose the potential of significantly improving certain aspects of hydrological calculations.

6 RECOMMENDATIONS

The method of deriving the areal reduction factor, using radar data, is extensive enough to be considered reliable. It is recommended that the radar data be improved by applying the suitable Marshall-Palmer reflectivity relationship for each individual storm. This would produce results that could better identify influences such as storm type, on the ARF.

For accuracy, it is recommended that rain gauge data be used for validation and possible calibration of the radar data. With this, a longer historic record should be analysed in order to consider the influence of return period on the ARF. Storm duration instead of storm rainfall accumulations for specific durations could be considered. Shorter storm durations, specifically 6 and 12 hour storm durations, as well as longer storm durations, specifically more than 1 day, should be considered. Categorising storms based on storm areas and accordingly carrying out analyses would expose a more detailed influence of storm area on ARFs.

7 REFERENCES

Alexander, W. (1980) 'Depth-Area-Duration-Frequency Properties of Storm Rainfall in South Africa', *Technical Report TR83*.

Alexander, W. (1990) 'Flood Hydrology for Southern Africa'.

Alexander, W. (2001) 'Flood Risk Reduction Measures: Incorporating Flood Hydrology for Southern Africa'.

Alexander, W. (2010) 'Analytical Methods for Water Resource Development and Managment: Handbook for Pratitioners and Decision Makers'. Available at: http://www.droughtsandfloods.com/.

Allen, R. J. and DeGaetano, A. T. (2005a) 'Areal Reduction Factors for Two Eastern United States Regions with High Rain-Gauge Density', *Journal of Hydrologic Engineering*, 10(4), pp. 327–335. doi: 10.1061/(asce)1084-0699(2005)10:4(327).

Allen, R. J. and DeGaetano, A. T. (2005b) 'Considerations for the use of radar-derived precipitation estimates in determining return intervals for extreme areal precipitation amounts', *Journal of Hydrology*, 315(1–4), pp. 203–219. doi: 10.1016/j.jhydrol.2005.03.028.

Asquith, W. H. and Famiglietti, J. S. (2000) 'Precipitation areal-reduction factor estimation using an annual-maxima centered approach', *Journal of Hydrology*, 230(1–2), pp. 55–69. doi: 10.1016/S0022-1694(00)00170-0.

Bacchi, B. and Ranzi, R. (1996) 'On the derivation of the areal reduction factor of storms', *Atmospheric Research*, 42(1–4), pp. 123–135. doi: 10.1016/0169-8095(95)00058-5.

Bárdossy, A. and Pegram, G. (2018) 'Intensity–duration–frequency curves exploiting neighbouring extreme precipitation data', *Hydrological Sciences Journal*. Taylor & Francis, 63(11), pp. 1593–1604. doi: 10.1080/02626667.2018.1524987.

Beard, L. R. (1967) 'Optimization techniques for hydrologic engineering', *Water Resources Research*, 3(3), pp. 809–815. doi: 10.1029/WR003i003p00809.

Becker, E. H. and Pegram, G. (2014) *College of Agriculture , Engineering and Science Handbook for 2013*.

Bell, F. (1976) 'The Areal Reduction Factor in Rainfall Frequency Estimation', *Report No. 35*.

Bengtsson, L. and Niemczynowicz, J. (1986) 'Areal Reduction Factors from Rain Movement', *Hydrology Research*, 17(2), pp. 65–82. doi: 10.2166/nh.1986.0005.

Bureau, U. W. (1957) '1957. Rainfall intensity–frequency regime', *Technical Paper 29*.

Cunnane, C. and Lynn, M. A. (1975) 'Flood Estimation following the Flood Studies Report', *The*

Institution of Engineers of Ireland, (February), p. 39.

Davies, B. and Day, J. (1998) 'Vanishing Waters'.

Dixon, M. (2006) 'MDV FORMAT Interface Control Document (ICD)', (November), pp. 1–30.

Gill, T. D. (2005) 'Transformation of Point Rainfall To Areal Rainfall By', (May).

Haarhoff, J. and Cassa, A. (2009) 'Introduction to Flood Hydrology'.

Hershfield, D. (1962) 'Extreme rainfall relationships', , *American Society of Civil Engineers HY6 (11)*, pp. 73–92.

Huff, F. (1995) 'Characteristics and contributing causes of an abnormal frequency of flood-producing rainstorms at Chicago', *Journal of the American Water Resources Association*, 31(4), pp. 703–714.

Huff, F. A. and Shipp, W. L. (2002) 'Spatial Correlations of Storm, Monthly and Seasonal Precipitation', *Journal of Applied Meteorology*, pp. 542–550. doi: 10.1175/1520-0450(1969)008<0542:scosma>2.0.co;2.

Kim, J. *et al.* (2019) 'The role of rainfall spatial variability in estimating areal reduction factors', *Journal of Hydrology*. Elsevier, 568(June 2018), pp. 416–426. doi: 10.1016/j.jhydrol.2018.11.014.

Lambourne, J. and Stephenson, D. (1986) 'Research in Urban Hydrology and Drainage: Factors affecting Storm Runoff in South Africa', *Water Systems Research Programme*, Report No.

Lombardo, F., Napolitano, F. and Russo, F. (2006) 'On the use of radar reflectivity for estimation of the areal reduction factor', *Natural Hazards and Earth System Science*, 6(3), pp. 377–386. doi: 10.5194/nhess-6-377-2006.

Olivara, F. *et al.* (2006) 'CALCULATION OF AREAL REDUCTION FACTORS USING NEXRAD PRECIPITATION ESTIMATES'.

Omolayo, A. S. (1993) 'On the transposition of areal reduction factors for rainfall frequency estimation', *Journal of Hydrology*, 145(1–2), pp. 191–205. doi: 10.1016/0022-1694(93)90227-Z.

Op ten Noort, T. and Stephenson, D. (1982) 'Flood peak calculation in South Africa', *Water Systems Research Programme Report*, 2/1982.

Overeem, A. *et al.* (2010) 'Extreme value modeling of areal rainfall from weather radar', *Water Resources Research*, 46(9), pp. 1–13. doi: 10.1029/2009WR008517.

Pavlovic, S. *et al.* (2016) 'Intercomparison of selected fixed-area areal reduction factor methods', *Journal of Hydrology*. Elsevier B.V., 537, pp. 419–430. doi: 10.1016/j.jhydrol.2016.03.027.

Picus, C. *et al.* (2008) 'Kernel-based storm tracking in radar data', *2008 IEEE Radar Conference,*

RADAR 2008. doi: 10.1109/RADAR.2008.4721112.

Pietersen, J., Gericke, O. J. and Woyessa, Y. E. (2016) 'OVERVIEW AND EVALUATION OF AREAL REDUCTION FACTOR METHODS', (August).

Pietersen, J. P. J. *et al.* (2015) 'Review of current methods for estimating areal reduction factors applied to South African design point rainfall and preliminary identification of new methods', *Journal of the South African Institution of Civil Engineering*, 57(1), pp. 16–30. doi: 10.17159/2309-8775/2015/v57n1a2.

Du Plessis, J. A. and Loots, W. (2019) 'Re-evaluation of area reduction factors and their impact on floods in South Africa', *Arabian Journal of Geosciences*. Arabian Journal of Geosciences, 12(11). doi: 10.1007/s12517-019-4507-9.

Prudhomme, C. (1999) 'Mapping a statistic of extreme rainfall in a mountainous region', *Physics and Chemistry of the Earth, Part B: Hydrology, Oceans and Atmosphere*, 24(1–2), pp. 79–84. doi: 10.1016/S1464-1909(98)00015-X.

Pullen, R., Wiederhold, J. and Midgley, D. (1966) 'STORM STUDIES IN SOUTH AFRICA : LARGE- AREA STORMS : DEPTH-AREA-DU RATION ANALY-SIS BY DIGITAL COMPUTER', *The Civil Engineer in South Africa*, pp. 173–187.

Rodriguez-Iturbe, I. and Mejía, J. (1974) 'On the transformation of point rainfall to areal rainfall', *Water Resour. Res., 10 (4)*, pp. 729–735.

SANRAL (2013) *Drainage Manual*. South African National Roads Agency Limited.

Sinclair, S. and Pegram, G. (2005) 'Combining radar and rain gauge rainfall estimates using conditional merging', *Atmospheric Science Letters*, 6(1), pp. 19–22. doi: 10.1002/asl.85.

Siriwardena, L. and Wienmann, P. (1996) 'Derivation of Areal Reduction Factors for Design Rainfalls in Victoria', (Report No 96/4).

Skaugen, T. (1997) 'Classification of rainfall into small- and large-scale events by statistical pattern recognition', *Journal of Hydrology*, 200(1–4), pp. 40–57. doi: 10.1016/S0022-1694(97)00003-6.

Van der Spuy, D. and Rademeyer, P. (2018) 'Flood Frequency Estimation Methods as Applied in the Department of Water and Sanitation'.

Stewart, E. J. (1989) 'Areal reduction factors for design storm construction: Joint use of raingauge and radar data', *IAHS Publ.*, 181(181), pp. 31–49.

Supino, G. (1964) 'Le reti idrauliche'.

Svensson, C. and Jones, D. A. (2010) 'Review of methods for deriving areal reduction factors',

Journal of Flood Risk Management, 3(3), pp. 232–245. doi: 10.1111/j.1753-318X.2010.01075.x.

Terblanche, D. (1996) 'A simple digital signal processing method to simulate linear and quadratic responses from a radar's loga- rithmic receiver. J. Atmos. Ocean. Technol. 10, 785–797', *Journal of Atmospheric Oceanic Technology*, 10, pp. 785–797.

Terblanche, D. E., Pegram, G. G. S. and Mittermaier, M. P. (2001) 'The development of weather radar as a research and operational tool for hydrology in south africa', *Journal of Hydrology*, 241(1–2), pp. 3–25. doi: 10.1016/S0022-1694(00)00372-3.

Veneziano, D. and Langousis, A. (2005) 'The areal reduction factor : A multifractal analysis', 41, pp. 1–15. doi: 10.1029/2004WR003765.

Waymire, E., Gupta, V. and Rodriguez-Iturbe, I. (1984) 'A spectral theory of a rainfall intensity field at the meso-β scale', *Water Resources Research*, 10(10), pp. 1453–1465.

Wolff, C. (2002) *Radar Basics*. Available at: http://www.radartutorial.eu/07.waves/Waves and Frequency Ranges.en.html.

Wright, D. B. *et al.* (2013) 'Estimating the frequency of extreme rainfall using weather radar and stochastic storm transposition', *Journal of Hydrology*. Elsevier B.V., 488, pp. 150–165. doi: 10.1016/j.jhydrol.2013.03.003.

Wright, D. B., Smith, J. A. and Baeck, M. L. (2014) 'Critical Examination of Area Reduction Factors', *Journal of Hydrologic Engineering*, 19(4), pp. 769–776. doi: 10.1061/(ASCE)HE.1943-5584.0000855.

Van Wyk, W. (1965) *Aids to the Prediction of Extreme Floods from Small Watersheds*. University of the Witwatersrand.

A. APPENDIX A

```
/**********************************************************************
 * TDRP params for MdvConvert
 **********************************************************************/

//======================================================================
//
// Program name: MdvConvert.
//
// MdvConvert reads mdv data, converts it in various ways, and writes it
//   out. The usage is 'MdvConvert -params params_file'.
//
//======================================================================

//======================================================================
// Convert UAE Merge for GCC use to NetCDF.
//======================================================================

//======================================================================
//
// DEBUGGING AND PROCESS CONTROL.
//
//======================================================================

////////////// debug ///////////////////////////////////
//
// Debug option.
// If set, debug messages will be printed appropriately.
//
// Type: enum
// Options:
//     DEBUG_OFF
//     DEBUG_NORM
//     DEBUG_VERBOSE
//

debug = DEBUG_OFF;

////////////// instance ////////////////////////////////
//
// Process instance.
// Used for registration with procmap.
// Type: string
//
```

```
instance = "precip";

////////////// reg_interval ////////////////////////////
//
// Registration interval.
// The number of seconds between expected procmap registrations.
// Type: int
//

reg_interval = 60;

//======================================================================
//
// DATA INPUT.
//
//======================================================================

////////////// mode ////////////////////////////////////
//
// Operating mode.
// In REALTIME mode, the program waits for a new input file.
//   LOCAL_FILEPATH_REALTIME is a realtime mode used when data resides on
//   the host where the application is running. This was added due to the
//   problems that the data server layer had distinguishing data times of
//   data written very close together. NOTE that in this mode the
//   input_url parameter should be set to an input directory, not an input
//   url. In ARCHIVE mode, it moves through the data between the start and
//   end times set on the command line. In SPEC_FCAST_REALTIME mode, the
//   program waits for a new input file that is a forecast file with the
//   specified forecast lead time. The forecast lead time is specified in
//   the fcast_lead_time parameter. In FILELIST mode, it moves through the
//   list of file names specified on the command line. Paths (in FILELIST
//   mode, at least) MUST contain a day-directory below the data file --
//   ./data_file.mdv will not work as a file path. In ARCHIVE_FCST mode,
//   it moves through the data between the start and end times set on the
//   comand line, and processes all lead times found in the forecast
//   files. In SPEC_FCST_ARCHIVE mode, it moves through the data between
//   the start and end times set on the comand line, and processes
//   forecast files with the specified forecast lead time.
//
// Type: enum
// Options:
//     ARCHIVE
//     REALTIME
//     FILELIST
```

```
//      SPEC_FCAST_REALTIME
//      REALTIME_FCST_DATA
//      LOCAL_FILEPATH_REALTIME
//      ARCHIVE_FCST
//      SPEC_FCST_ARCHIVE
//

mode = FILELIST;

////////////// local ///////////////////////////////////
//
// Setup for LOCAL_FILEPATH_REALTIME mode ONLY. Max age of input,
//   seconds, if we use latest data info to trigger, and if we should only
//   process the latest file.
// Defaults should generally be fine.
//
// Type: struct
//   typedef struct {
//      int lookback;
//      boolean use_ldata_info;
//      boolean latest_file_only;
//   }
//
//

local = {
    lookback = 1200,
    use_ldata_info = TRUE,
    latest_file_only = FALSE
};

////////////// input_url ///////////////////////////////
//
// URL for input data.
// This is used in REALTIME and ARCHIVE modes only. In FILELIST mode,
//   the file paths are specified on the command line. In
//   LOCAL_FILEPATH_REALTIME mode, set this to a directory, not a URL.
// Type: string
//

input_url = "$(DATA_DIR)/mdv/precip/1hr";

////////////// writeLdataInfo //////////////////////////
//
// Write _latest_data_info files for output files.
```

```
// If false, will suppress writing of _latest_data_info files.
// Type: boolean
//

writeLdataInfo = TRUE;

////////////// fcast_lead_time ////////////////////////
//
// Forecast lead time information for forecast files to be processed.
// Used only if mode is set to SPEC_FCAST_REALTIME or SPEC_FCST_ARCHIVE.
//
// Type: struct
//   typedef struct {
//      int lead_time_secs;
//      boolean use_gen_time;
//   }
//
//

fcast_lead_time = {
    lead_time_secs = 0,
    use_gen_time = FALSE
};

////////////// do_lead_time_subsampling ////////////////
//
// Lead time subsampling flag.
// Set to true to enable lead time subsampling.  Used only if mode is
//   REALTIME_FCST_DATA or ARCHIVE_FCST.
// Type: boolean
//

do_lead_time_subsampling = FALSE;

////////////// subsample_lead_time_hour ////////////////
//
// The subsampled lead times to process.
// Type: double
// 1D array - variable length.
//

subsample_lead_time_hour = { 0 };

////////////// set_field_nums //////////////////////////
//
```

```
// Option to set field numbers.
// Type: boolean
//

set_field_nums = FALSE;

////////////// field_nums ////////////////////////////
//
// Field number list.
// Type: int
// 1D array - variable length.
//

field_nums = {
 0
};

////////////// set_field_names ////////////////////////
//
// Option to set field names.
// Type: boolean
//

set_field_names = FALSE;

////////////// field_names ////////////////////////////
//
// Field name list.
// Type: string
// 1D array - variable length.
//

field_names = {
 "0"
};

////////////// rename_fields //////////////////////////
//
// Option to set field names.
// Type: boolean
//

rename_fields = FALSE;

////////////// new_names ////////////////////////////
```

```
//
// Provides a map from old field name to new field name. Note that
//   either the filed name or the long field name must match the
//   old_field_name specified for the renaming to take effect, and that if
//   the renaming happens then both the field name and the long field name
//   are renamed to the new_field_name.
//
// Type: struct
//   typedef struct {
//      string old_field_name;
//      string new_field_name;
//   }
//
// 1D array - variable length.
//

new_names = {
  {
    old_field_name = "",
    new_field_name = ""
  }
};

////////////// apply_thresholds_to_field_values ////////
//
// Option to threshold field values. Points with values outside the
//   specified limits will be set to missing.
// NOTE: this works on the output field names. If rename_fields is
//   false, then the input and output field names are the same. If rename
//   fields is true, the field name change is performed first, before the
//   field values are thresholded.
// Type: boolean
//

apply_thresholds_to_field_values = TRUE;

////////////// thresholded_fields ///////////////////////
//
// Limit the values in specified fields to between min_threshold and
//   max_threshold. Values outside this range will be set to missing.
//
// Type: struct
//   typedef struct {
//      string output_field_name;
//      double threshold_min;
```

```
//      double threshold_max;
//   }
//
// 1D array - variable length.
//

thresholded_fields = {
  {
    output_field_name = "precip",
    threshold_min = 0,
    threshold_max = 250
  }
};

//========================================================================
//
// DATA OUTPUT.
//
//========================================================================

////////////// output_url ////////////////////////////
//
// Output URL.
// Output data is written to this URL.
// Type: string
//

output_url = "$(DATA_DIR)/netcdf/precip1hr";

////////////// output_as_forecast ////////////////////
//
// Set to output the data as forecast in mdv format.
// This forces a forecast-style output, whether the data is of forecast
//   type or not.
// Type: boolean
//

output_as_forecast = FALSE;

////////////// if_forecast_output_as_forecast //////////
//
// Set to output the data as forecast, if the data is of a forecast
//   type.
// This only writes out in forecast-style output if the
//   data_collection_type in the master header is of type FORECAST or
```

```
//   EXTRAPOLATED.
// Type: boolean
//

if_forecast_output_as_forecast = FALSE;

////////////// output_format ////////////////////////////
//
// Specify format of file on output.
// FORMAT_MDV: normal MDV formal. FORMAT_XML: XML format. XML format
//   writes out 2 files: *.mdv.xml and *.mdv.buf. The xml file contains
//   the meta-data. The buf file contains the binary fields.
// NOTE: only COMPRESSION_NONE and COMPRESSION_GZIP_VOL are supported in
//   XML. FORMAT_NCF: write file in netCDF CF format. Extension will be
//   .nc.
//
// Type: enum
// Options:
//     OUTPUT_FORMAT_MDV
//     OUTPUT_FORMAT_XML
//     OUTPUT_FORMAT_NCF
//

output_format = OUTPUT_FORMAT_NCF;

////////////// write_to_path ////////////////////////////
//
// Write the file to a specified path.
// This overrides output_url.
// Type: boolean
//

write_to_path = FALSE;

////////////// output_path ////////////////////////////
//
// Output path.
// See 'write_to_path'.
// Type: string
//

output_path = "./output/test.mdv";

//======================================================================
//
```

```
// GEOMETRY CONVERSION.
//
//=========================================================================

////////////// set_horiz_limits ////////////////////////
//
// Option to set horizontal limits.
// Type: boolean
//

set_horiz_limits = FALSE;

////////////// horiz_limits ////////////////////////////
//
// Set horizontal limits.
//
// Type: struct
//   typedef struct {
//      float min_lat;
//      float min_lon;
//      float max_lat;
//      float max_lon;
//   }
//
//

horiz_limits = {
    min_lat = -90,
    min_lon = -180,
    max_lat = 90,
    max_lon = 180
};

////////////// set_vlevel_limits ///////////////////////
//
// Option to set plane vlevel limits.
// Mutually exclusive with set_plane_num_limits.
// Type: boolean
//

set_vlevel_limits = FALSE;

////////////// lower_vlevel ////////////////////////////
//
// Lower plane vlevel limit.
```

```
// Type: float
//

lower_vlevel = 0;

////////////// upper_vlevel ////////////////////////////
//
// Upper plane vlevel limit.
// Type: float
//

upper_vlevel = 0;

////////////// override_vlevels ////////////////////////
//
// Option to override the vlevels in the vlevel header.
// If true, will replace the vlevels in the header with those specified
//   in 'vlevel_array'. This does not affect the actual data in the file.
// Type: boolean
//

override_vlevels = FALSE;

////////////// vlevel_array ////////////////////////////
//
// vlevel values to override what is already in the file.
// See 'override_vlevels'.
// Type: double
// 1D array - variable length.
//

vlevel_array = {
 0
};

////////////// set_plane_num_limits ////////////////////
//
// Option to set plane number limits.
// Mutually exclusive with set_vlevel_limits.
// Type: boolean
//

set_plane_num_limits = FALSE;

////////////// lower_plane_num /////////////////////////
```

```
//
// Lower plane num limit.
// Type: int
//

lower_plane_num = 0;

////////////// upper_plane_num ////////////////////////
//
// Upper plane num limit.
// Type: int
//

upper_plane_num = 0;

////////////// composite ///////////////////////////////
//
// Option for creating composite.
// Composite is a plane in which each grid location contains the maximum
//   value at any height.
// Type: boolean
//

composite = FALSE;

////////////// remap_z_to_constant_grid ////////////////
//
// Option to remap the Z levels onto a grid with constant dz.
// Field data will be remapped onto the specified Z levels using the
//   nearest neighbor method. See 'remap_z_grid'. Note that this actually
//   changes the data. Whereas 'override_vlevels' only changes the vlevels
//   in the headers, and does not change the data.
// Type: boolean
//

remap_z_to_constant_grid = FALSE;

////////////// remap_z_grid ////////////////////////////
//
// Specified Z levels for remapping.
//
// Type: struct
//   typedef struct {
//      int nz;
//      double minz;
```

```
//      double dz;
//   }
//
//

remap_z_grid = {
    nz = 18,
    minz = 0,
    dz = 1
};

////////////// remap_xy ////////////////////////////////
//
// Option to remap grid in x,y.
// If true, set the remap parameters below.
// Type: boolean
//

remap_xy = FALSE;

////////////// auto_remap_to_latlon ////////////////////
//
// Option to automatically remap the grid to a lat-lon projection.
// If true, the data in the file will be remapped to a latlon grid which
//   matches the existing grid in resolution and extent. Other remap
//   parameters will be ignored.
// Type: boolean
//

auto_remap_to_latlon = FALSE;

////////////// remap_at_source /////////////////////////
//
// Flag indicating where to do the remapping.
// If set to true, the remapping is done on the source machine by
//   setting the remapping in the MDV read request. This is the default.If
//   set to false, the remapping is done on the destination machine by
//   doing a remap command after the read is done. This is useful if you
//   are reading the data from a machine that is overloaded.
// Type: boolean
//

remap_at_source = FALSE;

////////////// remap_projection ////////////////////////
```

```
//
// Projection for remapping in x,y. See projection param below.
//     PROJ_LATLON: simple lat/lon grid (Equidistant Cylindrical)
//     PROJ_FLAT: Azimuthal Equidistant (Radar)
//     PROJ_LAMBERT_CONF: Lambert Conformal Conic
//     PROJ_LAMBERT_AZIM: Lambert Azimuthal Equal Area
//     PROJ_MERCATOR: Mercator - EW orientation
//     PROJ_TRANS_MERCATOR: Tranverse Mercator - NS orientation
//     PROJ_POLAR_STEREO: Stereographic- polar aspect
//     PROJ_OBLIQUE_STEREO: Stereographic - oblique aspect
//     PROJ_ALBERS: Albers Equal Area Conic
//     PROJ_VERT_PERSP: Vertical Perspective (satellite view).
//
// Type: enum
// Options:
//     PROJ_LATLON
//     PROJ_LAMBERT_CONF
//     PROJ_MERCATOR
//     PROJ_POLAR_STEREO
//     PROJ_FLAT
//     PROJ_OBLIQUE_STEREO
//     PROJ_TRANS_MERCATOR
//     PROJ_ALBERS
//     PROJ_LAMBERT_AZIM
//     PROJ_VERT_PERSP
//

remap_projection = PROJ_LATLON;

////////////// remap_grid ///////////////////////////////
//
// Grid parameters for remapping in x,y.
// Units in km, except for LATLON, which is in degrees.
//
// Type: struct
//   typedef struct {
//      int nx;
//      int ny;
//      double minx;
//      double miny;
//      double dx;
//      double dy;
//   }
//
//
```

```
remap_grid = {
    nx = 1,
    ny = 1,
    minx = 0,
    miny = 0,
    dx = 1,
    dy = 1
};

////////////// remap_rotation ////////////////////////
//
// Remapped grid rotation.
// This applies only to PROJ_FLAT projections.
// Type: double
//

remap_rotation = 0;

////////////// remap_origin_lat ////////////////////////
//
// Remapped grid origin latitude.
// This applies to all projections except LATLON.
// Type: double
//

remap_origin_lat = 0;

////////////// remap_origin_lon ////////////////////////
//
// Remapped grid origin longitude.
// This applies to all projections except LATLON.
// Type: double
//

remap_origin_lon = 0;

////////////// remap_lat1 ////////////////////////////
//
// Remapped grid reference latitude 1.
// This applies to LAMBERT_CONF and ALBERS projections.
// Type: double
//

remap_lat1 = 0;
```

```
////////////// remap_lat2 ////////////////////////////
//
// Remapped grid reference latitude 2.
// This applies to LAMBERT_CONF and ALBERS projections.
// Type: double
//

remap_lat2 = 0;

////////////// remap_central_scale //////////////////////
//
// Central scale for remapped projections.
// This applies to POLAR_STEREO, OBLIQUE_STEREO and TRANSVERSE_MERCATOR
//   projections.
// Type: double
//

remap_central_scale = 1;

////////////// remap_tangent_lat ////////////////////////
//
// Remapped tangent latitude (deg).
// This applies to OBLIQUE_STEREO only.
// Type: double
//

remap_tangent_lat = 0;

////////////// remap_tangent_lon ////////////////////////
//
// Remapped tangent longitude (deg).
// This applies to OBLIQUE_STEREO and POLAR_STEREO.
// Type: double
//

remap_tangent_lon = 0;

////////////// remap_pole_is_north //////////////////////
//
// Flag indicating stereogtraphic is over the NORTH pole.
// This applies to POLAR_STEREO. If false, the projection is over the
//   south pole.
// Type: boolean
//
```

```
remap_pole_is_north = TRUE;

////////////// remap_persp_radius ///////////////////////
//
// Radius of perspective point (km).
// This applies to VERT_PERSP.
// Type: double
//

remap_persp_radius = 35786;

////////////// remap_false_northing ////////////////////
//
// Remapped false northing correction.
// Occasionally, this is added to the Y coordinate so that all
//   coordinates are positive. Normally 0. As an alternative to
//   false_northing and false_easting, you can set the offset_latitude and
//   offset_longitude.
// Type: double
//

remap_false_northing = 0;

////////////// remap_false_easting /////////////////////
//
// Remapped false easting correction.
// Occasionally, this is added to the X coordinate so that all
//   coordinates are positive. Normally 0.
// Type: double
//

remap_false_easting = 0;

////////////// remap_set_offset_origin /////////////////
//
// Do you want to specify an offset origin using lat/lon instead of
//   false_northing and false_easting?.
// If true, set remap_offset_origin_latitude and
//   remap_offset_origin_longitude.
// Type: boolean
//

remap_set_offset_origin = FALSE;
```

```
////////////// remap_offset_origin_latitude ////////////
//
// Latitude of offset origin.
// See remap_set_offset_origin.
// Type: double
//

remap_offset_origin_latitude = 0;

////////////// remap_offset_origin_longitude ///////////
//
// Longitude of offset origin.
// See remap_set_offset_origin.
// Type: double
//

remap_offset_origin_longitude = 0;

//=============================================================================
//
// ENCODING AND COMPRESSION CONVERSION.
//
//=============================================================================

////////////// encoding_type ///////////////////////////
//
// Set encoding type.
//
// Type: enum
// Options:
//     ENCODING_ASIS
//     ENCODING_INT8
//     ENCODING_INT16
//     ENCODING_FLOAT32
//

encoding_type = ENCODING_ASIS;

////////////// compression_type ////////////////////////
//
// Set compression type.
// See <toolsa/compress> for details on the compression types.
//
// Type: enum
// Options:
```

```
//     COMPRESSION_ASIS
//     COMPRESSION_NONE
//     COMPRESSION_RLE
//     COMPRESSION_LZO
//     COMPRESSION_ZLIB
//     COMPRESSION_BZIP
//     COMPRESSION_GZIP
//     COMPRESSION_GZIP_VOL
//     COMPRESSION_TYPES_N
//

compression_type = COMPRESSION_GZIP;

////////////// force_scale_change //////////////////////
//
// Option to force a scaling change in the data.
// If this option is chosen, the data is read in as float data and then
//   is converted to the chosen output encoding type using the scaling
//   options specified below.
// NOTE: When using this option, if you set the encoding_type option to
//   ENCODING_ASIS, the output will use FLOAT32 encoding.
// Type: boolean
//

force_scale_change = FALSE;

////////////// scaling_type ////////////////////////////
//
// Set scaling type.
// This is only relevant when converting from float32 to int8 or int16
//   or if force_scale_change is set.
//
// Type: enum
// Options:
//     SCALING_ASIS
//     SCALING_NONE
//     SCALING_ROUNDED
//     SCALING_INTEGRAL
//     SCALING_DYNAMIC
//     SCALING_SPECIFIED
//

scaling_type = SCALING_ROUNDED;

////////////// scale ///////////////////////////////////
```

```
//
// Input scaling scale.
// For SCALING_SPECIFIED only.
// Type: float
//

scale = 1;

////////////// bias ////////////////////////////////
//
// Input scaling bias.
// For SCALING_SPECIFIED only.
// Type: float
//

bias = 0;

//=====================================================================
//
// DECIMATION.
//
//=====================================================================

////////////// decimate ////////////////////////////////
//
// Option to decimate in x,y.
// If true, each plane is decimated to force the number of grid points
//   to be less than 'decimate_max_nxy'.
// Type: boolean
//

decimate = FALSE;

////////////// decimate_max_nxy ////////////////////////
//
// Max number of xy grid points in decimation.
// See 'decimate'.
// Type: int
//

decimate_max_nxy = 1000000;

//=====================================================================
//
// INVERT PLANES IN THE VERTICAL SENSE.
```

```
//
//=========================================================================

///////////// invert_vertically ///////////////////////
//
// Invert the vertical levels in all fields.
// This inversion is applied after the remap, forced scale change,
//   overriding of V levels, and linear transformations.
// Type: boolean
//

invert_vertically = FALSE;

//=========================================================================
//
// BYTE ORDERING.
//
//=========================================================================

///////////// input_be ////////////////////////////////
//
// Are input files big-endian.
// Type: boolean
//

input_be = TRUE;

///////////// output_be ///////////////////////////////
//
// Are output files big-endian.
// Type: boolean
//

output_be = TRUE;

//=========================================================================
//
// APPLY LINEAR TRANSFORM FUNCTION TO SELECTED FIELDS.
//
//=========================================================================

///////////// apply_linear_transform //////////////////
//
// Option to apply a linear transform function to the data in selected
//   data fields.
```

```
// Field names and transform parameters are given in linear_transforms
//   parameter.
// Type: boolean
//

apply_linear_transform = FALSE;

////////////// linear_transforms ///////////////////////
//
// Array specifying the transform functions and the field names to which
//   they apply.
// The transform will only be applied to the specified fields. If a
//   field which is specified does not exist, a warning will be issued.
//
// Type: struct
//   typedef struct {
//      string field_name;
//      double scale;
//      double bias;
//   }
//
// 1D array - variable length.
//

linear_transforms = {
  {
    field_name = "DBZ",
    scale = 1,
    bias = 0
  }
};

//========================================================================
//
// WRITE USING EXTENDED PATHS.
//
// This will be overridden if the environment variable
//   MDV_WRITE_USING_EXTENDED_PATHS exists and is set to TRUE.
//
//========================================================================

////////////// write_using_extended_paths //////////////
//
// Option to write files with extended paths.
// If specified, this will override that specified by the client.
```

```
//   Default is FALSE.

// If set, paths will include a separate year subdirectory, and the file
//   name will include date and time.

// Non-forecast path:
//   dir/yyyy/yyyymmdd/yyyymmdd_hhmmss.mdv.

// Forecast path:
//   dir/yyyy/yyyymmdd/yyyymmdd_g_hhmmss_f_llllllll.mdv.
// Type: boolean
//

write_using_extended_paths = TRUE;

//========================================================================
//
// CONTROL OF CONVERSION TO NETCDF.
//
// The following parameters control conversion of MDV files to NetCDF
//   CF-compliant files.
//
//========================================================================

////////////// ncf_set_global_attributes ///////////////
//
// Option to set specify global attributes in the NCF file.
// The global attributes are 'institution', 'references' and 'comment'.
// Type: boolean
//

ncf_set_global_attributes = TRUE;

////////////// ncf_global_attributes ///////////////////
//
// Global attributes for netCDF file.
// These strings will be included as global attributes in the NetCDF
//   file. Other global attributes will be determined from the MDV
//   headers.
//
// Type: struct
//   typedef struct {
//      string institution;
//      string references;
//      string comment;
```

```
//   }
//
//

ncf_global_attributes = {
    institution = "SAWS",
    references = "SA Radar Merge Precip 1hr",
    comment = "Converted by MdvConvert"
};

////////////// ncf_transform_fields ////////////////////
//
// Option to tranform field names, units and values when converting MDV
//   to NCF.
// Type: boolean
//

ncf_transform_fields = FALSE;

////////////// ncf_field_transforms ////////////////////
//
// List of transforms. If mdv_field_name is found in the MDV data, these
//   other parameters will be used to set the field variable in the netCDF
//   file.
// See mdv2ncf_transform_fields.
//
// Type: struct
//   typedef struct {
//      string mdv_field_name;
//      string ncf_field_name;
//      string ncf_standard_name;
//      string ncf_long_name;
//      string ncf_units;
//      boolean do_linear_transform;
//      float linear_multiplier;
//      float linear_const;
//      data_pack_t packed_data_type;
//        Options:
//          DATA_PACK_FLOAT
//          DATA_PACK_SHORT
//          DATA_PACK_BYTE
//          DATA_PACK_ASIS
//   }
//
// 1D array - variable length.
```

```
//

ncf_field_transforms = {
  {
    mdv_field_name = "mdv_field_name",
    ncf_field_name = "ncf_field_name",
    ncf_standard_name = "ncf_standard_name",
    ncf_long_name = "ncf_long_name",
    ncf_units = "ncf_units",
    do_linear_transform = FALSE,
    linear_multiplier = 1,
    linear_const = 0,
    packed_data_type = DATA_PACK_ASIS
  }
};

////////////// ncf_compress_data ///////////////////////
//
// Option to compress field data.
// Only applies to NETCDF4 and  NETCDF4_CLASSIC files.
// Type: boolean
//

ncf_compress_data = TRUE;

////////////// ncf_compression_level ///////////////////
//
// Compression level from 1 to 9 with 9 being the greatest compression.
//   Default is 9.
// Only applies to NETCDF4 and  NETCDF4_CLASSIC files.
// Type: int
//

ncf_compression_level = 9;

////////////// ncf_filename_suffix /////////////////////
//
// Suffix of netCDF files.
// File extension is always .nc. File name will end with mdv.suffix.nc.
//   Set to the empty string for no suffix, in which case file name will
//   end with .mdv.nc.
// Type: string
//

ncf_filename_suffix = "";
```

```
////////////// ncf_file_format ////////////////////////
//
// NetCDF file format.
// netCDF classic format, netCDF 64-bit offset format, netCDF4 using
//   HDF5 format, netCDF4 using HDF5 format but only netCDF3 calls.
//
// Type: enum
// Options:
//     CLASSIC
//     NC64BIT
//     NETCDF4
//     NETCDF4_CLASSIC
//

ncf_file_format = NETCDF4;

////////////// ncf_polar_radar_file_type ///////////////
//
// Output format for polar radar data.
//
// Type: enum
// Options:
//     FILE_TYPE_CF
//     FILE_TYPE_CF_RADIAL
//     FILE_TYPE_DORADE
//     FILE_TYPE_UF
//

ncf_polar_radar_file_type = FILE_TYPE_CF;

////////////// ncf_output_latlon_arrays ////////////////
//
// If true latitude and longitude arrays of each grid point are output.
// The CF convention requires that these arrays are present in the
//   netCDF file; however, the information is redundant since the lat and
//   lon arrays could be constructed using the other projection and grid
//   information required with a gridded data field.
// Type: boolean
//

ncf_output_latlon_arrays = TRUE;

////////////// ncf_output_mdv_attributes ///////////////
//
```

```
// Option to output non-CF compliant MDV attributes.
// If true, MDV attributes which are not CF compliant will be output.
//   This will facilitate the translation of the data back into MDV with
//   the minimal loss of information.
// Type: boolean
//

ncf_output_mdv_attributes = TRUE;

////////////// ncf_output_mdv_chunks ////////////////////
//
// Option to output non-CF compliant MDV chunks.
// If true, MDV chunks will be included as byte binary variables.
// Type: boolean
//

ncf_output_mdv_chunks = T
```

B. APPENDIX B

Table B.1: Results

	Date	Cell Count	Rainfall			Area of Storm (km²)		Max Point Precipitation (mm)	Max Point Intensity	ARF		Region (Convective/ Frontal)
			Areal Average (mm)	Isohyetal (mm)	ArcGIS (mm)	Precipitation Array	ArcGIS			ARF Isohyetal (%)	ARF ArcGIS (%)	
1 hr	24/01/2016	357	28.05	28.58	27.54	1054.75	1187.39	57.50	57.50	49.70%	47.89%	Frontal
1 hr	06/02/2016	142	24.50	24.89	24.80	419.54	430.39	32.20	32.20	77.31%	77.03%	Convective
1 hr	25/02/2016	89	35.72	36.38	38.49	262.95	262.51	62.50	62.50	58.20%	61.58%	Costal
1 hr	09/03/2016	85	31.62	32.26	30.64	251.13	311.35	53.50	53.50	60.31%	57.27%	Convective
1 hr	10/03/2016	11	27.11	27.95	27.50	32.50	33.58	37.00	37.00	75.55%	74.32%	Frontal
1 hr	14/03/2016	264	26.29	26.63	26.42	779.98	775.32	38.60	38.60	68.99%	68.44%	Convective
1 hr	17/03/2016	181	36.57	36.95	37.32	534.76	521.96	56.50	56.50	65.39%	66.06%	Frontal
1 hr	22/10/2016	1852	28.88	29.26	28.85	5471.70	5744.67	70.00	70.00	41.80%	41.21%	Frontal
1 hr	23/10/2016	1625	27.70	28.11	28.05	4801.03	4847.25	50.50	50.50	55.67%	55.55%	Frontal
1 hr	26/10/2016	203	38.12	38.51	38.23	599.76	644.06	60.50	60.50	63.65%	63.20%	Convective
1 hr	05/11/2016	18	23.71	24.44	24.04	53.18	39.68	30.00	30.00	81.48%	80.13%	Frontal
1 hr	10/11/2016	2857	37.39	37.65	37.44	8440.96	9013.81	81.50	81.50	46.19%	45.94%	Convective
1 hr	11/11/2016	2044	32.82	33.14	32.48	6038.96	7057.21	54.50	54.50	60.81%	59.60%	Convective
1 hr	30/11/2016	257	32.09	32.48	32.37	759.30	802.79	48.50	48.50	66.97%	66.74%	Frontal
1 hr	13/12/2016	168	29.05	29.35	28.85	496.35	521.96	47.60	47.60	61.65%	60.85%	Convective
1 hr	19/12/2016	568	32.50	32.90	33.15	1678.15	1654.42	60.00	60.00	54.83%	55.24%	Frontal
1 hr	03/01/2017	122	44.13	44.47	44.42	360.45	345.42	81.00	81.00	54.90%	54.84%	Convective
1 hr	04/01/2017	233	35.87	36.17	36.08	688.39	699.01	59.50	59.50	60.79%	60.64%	Convective
1 hr	06/01/2017	144	24.38	24.83	24.74	425.45	436.50	33.00	33.00	75.23%	74.96%	Convective
1 hr	07/01/2017	63	28.96	28.85	29.61	186.13	137.36	44.20	44.20	65.27%	66.10%	Convective
1 hr	26/01/2017	130	34.29	34.58	34.38	384.08	381.55	69.50	69.50	49.75%	49.47%	Convective

	Date	Cell Count	Rainfall			Area of Storm (km²)		Max Point Precipitation (mm)	Max Point Intensity	ARF		Region (Convective/ Frontal)
			Areal Average (mm)	Isohyetal (mm)	ArcGIS (mm)	Precipitation Array	ArcGIS			ARF Isohyetal (%)	ARF ArcGIS (%)	
1 hr	27/01/2017	94	34.73	35.27	33.51	277.72	210.62	59.50	59.50	59.27%	56.33%	Frontal
1 hr	30/01/2017	173	32.93	33.16	33.15	511.13	515.86	57.00	57.00	58.18%	58.16%	Convective
1 hr	09/02/2017	16	28.76	28.75	29.09	47.27	67.15	38.60	38.60	74.48%	75.37%	Convective
1 hr	20/02/2017	118	22.65	23.39	22.50	348.63	3.05	31.00	31.00	75.45%	72.58%	Convective
1 hr	21/02/2017	76	22.79	23.36	23.50	224.54	30.52	31.40	31.40	74.38%	74.84%	Convective
1 hr	06/04/2017	129	29.43	29.90	29.79	381.13	360.19	42.50	42.50	70.36%	70.09%	Frontal
1 hr	30/09/2017	74	29.72	30.20	30.17	218.63	222.83	44.20	44.20	68.33%	68.26%	Convective
1 hr	23/11/2017	106	27.88	27.88	27.76	313.18	351.03	39.60	39.60	70.40%	70.10%	Convective
1 hr	27/11/2017	45	23.90	24.39	26.73	132.95	39.68	31.80	31.80	76.69%	69.98%	Convective
1 hr	06/12/2017	58	32.61	32.76	32.35	171.36	100.73	65.50	65.50	50.01%	49.39%	Convective
1 hr	29/12/2017	67	31.37	31.75	32.28	197.95	210.62	53.50	53.50	59.35%	60.34%	Frontal
3 hr	08/03/2016	78	33.91	34.04	34.31	230.45	210.62	48.44	16.15	70.27%	70.83%	Convective
3 hr	09/03/2016	175	34.74	34.87	35.00	517.03	567.75	55.52	18.51	62.81%	63.04%	Convective
3 hr	16/03/2016	515	48.84	48.73	51.91	1521.56	1251.49	130.71	43.57	37.28%	39.72%	Frontal
3 hr	26/04/2016	274	47.36	47.59	47.54	809.53	778.37	97.60	32.53	48.76%	48.71%	Convective
3 hr	26/04/2016	818	47.55	47.61	47.73	2416.77	2521.30	101.76	33.92	46.79%	46.91%	Convective
3 hr	14/05/2016	337	57.00	57.13	56.78	995.66	1031.72	114.15	38.05	50.05%	49.74%	Convective
3 hr	26/07/2016	922	44.51	44.64	44.74	2724.03	2734.97	142.71	47.57	31.28%	31.35%	Frontal
3 hr	22/10/2016	524	41.06	41.16	41.52	1548.15	1611.68	71.90	23.97	57.26%	57.76%	Convective
3 hr	22/10/2016	2125	39.99	40.13	40.05	6278.28	6559.66	105.43	35.14	38.06%	37.99%	Convective
3 hr	26/10/2016	192	52.62	52.81	53.02	567.26	613.54	98.60	32.87	53.56%	53.77%	Convective
3 hr	11/11/2016	1016	54.69	54.71	55.99	3001.75	2960.85	127.02	42.34	43.08%	44.08%	Convective
3 hr	20/11/2016	951	45.52	45.64	45.46	2809.71	2869.28	86.10	28.70	53.01%	52.80%	Convective
3 hr	26/11/2016	63	42.65	42.66	41.78	186.13	210.62	90.70	30.23	47.03%	46.06%	Convective
3 hr	30/11/2016	60	29.62	29.92	29.96	177.27	198.41	39.55	13.18	75.64%	75.75%	Convective

	Date	Cell Count	Rainfall			Area of Storm (km²)		Max Point Precipitation (mm)	Max Point Intensity	ARF		Region (Convective/ Frontal)
			Areal Average (mm)	Isohyetal (mm)	ArcGIS (mm)	Precipitation Array	ArcGIS			ARF Isohyetal (%)	ARF ArcGIS (%)	
3 hr	04/12/2016	38	48.30	48.42	48.42	112.27	115.99	75.86	25.29	63.83%	63.83%	Convective
3 hr	07/12/2016	243	51.92	51.97	52.48	717.94	753.95	116.43	38.81	44.63%	45.07%	Convective
3 hr	19/12/2016	241	38.89	38.93	39.47	712.03	744.79	68.17	22.72	57.11%	57.90%	Convective
3 hr	03/01/2017	218	38.33	38.49	38.37	644.08	613.54	69.87	23.29	55.08%	54.92%	Convective
3 hr	04/01/2017	543	63.51	63.47	63.09	1604.28	1672.73	161.53	53.84	39.29%	39.06%	Convective
3 hr	07/01/2017	490	33.41	33.60	33.35	1447.70	1510.95	67.46	22.49	49.81%	49.43%	Convective
3 hr	07/01/2017	213	39.12	39.24	39.00	629.30	680.69	115.94	38.65	33.84%	33.64%	Convective
3 hr	20/01/2017	54	45.95	46.20	46.89	159.54	201.46	98.82	32.94	46.75%	47.45%	Convective
3 hr	26/01/2017	125	50.21	50.30	49.38	369.31	366.29	100.53	33.51	50.03%	49.11%	Convective
3 hr	30/01/2017	504	42.90	43.13	42.63	1489.06	1514.00	147.37	49.12	29.26%	28.93%	Convective
3 hr	21/02/2017	268	30.78	31.10	31.15	791.80	769.21	44.95	14.98	69.20%	69.31%	Convective
3 hr	09/03/2017	453	43.63	43.69	40.70	1338.38	2213.01	105.84	35.28	41.28%	38.45%	Convective
3 hr	10/04/2017	140	39.37	39.46	39.77	413.63	424.29	79.11	26.37	49.89%	50.27%	Frontal
3 hr	14/04/2017	130	33.12	33.23	33.28	384.08	393.76	52.52	17.51	63.27%	63.35%	Convective
3 hr	12/05/2017	33	29.91	29.92	30.18	97.50	125.15	39.80	13.27	75.19%	75.84%	Frontal
3 hr	13/05/2017	36	29.54	30.00	30.00	106.36	115.99	40.28	13.43	74.49%	74.49%	Convective
3 hr	02/10/2017	59	30.87	31.14	30.56	174.31	189.25	42.26	14.09	73.70%	72.32%	Convective
3 hr	23/11/2017	977	42.56	42.69	43.18	2886.53	2933.38	87.47	29.16	48.80%	49.37%	Convective
3 hr	28/11/2017	88	34.62	35.11	35.18	259.99	250.30	45.03	15.01	77.98%	78.13%	Convective
24 hr	13/03/2016	599	54.65	55.25	54.48	1769.74	1709.36	101.00	4.21	54.71%	53.94%	Convective
24 hr	15/03/2016	78	50.40	50.64	50.23	230.45	235.04	63.50	2.65	79.75%	79.10%	Convective
24 hr	12/06/2016	46	48.20	48.59	48.15	135.91	140.41	71.00	2.96	68.43%	67.82%	Frontal
24 hr	25/07/2016	1120	48.99	49.68	51.01	3309.02	2359.53	80.00	3.33	62.10%	63.77%	Frontal
24 hr	18/10/2016	23	47.43	47.72	47.26	67.95	64.10	59.00	2.46	80.88%	80.10%	Convective
24 hr	20/10/2016	461	54.74	55.08	54.29	1362.02	1254.55	107.50	4.48	51.24%	50.50%	Frontal

	Date	Cell Count	Rainfall			Area of Storm (km²)		Max Point Precipitation (mm)	Max Point Intensity	ARF		Region (Convective/ Frontal)
			Areal Average (mm)	Isohyetal (mm)	ArcGIS (mm)	Precipitation Array	ArcGIS			ARF Isohyetal (%)	ARF ArcGIS (%)	
24 hr	25/10/2016	202	61.96	62.35	61.98	596.81	592.17	96.00	4.00	64.95%	64.57%	Frontal
24 hr	01/11/2016	167	56.70	56.93	56.51	493.40	509.76	100.00	4.17	56.93%	56.51%	Convective
24 hr	04/11/2016	374	59.18	59.91	61.63	1104.98	934.04	126.00	5.25	47.54%	48.92%	Frontal
24 hr	09/11/2016	99	64.08	64.47	64.24	292.49	271.67	118.00	4.92	54.64%	54.44%	Convective
24 hr	29/11/2016	85	48.99	49.44	48.31	251.13	262.51	63.00	2.63	78.48%	76.69%	Convective
24 hr	04/12/2016	69	46.42	47.21	47.00	203.86	183.15	70.00	2.92	67.44%	67.14%	Frontal
24 hr	06/12/2016	59	58.97	59.62	56.81	174.31	155.67	86.00	3.58	69.32%	71.92%	Convective
24 hr	09/12/2016	206	73.09	73.45	72.50	608.62	634.90	158.00	6.58	46.49%	47.08%	Convective
24 hr	18/12/2016	58	57.12	57.59	57.23	171.36	167.88	100.00	4.17	57.59%	57.23%	Frontal
24 hr	27/12/2016	2199	58.80	59.12	60.08	6496.91	6849.64	117.50	4.90	50.32%	51.14%	Frontal
24 hr	03/01/2017	257	55.44	55.75	55.98	759.30	741.74	96.00	4.00	58.07%	58.31%	Frontal
24 hr	06/01/2017	887	48.31	48.75	48.66	2620.63	2499.94	68.50	2.85	71.17%	72.09%	Convective
24 hr	12/01/2017	134	65.66	65.82	65.72	395.90	412.08	123.00	5.13	53.51%	53.43%	Convective
24 hr	25/01/2017	55	73.20	73.41	73.43	162.50	164.83	155.00	6.46	47.36%	47.37%	Frontal
24 hr	29/01/2017	34	56.71	56.76	56.83	100.45	91.57	73.00	3.04	77.76%	77.85%	Convective
24 hr	09/02/2017	121	66.94	67.54	69.46	357.49	366.29	149.00	6.21	45.33%	46.62%	Convective
24 hr	19/02/2017	147	84.29	84.74	85.51	434.31	436.50	147.00	6.13	57.65%	58.17%	Frontal
24 hr	24/02/2017	487	48.71	49.40	51.85	1438.83	1407.17	64.00	2.67	77.19%	81.01%	Convective
24 hr	09/04/2017	230	61.89	62.57	62.38	679.53	650.17	116.00	4.83	53.94%	53.78%	Convective
24 hr	12/05/2017	3159	56.63	57.25	57.48	9333.21	8519.32	141.00	5.88	40.61%	40.77%	Frontal
24 hr	14/05/2017	161	53.92	54.33	54.25	475.67	479.23	83.00	3.46	65.46%	65.36%	Convective
24 hr	30/09/2017	241	50.62	51.19	50.38	712.03	726.48	80.00	3.33	63.99%	62.97%	Convective
24 hr	02/10/2017	58	60.78	61.03	60.83	171.36	155.67	101.00	4.21	60.43%	60.23%	Convective
24 hr	04/10/2017	18	57.28	57.78	60.83	53.18	155.67	77.50	3.23	74.55%	75.05%	Frontal
24 hr	26/11/2017	724	48.96	49.60	49.42	2139.05	2014.60	77.00	3.21	64.41%	64.18%	Convective

	Date	Cell Count	Rainfall			Area of Storm (km²)		Max Point Precipitation (mm)	Max Point Intensity	ARF		Region (Convective/ Frontal)
			Areal Average (mm)	Isohyetal (mm)	ArcGIS (mm)	Precipitation Array	ArcGIS			ARF Isohyetal (%)	ARF ArcGIS (%)	
24 hr	29/12/2017	315	52.19	54.69	54.87	930.66	637.96	80.00	3.33	68.36%	68.59%	Convective

Table B.2: Comparison of Radar Derived ARFs with Smaller Catchment ARFs

Duration	Date	Time	ArcGIS area (km^2)	Max Point Precipitation (mm)	ARCGIS Point Intensity (mm/h)	ARF ArcGIS	Van Wyk ARF	Van Wyk ARF - Radar ARF	Op Ten Noort	OTN ARF - Radar ARF
1	20/02/2017	04:00:00	3.05	31	31.00	72.58%	99.76%	27.18%	99.36%	26.78%
1	21/02/2017	09:00:00	30.52	31	31.40	74.84%	96.49%	21.65%	93.69%	18.85%
1	10/03/2016	01:00:00	33.58	37	37.00	74.32%	95.54%	21.21%	91.90%	17.57%
1	05/11/2016	16:00:00	39.68	30	30.00	80.13%	95.81%	15.68%	92.22%	12.10%
1	27/11/2017	18:00:00	39.68	32	31.80	69.98%	95.56%	25.59%	91.78%	21.80%
24	18/10/2016	06:00:00	64.10	59	2.46	80.10%	99.50%	19.40%	98.93%	18.83%
1	09/02/2017	21:00:00	67.15	39	38.60	75.37%	92.25%	16.88%	83.84%	8.47%
24	29/01/2017	06:00:00	91.57	73	3.04	77.85%	99.22%	21.37%	98.12%	20.27%
1	06/12/2017	17:00:00	100.73	66	65.50	49.39%	83.49%	34.10%	63.85%	14.46%
3	04/12/2016	15:00:00	115.99	76	25.29	63.83%	92.66%	28.83%	81.92%	18.09%
3	13/05/2017	10:00:00	115.99	40	13.43	74.49%	96.03%	21.55%	89.95%	15.47%
3	12/05/2017	13:00:00	125.15	40	13.27	75.84%	95.88%	20.04%	89.32%	13.49%
1	07/01/2017	12:00:00	137.36	44	44.20	66.10%	86.16%	20.06%	66.18%	0.08%
24	12/06/2016	06:00:00	140.41	71	2.96	67.82%	98.99%	31.17%	97.21%	29.39%
24	06/12/2016	06:00:00	155.67	86	3.58	71.92%	98.68%	26.77%	96.28%	24.36%
24	02/10/2017	06:00:00	155.67	101	4.21	60.23%	98.46%	38.22%	95.64%	35.41%
24	04/10/2017	06:00:00	155.67	78	3.23	75.05%	98.81%	23.76%	96.64%	21.59%
24	25/01/2017	06:00:00	164.83	155	6.46	47.37%	97.54%	50.17%	93.02%	45.65%
24	18/12/2016	06:00:00	167.88	100	4.17	57.23%	98.38%	41.16%	95.35%	38.13%
24	04/12/2016	06:00:00	183.15	70	2.92	67.14%	98.79%	31.65%	96.43%	29.29%
3	02/10/2017	16:00:00	189.25	42	14.09	72.32%	94.15%	21.83%	83.42%	11.10%
3	30/11/2016	15:00:00	198.41	40	13.18	75.75%	94.32%	18.57%	83.70%	7.95%

Duration	Date	Time	ArcGIS area (km^2)	Max Point Precipitation (mm)	ARCGIS Point Intensity (mm/h)	ARF ArcGIS	Van Wyk ARF	Van Wyk ARF - Radar ARF	Op Ten Noort	OTN ARF - Radar ARF
3	20/01/2017	17:00:00	201.46	99	32.94	47.45%	86.29%	38.83%	63.68%	16.23%
1	29/12/2017	21:00:00	210.62	54	53.50	60.34%	78.32%	17.98%	46.48%	-13.86%
3	26/11/2016	00:00:00	210.62	91	30.23	46.06%	87.10%	41.04%	64.86%	18.80%
1	27/01/2019	17:00:00	210.62	60	59.50	56.33%	76.20%	19.88%	42.65%	-13.68%
3	08/03/2016	16:00:00	210.62	48	16.15	70.83%	92.88%	22.05%	79.35%	8.52%
1	30/09/2017	20:00:00	222.83	44	44.20	68.26%	81.27%	13.01%	51.18%	-17.08%
24	15/03/2016	06:00:00	235.04	64	2.65	79.10%	98.73%	19.63%	95.86%	16.76%
3	28/11/2017	01:00:00	250.30	45	15.01	78.13%	92.80%	14.66%	77.45%	-0.68%
24	29/11/2016	06:00:00	262.51	63	2.63	76.69%	98.67%	21.98%	95.42%	18.73%
1	25/02/2016	15:00:00	262.51	63	62.50	61.58%	72.77%	11.19%	32.77%	-28.81%
24	09/11/2016	06:00:00	271.67	118	4.92	54.44%	97.47%	43.03%	91.32%	36.88%
1	09/03/2016	16:00:00	311.35	54	53.50	57.27%	74.14%	16.87%	32.22%	-25.05%
1	03/01/2017	22:00:00	345.42	81	81.00	54.84%	61.80%	6.96%	14.92%	-39.93%
1	23/11/2017	18:00:00	351.03	40	39.60	70.10%	78.79%	8.69%	38.86%	-31.24%
1	06/04/2017	21:00:00	360.19	43	42.50	70.09%	77.11%	7.02%	35.31%	-34.78%
24	09/02/2017	06:00:00	366.29	149	6.21	46.62%	96.23%	49.61%	85.67%	39.06%
3	26/01/2017	14:00:00	366.29	101	33.51	49.11%	81.28%	32.17%	43.40%	-5.71%
1	26/01/2017	20:00:00	381.55	70	69.50	49.47%	64.36%	14.90%	16.48%	-32.99%
3	14/04/2017	11:00:00	393.76	53	17.51	63.35%	89.28%	25.92%	62.58%	-0.78%
24	12/01/2017	06:00:00	412.08	123	5.13	53.43%	96.66%	43.23%	86.62%	33.19%
3	10/04/2017	23:00:00	424.29	79	26.37	50.27%	83.77%	33.50%	46.73%	-3.54%
1	06/02/2016	19:00:00	430.39	32	32.20	77.03%	80.45%	3.41%	38.97%	-38.06%
24	19/02/2017	06:00:00	436.50	147	6.13	58.17%	95.92%	37.75%	83.38%	25.21%
1	06/01/2017	23:00:00	436.50	33	33.00	74.96%	79.90%	4.94%	37.55%	-37.41%

Duration	Date	Time	ArcGIS area (km^2)	Max Point Precipitation (mm)	ARCGIS Point Intensity (mm/h)	ARF ArcGIS	Van Wyk ARF	Van Wyk ARF - Radar ARF	Op Ten Noort	OTN ARF - Radar ARF
24	14/05/2017	06:00:00	479.23	83	3.46	65.36%	97.57%	32.20%	89.34%	23.98%
24	01/11/2016	06:00:00	509.76	100	4.17	56.51%	96.99%	40.47%	86.55%	30.04%
1	30/01/2017	15:00:00	515.86	57	57.00	58.16%	65.80%	7.64%	13.54%	-44.62%
1	13/12/2016	03:00:00	521.96	48	47.60	60.85%	70.33%	9.48%	18.46%	-42.39%
1	17/03/2016	10:00:00	521.96	57	56.50	66.06%	65.88%	-0.18%	13.46%	-52.60%
3	09/03/2016	04:00:00	567.75	56	18.51	63.04%	86.64%	23.59%	48.95%	-14.10%
24	25/10/2016	06:00:00	592.17	96	4.00	64.57%	96.87%	32.30%	85.12%	20.56%
3	03/01/2017	19:00:00	613.54	70	23.29	54.92%	82.85%	27.93%	37.85%	-17.07%
3	26/10/2016	16:00:00	613.54	99	32.87	53.77%	76.70%	22.93%	25.38%	-28.39%
24	09/12/2016	06:00:00	634.90	158	6.58	47.08%	94.71%	47.63%	75.26%	28.18%
24	29/12/2017	06:00:00	637.96	80	3.33	68.59%	97.28%	28.69%	86.54%	17.95%
1	26/10/2016	20:00:00	644.06	61	60.50	63.20%	60.65%	-2.55%	7.07%	-56.13%
24	09/04/2017	06:00:00	650.17	116	4.83	53.78%	96.04%	42.26%	80.76%	26.98%
3	07/01/2017	20:00:00	680.69	116	38.65	33.64%	71.83%	38.19%	16.72%	-16.92%
1	04/01/2017	01:00:00	699.01	60	59.50	60.64%	59.66%	-0.98%	5.91%	-54.73%
24	30/09/2017	06:00:00	726.48	80	3.33	62.97%	97.07%	34.10%	84.82%	21.84%
24	03/01/2017	06:00:00	741.74	96	4.00	58.31%	96.45%	38.14%	81.73%	23.42%
3	19/12/2016	22:00:00	744.79	68	22.72	57.90%	81.41%	23.51%	31.64%	-26.26%
3	07/12/2016	19:00:00	753.95	116	38.81	45.07%	70.21%	25.14%	13.67%	-31.40%
3	21/02/2017	17:00:00	769.21	45	14.98	69.31%	87.08%	17.77%	45.67%	-23.63%
1	14/03/2016	18:00:00	775.32	39	38.60	68.44%	69.90%	1.46%	13.07%	-55.37%
3	26/04/2016	15:00:00	778.37	98	32.53	48.71%	73.89%	25.18%	17.87%	-30.84%

Table B.3: Comparison of Radar Derived ARFs with Larger Catchment ARFs

Duration	Date	Time	ArcGIS area (km^2)	Max Point Precipitation (mm)	ARCGIS Point Intensity	ARF ArcGIS (%)	Wiederhold ARF	Wiederhold ARF – Radar ARF	Op Ten Noort	OTN ARF – Radar ARF
1	30/11/2016	19:00:00	802.79	49	48.50	66.74%	51.89%	-14.85%	74.11%	7.37%
24	04/11/2016	06:00:00	934.04	126	5.25	48.92%	75.05%	26.13%	103.19%	54.28%
3	14/05/2016	15:00:00	1031.72	114	38.05	49.74%	57.73%	7.99%	81.27%	31.53%
1	24/01/2016	01:00:00	1187.39	58	57.50	47.89%	50.30%	2.41%	70.58%	22.69%
3	16/03/2016	04:00:00	1251.49	131	43.57	39.72%	56.83%	17.11%	79.67%	39.95%
24	20/10/2016	06:00:00	1254.55	108	4.48	50.50%	73.81%	23.31%	101.45%	50.95%
24	24/02/2017	06:00:00	1407.17	64	2.67	81.01%	73.22%	-7.79%	100.78%	19.76%
3	07/01/2017	05:00:00	1510.95	67	22.49	49.43%	55.77%	6.33%	78.10%	28.67%
3	30/01/2017	08:00:00	1514.00	147	49.12	28.93%	55.76%	26.83%	78.09%	49.16%
3	22/10/2016	19:00:00	1611.68	72	23.97	57.76%	55.36%	-2.40%	77.57%	19.81%
1	19/12/2016	17:00:00	1654.42	60	60.00	55.24%	48.37%	-6.87%	67.60%	12.36%
3	04/01/2017	01:00:00	1672.73	162	53.84	39.06%	55.11%	16.05%	77.26%	38.20%
24	13/03/2016	06:00:00	1709.36	101	4.21	53.94%	72.05%	18.11%	99.63%	45.69%
24	26/11/2017	06:00:00	2014.60	77	3.21	64.18%	70.87%	6.70%	98.66%	34.48%
3	09/03/2017	17:00:00	2213.01	106	35.28	38.45%	52.89%	14.44%	74.93%	36.47%
24	25/07/2016	06:00:00	2359.53	80	3.33	63.77%	69.54%	5.78%	97.73%	33.96%
24	06/01/2017	06:00:00	2499.94	69	2.85	72.09%	69.00%	-3.09%	97.38%	25.29%
3	26/04/2016	18:00:00	2521.30	102	33.92	17.69%	51.63%	33.94%	73.84%	56.15%
3	26/07/2016	20:00:00	2734.97	143	47.57	31.35%	50.75%	19.40%	73.15%	41.81%
3	20/11/2016	18:00:00	2869.28	86	28.70	52.80%	50.20%	-2.60%	72.75%	19.95%
3	23/11/2017	16:00:00	2933.38	87	29.16	49.37%	49.94%	0.57%	72.57%	23.20%

Duration	Date	Time	ArcGIS area (km^2)	Max Point Precipitation (mm)	ARCGIS Point Intensity	ARF ArcGIS (%)	Wiederhold ARF	Wiederhold ARF – Radar ARF	Op Ten Noort	OTN ARF – Radar ARF
3	11/11/2016	16:00:00	2960.85	127	42.34	44.08%	49.83%	5.75%	72.49%	28.41%
1	23/10/2016	00:00:00	4847.25	51	50.50	55.55%	35.18%	-20.37%	57.92%	2.37%
1	22/10/2016	21:00:00	5744.67	70	70.00	41.21%	31.47%	-9.74%	56.40%	15.18%
3	22/10/2016	22:00:00	6559.66	105	35.14	37.99%	35.07%	-2.91%	65.76%	27.78%
24	27/12/2016	06:00:00	6849.64	118	4.90	51.14%	52.18%	1.05%	91.33%	40.20%
1	11/11/2016	21:00:00	7057.21	55	54.50	59.60%	26.05%	-33.55%	54.54%	-5.05%
24	12/05/2017	06:00:00	8519.32	141	5.88	40.77%	45.73%	4.96%	89.98%	49.22%
1	10/11/2016	23:00:00	9013.81	82	81.50	45.94%	17.96%	-27.98%	52.34%	6.40%

Table B.4: Statistical Results

X variable	Y variable	R^2 value	r-value	p-value
ArcGIS Area	Precipitation Array Area	0.9861	0.9930	5.22E-90
Precipitation Array Isohyetal Rainfall	ArcGIS Isohyetal Rainfall	0.9952	0.9976	7.7E-112
Precipitation Array Isohyetal Rainfall	Precipitation Array Average Rainfall	0.9995	0.9997	1.1E-156
Precipitation Array Isohyetal Rainfall ARFs	ArcGIS ARFs	0.9896	0.9948	4.71E-96
Max Point Precipitation	ArcGIS ARF	0.5587	-0.7475	3.19E-18
Log ArcGIS Area 1 hr storm duration	ArcGIS ARF	0.3792	-0.6158	0.000176
Log ArcGIS Area 3 hr storm duration	ArcGIS ARF	0.4733	-0.6879	9.69E-06
Log ArcGIS 24 hr storm duration	ArcGIS ARF	0.1738	-0.4169	0.017595
Log ArcGIS All Areas	ArcGIS ARF	0.3269	-0.5718	9.51E-10
Log All Max Point Intensity	ArcGIS ARF	0.1029	-0.3207	0.001361
Log 1 hr Max Point Intensity	ArcGIS ARF	0.7892	-0.8884	1.17E-11
Log 3 hr Max Point Intensity	ArcGIS ARF	0.8878	-0.9422	2.85E-16
Log 24 hr Max Point Intensity	ArcGIS ARF	0.8363	-0.9145	2.56E-13
ArcGIS ARFs	Van Wyk ARF	0.1295	0.3598	0.0026
ArcGIS ARFs	Op Ten Noort and Stephenson Equation 2	0.1624	0.4029	0.00066
Van Wyk ARF	Op Ten Noort and Stephenson Equation 2	0.9486	0.9740	2.86E-44
ArcGIS ARFs	Pullen, Wiederhold and Midgley's ARFs	0.1066	0.3265	0.083914
ArcGIS ARFs	Op Ten Noort and Stephenson Equation 3	0.1254	0.3541	0.059481
Pullen, Wiederhold and Midgley's ARFs	Op Ten Noort and Stephenson Equation 3	0.8591	0.9269	5.29E-13